Published in final edited form as:
Am Mineral. 2020 October 29; 105(10): 1508–1535. doi:10.2138/am-2020-7447.

An evolutionary system of mineralogy. Part II: Interstellar and solar nebula primary condensation mineralogy (>4.565 Ga)

Shaunna M. Morrison[1], **Robert M. Hazen**[1,*]

[1]Earth and Planets Laboratory, Carnegie Institution for Science, 5251 Broad Branch Road NW, Washington, D.C. 20015, U. S. A.

Abstract

The evolutionary system of mineralogy relies on varied physical and chemical attributes, including trace elements, isotopes, solid and fluid inclusions, and other information-rich characteristics, to understand processes of mineral formation and to place natural condensed phases in the deep-time context of planetary evolution. Part I of this system reviewed the earliest refractory phases that condense at $T > 1000$ K within the turbulent expanding and cooling atmospheres of highly evolved stars. Part II considers the subsequent formation of primary crystalline and amorphous phases by condensation in three distinct mineral-forming environments, each of which increased mineralogical diversity and distribution prior to the accretion of planetesimals >4.5 billion years ago.

(1) Interstellar molecular solids: Varied crystalline and amorphous molecular solids containing primarily H, C, O, and N are observed to condense in cold, dense molecular clouds in the interstellar medium ($10 < T < 20$ K; $P < 10^{-13}$ atm). With the possible exception of some nanoscale organic condensates preserved in carbonaceous meteorites, the existence of these phases is documented primarily by telescopic observations of absorption and emission spectra of interstellar molecules in radio, microwave, or infrared wavelengths.

(2) Nebular and circumstellar ice: Evidence from infrared observations and laboratory experiments suggest that cubic H_2O ("cubic ice") condenses as thin crystalline mantles on oxide and silicate dust grains in cool, distant nebular and circumstellar regions where $T \sim 100$ K.

(3) Primary condensed phases of the inner solar nebula: The earliest phase of nebular mineralogy saw the formation of primary refractory minerals that solidified through high-temperature condensation ($1100 < T < 1800$ K; $10^{-6} < P < 10^{-2}$ atm) in the solar nebula more than 4.565 billion years ago. These earliest mineral phases originating in our solar system formed prior to the accretion of planetesimals and are preserved in calcium-aluminum-rich inclusions, ultra-refractory inclusions, and amoeboid olivine aggregates.

Keywords

Classification; mineral evolution; natural kinds; vapor deposition; condensation; nebular mineralogy; interstellar mineralogy; chondrite meteorites

* rhazen@carnegiescience.edu.

Introduction

The incremental, episodic emergence of mineral diversity and distribution through more than 13 billion years of cosmic evolution provides the basis for an “evolutionary system” of mineral classification—one that emphasizes the formation of solid phases by a progression of physical, chemical, and ultimately biological processes (Hazen et al. 2008; Hazen and Ferry 2010; Hazen 2019; Hazen and Morrison 2020). This system amplifies the official classification protocols of the International Mineralogical Association’s Commission on New Minerals, Nomenclature and Classification (IMA, CNMNC; e.g., Burke 2006; Mills et al. 2009; Schertl et al. 2018), which defines each mineral “species” on the basis of its unique combination of end-member composition and idealized crystal structure. More than 5500 approved mineral species are now recognized by the IMA system (https://rruff.info/ima; accessed 27 March 2020).

By design, the IMA classification system is predicated on identifying the minimum amount of information (as measured in bits; e.g., Krivovichev 2012, 2013) required to distinguish one species from another. Consequently, IMA procedures cannot capture the information-rich complexity of natural mineral specimens—their trace and minor elements, fractionated isotopes, structural defects, varied magnetic and electrical properties, external morphologies, solid and fluid inclusions, spectral features, petrologic environment, ages of both formation and subsequent diagenetic episodes, and myriad other attributes that have the potential to tell the story of each individual sample’s origin and alteration via interactions with a succession of environments through deep time. We conclude that IMA protocols are insufficient to classify minerals in their evolutionary contexts.

Accordingly, we propose an “evolutionary system of mineralogy” that amplifies and modifies the IMA scheme in three ways, each of which is informed by those information-rich aspects of natural mineral specimens—attributes that are the essence of historical science discovery in the “messy, uncontrollable world of nature” (Cleland 2013; see also Cleland 2011). We split some IMA species into two or more “natural kinds”—subdivisions that recognize fundamentally different idiosyncratic combinations of attributes that arise from distinct paragenetic modes. Thus, for example, we view isotopically anomalous nanoscale diamond condensed from a high-temperature, low-pressure carbon-rich vapor in the expanding atmosphere of an exploding star as intrinsically different from macroscopic Type I “gem” diamond crystallized in high-temperature, high-pressure, carbon-saturated aqueous fluids in Earth’s mantle, which in turn differs from diamond formed by the impact of an asteroid on near-surface carbonaceous material (Hazen 2019). Such splitting of IMA species into multiple “natural kinds” is appropriate for many of Earth’s commonest mineral species, including calcite, hydroxylapatite, pyrite, and quartz, all of which have both abiotic and biotic paragenetic modes.

In other instances, we propose lumping two or more IMA species into a single “natural kind.” Notable examples of species that are lumped according to their evolutionary contexts occur in chemically diverse structural groups of rock-forming silicates, including amphibole, mica, pyroxene, and tourmaline group minerals, for which a given specimen formed in a single geological setting and in one continuous phase domain may display a range of zoning

and solid solution that overlaps the compositional ranges of two or more end-member species as defined by IMA protocols. Other examples of IMA species that we lump into a single natural kind include groups of isostructural rare earth element minerals, some Mg-Fe oxides and silicates, and natural metal alloys, for which small variations in the ratios of crystal chemically similar elements that occur within one paragenetic environment may require multiple IMA end-member mineral species.

Third, the evolutionary system catalogs a variety of non-crystalline or aperiodic condensed phases, including glasses (e.g., stellar amorphous carbon, impact maskelynite, volcanic obsidian) and mixed-phase nano-materials (bauxite, coal, and limonite, for example)—materials not usually considered in the current IMA scheme (e.g., Hazen et al. 2013, Table 3 therein), though many of these phases were included in the revolutionary third edition of James Dwight Dana's *System of Mineralogy* (Dana 1850), from which the modern IMA formalisms have evolved.

Meteorite minerals

An important illustration of the demonstrable benefits and potential pitfalls of the IMA system is provided by the diversity, distribution, and modes of formation of meteorite minerals, as reviewed by Rubin and Ma (2017, 2020), who tabulate more than 400 types of minerals known from meteorites, the majority of which (including dozens of intriguing micro- or nano-scale phases discovered by Chi Ma) have been approved as official IMA species. However, more than 50 of the listed meteorite phases are not officially recognized by the IMA (see https://rruff.info/ima; accessed 27 March 2020), because they fail to meet IMA criteria for legitimate species owing to a range of reasons.

At least a dozen minerals in Rubin and Ma's list, including native Mo, Nb, and Re; carbides of Fe, Mo, and Zr; Ca and Nb oxides, and other primarily micrometer-scale phases, may eventually receive approval but have not yet been accepted by the IMA. However, many of Rubin and Ma's listed phases do not meet IMA requirements for end-member compositional variants of natural crystalline phases. In some cases, they list phases that effectively split IMA species as a consequence of additional minor elements. For example, they record "Ti-rich" and "V-rich" varieties of magnetite (in addition to magnetite), "pleonaste" (a varietal name for Mg-Fe^{2+} oxide spinel), "sodium phlogopite," "Ca-armalcolite," and "carbonate-fluorapatite." They also split graphite into two polytypes—graphite 2*H* and graphite 3*R*.

On the other hand, in some instances, Rubin and Ma (2017, 2020) lump mineral species into broadly inclusive mineral groups—e.g., apatite, feldspar, mica, olivine, and orthopyroxene. They also implicitly lump two or more approved minerals with end-member compositions into one solid solution; for example, their list includes "magnesiowüstite," which is an unapproved name for the solid solution between periclase (MgO) and wüstite (FeO), both of which end-members are also listed. Similarly, IMA-approved magnesite ($MgCO_3$) and siderite ($FeCO_3$) are listed along with "breunnerite," an obsolete, though useful, name for Mg-dominant rhombohedral carbonates in the magnesite-siderite solid solution. "Plagioclase" also appears in the tabulation along with the two end-members of the albite-anorthite solid solution. Similarly, "biotite," "Au-dominated alloys," and "PGE-dominated

alloys" are names for chemically complex phase regions that encompass multiple approved IMA species.

Finally, Rubin and Ma (2017, 2020) catalog several amorphous or composite nanophases that are excluded from the current IMA list (illite, martinsite, and maskelynite, for example). In these particulars, Rubin and Ma's tabulation of meteorite minerals mirrors the evolutionary system of mineralogy, as it underscores both the need for the exacting IMA nomenclature and the desirability of additional classification protocols to address complex natural condensed phases—varied split, lumped, and non-crystalline phases that are critical to describing the diverse modes of mineral formation in the natural world.

The potential benefits of the evolutionary system are further highlighted by Rubin and Ma (2017), who list 17 different processes by which the hundreds of documented meteorite minerals have formed (Table 1). They note, "Some meteoritic minerals form by only a single mechanism (e.g., ringwoodite and ahrensite by high-pressure shock metamorphism of olivine); other minerals form by several mechanisms (e.g., olivine by condensation around red giant and AGB stars, condensation in the solar nebula, crystallization in [high-temperature nebular] melts, crystallization in chondrule melts, thermal metamorphism, crystallization from impact melts, condensation within impact plumes, crystallization in magmatic bodies on differentiated asteroids, annealing of amorphous material, and aqueous alteration)" (Rubin and Ma 2017, page 339). They emphasize that "In this overview, no attempt has been made to describe every mode of formation of every meteoritic mineral. That monumental task would require a multi-volume book-length treatment."

We suggest that such varied modes of formation usually result in diagnostic sets of attributes that point to multiple natural kinds—the mineralogical key to understanding the evolution of planetary systems. Our multi-part endeavor, though far from the encyclopedic "monumental task" envisioned by Rubin and Ma for meteorite minerals, nevertheless will attempt to enumerate mineral natural kinds in the context of their paragenetic modes.

Pre-terrestrial stages of mineral formation

In Part I of this series, Hazen and Morrison (2020) described the earliest phase of mineral evolution commencing more than 13 billion years ago—the condensation of more than 40 kinds of extremely refractory nanoscale minerals, representing 22 IMA-approved mineral species, as well as two as yet unapproved crystalline phases and amorphous forms of carbon, alumina, and silicates (i.e., Mode 1 of Rubin and Ma's 17 modes of meteorite mineralization; Table 1). These varied phases were dispersed as micro- and nano-scale dust grains into the interstellar medium, along with hydrogen, helium, and other atomic and molecular species. A variety of highly evolved stars, including C- and O-rich asymptotic giant branch (AGB) stars, classical novae, and type II supernovae, seeded the interstellar environment with copious quantities of gas and mineral dust. Significant fractions of those raw materials eventually concentrated in subsequent generations of stars and their companion planets.

Here in Part II we examine the next two episodes of cosmic mineral evolution, which encompass the primary condensation, melt crystallization, and initial solid-state

transformation on cooling (e.g., exsolution, reversible phase transitions, and element ordering) of a variety of crystalline and amorphous phases from the dust and gaseous remnants of stars. These processes include modes of formation no. 2, no. 3, and no. 5 in Table 1, as well as additional processes that lead to interstellar and circumstellar condensed phases that are observed through telescopic spectral observations but are not preserved in meteorites.

In particular, we consider a few kinds of condensed molecular phases, sometimes collectively known as "ices," though in this review, the term ice refers exclusively to crystalline H_2O. Condensed molecular solids are observed by astronomical spectroscopy to form in the extremely low-temperature, high-vacuum conditions of "cool, dense" interstellar molecular clouds—the nurseries of new generations of stars. Perturbations to a molecular cloud can lead to a Jeans instability—a local density increase, followed by gravitationally induced collapse of the molecular cloud into a solar nebula, and ultimately star system formation (Jeans 1902; Mizuno et al. 1994; Longair 2008). In the case of our solar system, more than 99.8% of the solar nebula's mass formed the Sun, commencing ~4.567 billion years ago, while the remaining dust and gas experienced a complex history of thermal processing and chemical mixing that led to the formation of numerous additional solid phases (Rubin and Ma 2017, 2020).

In this contribution we focus on presumed primary phases—those that are thought to have formed by condensation directly from a gas phase, by subsequent solidification from a melt at pressures less than 0.01 atm, and solid-state transformations (e.g., exsolution, annealing, or ordering), as observed in calcium-aluminum-rich inclusions (CAIs), amoeboid olivine aggregates (AOAs), and ultra-refractory inclusions (URIs) of chondrite meteorites (Fig. 1). We also include condensation of cubic ice (H_2O), the low-temperature crystalline polymorph of water ice (e.g., Gaffney and Matson 1980), as <0.05 μm thick crystalline mantles on oxide and silicate dust particles in the cold, distant circumstellar regions of solar nebulae. It should be emphasized, however, that most primary condensed interstellar and solar nebular phases were either lost through sublimation or were eventually incorporated into larger bodies—asteroids, comets, and planetesimals that experienced subsequent alteration by large-scale differentiation; fluid-rock interactions; multiple thermal events, including heating by the decay of short-lived radioactive isotopes, radiative heating, and conversion of gravitational potential energy; and high-energy impacts. Thus, a continuum exists between pristine "primary" and altered "secondary" mineral grains (e.g., Brearley and Jones 1998; MacPherson 2014; Rubin and Ma 2017). Primary mineral phases preserved in chondrules, which formed by melt solidification and subsequent solid-state reactions (Brearley and Jones 1998; Scott and Krot 2014; Connolly and Jones 2016), are the subject of Part III of this series, whereas the rich variety of presumed secondary minerals, as processed in the dynamic environments of growing planetesimals and preserved in the diverse meteorites that fall to Earth, will be the focus of Parts IV and V.

The mineralogy of interstellar molecular clouds

Highly evolved mineral-producing stars eject a significant fraction of their atmospheric dust and gas in energetic solar winds. Much of this ejected mass continues to be collected

throughout the galaxy in a variety of molecular clouds, most of which are too warm and dispersed to form additional condensed phases (Greenberg 1991; Ferriere 2001). Only the so-called "cool, dense molecular clouds" have been the loci of a second significant pulse of cosmic condensation, albeit at significantly lower temperatures and pressures than their stellar precursors (Fig. 2). These distinctive interstellar molecular clouds, typically composed of 99% gas, predominantly H in the form of H atoms and H_2 molecules (Wakelam et al. 2017) and atomic He, with important contributions by O-, C-, and N-bearing molecular species (Fig. 1b), and ~1 wt% mineral dust (primarily oxides, silicates, carbides, and carbon allotropes), are the nurseries of new star systems (e.g., Herbst 1995).

The environments of cool, dense molecular clouds

"Cool, dense molecular clouds" might seem misnamed. They are relatively cold ($10 < T < 20$ K) regions of the interstellar medium that are characterized by the gradual condensation of a variety of molecular solids (Kouchi and Yamamoto 1995; Allamandola et al. 1999; Ferriere 2001; Gibb et al. 2004). Furthermore, "dense" in this context equates to approximately 10^2 to a maximum of 10^6 molecules per cubic centimeter—i.e., orders of magnitude lower pressure than the 10^{10} molecules per cm^3 in a typical laboratory "high vacuum," though significantly greater than the average galactic medium of fewer than one atom per cubic centimeter. Thus, the effective pressures of condensation in cool, dense molecular clouds are thought to be less than 10^{-13} atm (Fig. 1a).

Cool, dense molecular clouds are vast, sometimes exceeding 100 light years in diameter, and they appear as dark irregular shapes in silhouette against the twinkling background of more distant stars—a consequence of the cumulative effect of light-blocking dust (Ferriere 2001; Di Francesco et al. 2006). Of note is the Taurus Molecular Cloud, which at a distance of ~430 light years is the closest and among the best-studied large star-forming regions (Luhman et al. 2010). In addition to hundreds of relatively young stars, the Taurus Molecular Cloud hosts a diverse suite of molecular species (Freeman and Millar 1983), some of which (though not all; e.g., Güsten et al. 2019) condense into molecular crystals and amorphous solids.

Evidence for such interstellar condensed phases comes primarily from infrared absorption measurements, as light from more distant stars passes through a molecular cloud, as well as by IR and radio emission spectroscopy. Astronomical observations are interpreted using spectroscopic data from laboratory experiments on small molecules under cold vacuum (e.g., Allamandola et al. 1999; Ehrenfreund and Cami 2010, and references therein). These interstellar solids are nanoscale in dimensions, volatile in subsequent warmer solar nebular environments, and inaccessible from Earth; consequently, they will never grace the collections of mineralogical museums. Nevertheless, these ephemeral, submicroscopic condensed phases are among the largest molecular repositories in the cosmos; thus, they play a significant role in the origins and distribution of key volatile molecular species in planetary systems.

At 10 K, most molecular species have a "sticking coefficient" close to unity, meaning that almost all gaseous species except for H_2 and He adhere to cold surfaces. Under such conditions, gradual molecule-by-molecule condensation of the most abundant molecular

species, including H_2O, CO, CO_2, CH_3OH, and CH_4, is thought to occur on the surfaces of dust grains. By contrast, condensed molecular phases are not thought to be present in the warmer diffuse interstellar medium ($50 < T < 100$ K; $< 10^3$ atoms/cm^3; Ehrenfreund and Charnley 2000; Ferriere 2001).

The diversity and distribution of molecular components in interstellar solids reflect the initial gas phase composition, predominantly H and He with C, O, and N (Fig. 1b), that has been significantly modified by several factors, including relative rates of condensation and sublimation at low temperatures, the nature of dust grain substrates, intermolecular chemical reactions, photochemical alteration by UV radiation and cosmic rays, and gradual annealing (Seki and Hasegawa 1983; Kouchi and Kuroda 1990; Jenniskens and Blake 1994, 1996; Kouchi et al. 1994; Ehrenfreund and Charnley 2000; Ehrenfreund and Fraser 2003; Gibb et al. 2004; Williams 2005; Hollenbach et al. 2009). For example, Allamandola et al. (1999) review the important role of hydrogen speciation, notably the ratio of H to H_2, in molecular clouds. In regions where monatomic hydrogen dominates, hydrogenation reactions lead to the synthesis of H_2O, NH_3, and CH_4 as common condensed species. In H_2-rich environments, by contrast, O_2, N_2, CO, and CO_2 occur more abundantly in condensates. Accordingly, Allamandola et al. (1999) conclude that condensed molecular mantles on dust grains may fall into two principal populations distinguished by the dominant local hydrogen species.

Characterizing interstellar condensed phases

The first interstellar molecular condensates to be identified were CO (Wilson et al. 1971) and H_2O (Gillet and Forrest 1973), based on their strong absorption bands at 4.67 and 3.07 μm, respectively. Subsequent discoveries of absorption and emission features point to hundreds of molecular species, of which a few may condense and anneal in local concentrations that warrant designation as an interstellar mineral. The most detailed picture of the nature and distribution of these interstellar phases comes from orbiting telescopic measurements, for example as summarized by Gibb et al. (2004), who review spectra in the 2.5 to 30 μm range measured by the Short-Wavelength Spectrometer of the Infrared Space Observatory (ISO). ISO spectra reveal diagnostic absorption features from a range of molecular sources that point to more than a dozen forms of interstellar condensed molecules, of which at least five—H_2O, CO, CO_2, CH_3OH, and CH_4—occur as discrete nanoscale phases. Table 2 lists several phases that condense in the extremely cold, low-pressure environments of circumstellar and interstellar molecular clouds.

By far the most abundant interstellar molecular condensate is water in its low-density amorphous form (Jenniskens and Blake 1994, 1996), comprising more than 60% of observable molecular solids (Gibb et al. 2004). Water molecules are identified based on a characteristic O-H stretching infrared absorption feature at 3.05 μm, coupled with bending and combination absorption modes at 1.65, 4.5, and 6.0 μm (Whittet 2003; Hagen et al. 1981; Grundy and Schmitt 1998; Newman et al. 2008). Importantly, interstellar water ice and other condensates were the primary source of water and other volatiles on Earth (Alexander et al. 2018).

Four other common condensate species are CO (with a diagnostic C-O stretch mode at 4.67 μm), CO_2 (C-O stretch and O-C-O bending modes at 4.27 and 15.2 μm, respectively), CH_3OH (four bands at 3.54, 3.95, 8.90, and 9.75 μm), and CH_4 (7.676 μm), all of which have been confirmed to exist in the solid state. These molecular solids, which formed primarily by heterogeneous condensation and/or photoreactions on dust grains (Seki and Hasegawa 1983; Lacy et al. 1991; Kouchi and Yamamoto 1995; Gibb et al. 2004; Williams 2005), occur both as relatively pure phases and as condensed molecular mixtures.

In addition to the five most abundant solid-forming molecules noted above, strong evidence exists for other molecular species as generally minor, i.e., < 1 molecular percent (mol%) components of condensed phases, including N_2, O_2, OCS, H_2CO, HCOOH, *X*CN (where *X* may be oxygen; Whittet et al. 2001), and NH_3, while the molecular ions OCN^-, NH_4^+, and CN^- may also play a role in some condensed solids (Gibb et al. 2004).

Molecular clouds also reveal complex assemblages of organic species, the majority of which accumulate in carbonaceous condensates analogous to soot and coal (Henning and Salama 1998; Ehrenfreund and Charnley 2000; Pendleton and Allamandola 2002; Snow and McCall 2006; Alexander et al. 2007; Tielens 2008). Ehrenfreund and Cami (2010) review carbon chemistry in the interstellar medium, in which almost 800 molecular species have been identified in molecular clouds (http://www.astrochemistry.net; accessed 12 August 2019), including significant quantities of nitriles, ketones, and esters (Allamandola et al. 1999; Yan et al. 2005; Ehrenfreund and Cami 2010). Of special interest are polycyclic aromatic hydrocarbons, or “PAHs,” as well as a variety of fullerenes, both of which form in the high-temperature circumstellar envelopes of carbon-rich stars and have complex carbon chemistry analogous to soot formation in automobile exhaust or wood-fire smoke (Henning et al. 2004; Snow and Witt 1995; Ehfrendfreund and Cami 2010; Salama et al. 2011).

Systematic evolutionary mineralogy: Part IIA—Interstellar mineralogy

From the mineralogical perspective, the nature of interstellar molecular solids presents challenges when attempting to define discrete phases. At temperatures close to 10 K, almost all molecular species will condense onto the cold surfaces of mineral grains immediately on contact (Greenberg 1991; Gibb et al. 2004). The initial molecular distribution, therefore, is highly disordered—a randomly condensed, amorphous molecular mixture rather than discrete, relatively pure phases. Only the most abundant molecular species are likely to gradually anneal into homogeneous nanoscale crystalline or amorphous volumes that might be justifiably characterized as mineral kinds. Such phases may be as small as 1 to 2 nm in diameter; experimental and theoretical experiments by Moberg et al. (2019) suggest that in the case of H_2O fewer than 100 molecules are required to form a discrete phase with the structural properties of ice.

Water ice, which accounts for 60 to 70% of molecular condensates in most observed molecular clouds (Whittet 2003; Gibb et al. 2004), provides the least ambiguous case. Specific sharp infrared emission features at 44 and 60 μm, as well as peak shapes and intensities of peaks at 1.65, ~3.1, and 4.53 μm, point unambiguously to both crystalline and amorphous condensed regions (Hagen et al. 1981; Moore and Hudson 1992; Grundy and

Schmitt 1998; Newman et al. 2008). As noted above, at the relatively cold temperatures of dense molecular clouds, cubic ice is the expected crystalline form.

Carbon monoxide, often the second most abundant condensing molecular species at concentrations up to 20% (e.g., Gibb et al. 2004), presents an intriguing case with two spectral types; the IR absorption spectra of solid CO differs significantly depending on its molecular environment (Sandford et al. 1988; Elsila et al. 1997; Williams 2005). For matrices composed predominantly of polar species (predominantly H_2O), the ~4.67 mm peak has a broad component with a maximum at 4.682 μm. By contrast, a matrix of non-polar molecules (often CO, itself) is characterized by a narrower peak at 4.673 μm (Chiar et al. 1995, 1998). In the latter instance, a strong case can be made for discrete condensed amorphous CO as an interstellar phase.

Interstellar methanol is characterized by differences in absorption peak profiles that are also revealing, pointing to condensed regions of both relatively pure CH_3OH and methanol-water mixtures (Pontoppidan et al. 2003). However, for other less abundant interstellar molecules, of which hundreds have been cataloged (http://www.astrochemistry.net), the existence of discrete icy phases is inferred primarily on their relative abundances, rather than on specific spectroscopic characteristics.

Here we describe a few of the most abundant non-ionized interstellar molecules, including all C_1 molecules (those with only one carbon atom per molecule) and other species that are estimated to occur in some cool, dense molecular clouds at concentrations greater than 2 mol %. We catalog and name 8 condensed phases as likely interstellar minerals, while an additional 10 molecular species are labeled “unconfirmed as a discrete condensed phase” (Table 2).

Note that, with the exception of water ice, these 18 phases have not been identified in their crystalline forms naturally on Earth and are thus not in the current list of official IMA mineral species. Therefore, our nomenclature follows the conventions established by Hazen and Morrison (2020). The name of the molecule is preceded by the modifier interstellar (i.e., “*interstellar methane*”) to distinguish it from similar species that may condense in circumstellar, nebular (see below), or planetary (Maynard-Casely et al. 2018; Hazen 2018) environments.

Native elements

Interstellar hydrogen (H_2).—[unconfirmed as a discrete condensed phase] According to some models of molecular condensation, a fraction of di-molecular hydrogen could condense at the lowest temperatures (~10 K) in a cool dense molecular cloud. However, most hydrogen remains in its gaseous form as H_2 or H atoms at $T > 10$ K.

Interstellar nitrogen (N_2).—[unconfirmed as a discrete condensed phase] Molecular nitrogen (N_2) is a relatively minor component of cool dense molecular clouds, but it should condense heterogeneously with other molecules in environments with $T < 20$ K (Herbst and Klemperer 1973; Womack et al. 1992; Knauth et al. 2004; Maret et al. 2006; Daranlot et al.

2012). In addition, hydrogenation reactions of nitrogen play an important role in the formation of ammonia.

Interstellar oxygen (O_2).—[unconfirmed as a discrete condensed phase] Oxygen is the third most abundant element in most molecular clouds; nevertheless, molecular oxygen (O_2) is a minor component of cool dense molecular clouds (Hollenbach et al. 2009; Wang et al. 2015). A significant fraction of O_2 reacts with hydrogen to form water molecules.

Oxides

Interstellar cubic ice (H_2O).—Water (H_2O), both as an amorphous phase and crystalline ice, is the most abundant interstellar condensed molecular species, comprising 60% or more of condensates in cool dense molecular clouds (Whittet 2003; Gibb et al. 2004). The most familiar crystalline structure of H_2O is the hexagonal form of snowflakes. However, below ~170 K the stable crystalline form of ice condensed onto a cold substrate is “cubic ice” (Hobbs 1974). Because water ice condenses at temperatures significantly higher than other common molecular solids (as high as ~100 K), crystalline H_2O is also the only ice to commonly form mantles on silicate grains as they are ejected from oxygen-rich stars (Kouchi and Yamamoto 1995), based on distinctive IR absorption features (e.g., Whittet 2003).

“*Interstellar cubic ice (H_2O)*” in this evolutionary classification exclusively designates crystalline H_2O, which is thought to account for significantly less than half of water condensates in the interstellar medium. We retain the official IMA name, ice, for crystalline water, even though the term “ice” is also commonly applied generically to other cold condensed molecular solids, both crystalline and amorphous, in the cosmochemistry literature.

Interstellar amorphous H_2O.—Amorphous H_2O is the most abundant interstellar mineral and is a ubiquitous constituent of the icy mantles on presolar dust grains that form in cool dense molecular clouds (Gibb et al. 2004). Amorphous H_2O may form by direct condensation at temperatures in a molecular cloud, as well as by prolonged exposure of crystalline H_2O to ultraviolet or charged-particle radiation (Kouchi and Kuroda 1990; Kouchi and Yamamoto 1995).

A complication is the possibility of multiple forms of amorphous H_2O (e.g., Kouchi 1987, 1990; Sack and Baragiola 1993; Palumbo 2005), which depend on several factors, including the temperature of condensation, the molecular/atomic flux density, exposure to ionizing radiation, and the nature of the substrate.

The formation of amorphous vs. crystalline H_2O is a balance between the temperature and molecular/atomic flux. Crystalline water ices only form at relatively high temperature and low molecular fluxes (e.g., $<10^8$ molecules per cm^2 per second at 50 K; Kouchi et al. 1994). At the lower temperatures and higher fluxes of cool, dense molecular clouds there is insufficient time for molecular order to occur, so amorphous phases prevail. Gradual annealing to crystalline H_2O can occur, but the process is highly temperature dependent and is balanced by gradual sublimation at higher temperatures.

Interstellar amorphous carbon monoxide (CO).—Interstellar carbon monoxide is a common constituent of molecular clouds, identified by its prominent infrared absorption feature at 4.67 μm (Chiar et al. 1996; Elsila et al. 1997). Kouchi (1990) determined that CO condenses in part as a separate amorphous phase and, in part, as an impurity up to a few percent in amorphous H_2O (see also Collings et al. 2003). CO molecules can comprise a significant fraction (up to 25 mol%; Allamandola et al. 1999) of H_2O-dominated phases, with greater abundances in solids rich in other nonpolar molecules, such as CO_2, O_2, and N_2 (Elsila et al. 1997; Ehrenfreund et al. 1997).

Interstellar carbon monoxide (CO).—Crystalline interstellar carbon monoxide has been shown to form when amorphous CO warms to 23 K and anneals (Kouchi 1990).

Interstellar amorphous carbon dioxide (CO_2).—Interstellar carbon dioxide has been identified by its characteristic infrared absorption features at 4.27 and 15.2 μm as a ubiquitous condensed species (d'Hendecourt and de Muizon 1989; Chiar et al. 1998; Gerakines et al. 1999; Nummelin et al. 2001; Boogert and Ehfrenfreund 2004; Gibb et al. 2004; Pontoppidan et al. 2008). While carbon dioxide is relatively rare in the interstellar gas phase, it can represent as much as 20 mol% of a condensed molecular mixture in both single-phase form and in heterogeneous molecular mixtures. This situation has led several authors to suggest that CO_2 forms principally by oxidation of condensed CO in the solid state (Allamandola et al. 1999; Roser et al. 2001; Williams 2005).

Interstellar sulfur dioxide (SO_2).—[unconfirmed as a discrete condensed phase] Condensed interstellar sulfur dioxide is revealed by absorption at ~7.6 μm (Boogert et al. 1997; Zasowski et al. 2009).

Organic molecular solids

Interstellar amorphous methanol (CH_3OH).—The presence of interstellar methanol at abundances as high as 25 mol% is revealed by a distinctive suite of infrared absorption bands (Grim et al. 1991; Gibb et al. 2004). Pontoppidan et al. (2003) analyzed absorption peak profiles that indicate regions of relatively pure CH_3OH, as well as methanol-water mixtures. The measured methanol abundance in the interstellar medium is often significantly greater than that predicted from models of gas-phase chemistry, possibly as a result of solid-state hydrogenation reactions in mixed-phase water-CO condensed phases to make methanol (Williams 2005; Qasim et al. 2018)—further evidence that the molecular compositions of interstellar solids are not exclusively a consequence of condensation (Öberg et al. 2008).

Interstellar amorphous methane (CH_4). Interstellar methane at concentrations from ~1 to 4 mol% is revealed by a diagnostic 7.676 μm absorption band (Lacy et al. 1991; Boogert et al. 1996; d'Hendecourt et al. 1996; Gibb et al. 2004). Spectroscopic evidence for a much lower concentration of gas-phase methane suggests that CH_4 forms in the solid state through hydrogenation of atomic carbon (Boogert et al. 1998). An unknown fraction of condensed interstellar methane may occur in the form of clathrate hydrates (Ghose et al. 2019).

Interstellar cyanide (XCN).—[unconfirmed as a discrete condensed phase] The presence of a weak absorption feature at 4.62 μm in the spectra of some dense molecular clouds

points to the C-N stretch feature of cyanide, which may constitute up to a few mol% of some objects. Generally given as "*X*CN," Whittet et al. (2001) suggest that *X* may be oxygen, though HCN is likely present, as well (Snyder and Buhl 1971; Clark et al. 1974).

Interstellar formaldehyde (H_2CO).—[unconfirmed as a discrete condensed phase] Diagnostic microwave emissions at 4830 MHz (Snyder et al. 1969), as well as infrared features at 5.81 and 5.83 μm, point to molecular formaldehyde at abundances up to ~3 mol% (Grim et al. 1991; Gibb et al. 2004).

Interstellar formic acid (HCOOH).—[unconfirmed as a discrete condensed phase] The presence of formic acid at concentrations less than 2 mol% is revealed by radio emissions (Zuckerman et al. 1971; Winnewisser and Churchwell 1975), as well as by infrared absorption bands at 5.85 and 7.243 μm (Gibb et al. 2004). Peak profiles of IR bands reveal formic acid molecules in both gas and condensed states (Schutte et al. 1999; Bisschop et al. 2007).

Interstellar acetaldehyde (CH_3HCO).—[unconfirmed as a discrete condensed phase] An absorption band at 7.414 μm suggests the presence of condensed acetaldehyde in significant concentrations, perhaps as much as ~10 mol%, in many interstellar environments (Schutte et al. 1999; Gibb et al. 2004).

Interstellar carbonyl sulfide (OCS).—[unconfirmed as a discrete condensed phase] Characterized by a distinctive absorption feature at 4.91 μm, OCS is present at typically <1 mol% (Palumbo et al. 1995, 1997; Gibb et al. 2004).

Interstellar ammonia (NH_3).—[unconfirmed as a discrete condensed phase] The presence of interstellar ammonia is inferred from a minor absorption band at ~9 μm, close to the 9.3 μm absorption of pure NH_3 (Smith et al. 1989; Chiar et al. 2000; Dartois et al. 2002). Note that the position of the band shifts when the molecule is present in the polar environment of condensed H_2O. This interpretation is reinforced by a band at 3.5 μm, which matches a broad feature associated with ammonium hydrate (Gibb et al. 2004).

Interstellar kerogen.—Laboratory studies of the effects of UV radiation on simple molecular systems under high vacuum and low temperatures demonstrate the formation of complex insoluble mixtures of non-volatile organic matter, not unlike the "kerogen" component that can be extracted through acid dissolution of carbonaceous meteorites (Cronin and Pizzarello 1990; Greenberg et al. 1995; Widowiak et al. 1995; Ehrenfreund and Cami 2010). An absorption feature at ~3.47 μm corresponds to the C-H stretch in hydrocarbons (Chiar et al. 1996), while several bands (3.3, 6.2, 8.6, and 11.3 μm) are consistent with polycyclic aromatic hydrocarbons—important carbon-bearing components of carbonaceous meteorites (Grishko and Duley 2000). Kerridge (1983) discovered isotopic heterogeneities in meteoritic kerogen consistent with low-temperature interstellar origins. Ehrenfreund et al. (1991) demonstrated that distinctive features of the 3.4 μm absorption band in the interstellar medium and in carbonaceous chondrites match closely. Thus, it is likely that some, if not most, of the insoluble matter in the least altered (i.e., "3.0") carbon-rich meteorites represent relatively unaltered interstellar material.

Note that in spite of their comprehensive list of meteorite phases, Rubin and Ma (2017) do not include condensed organic material, i.e., “kerogen.”

Primary condensation mineralogy of the solar nebula

Diverse and abundant chondrite meteorites provide an unparalleled view of the earliest stages of our solar system’s formation (Brearley and Jones 1998; Krot et al. 2014; MacPherson 2014; Scott and Krot 2014; Connolly and Jones 2016). Data collected from these fascinating specimens, coupled with experimental measurements and theoretical modeling of high-temperature mineral condensation processes, provide an increasingly vivid picture of the first few million years of nebular evolution (e.g., Hashimoto 1983, 1992; Mysen et al. 1985; Mysen and Kushiro 1988; Davis et al. 1990; Nagahara et al. 1993; Wood and Hashimoto 1993; Ebel and Grossman 2000; Richter et al. 2002, 2007; Lodders 2003; Ebel 2006; Ebel and Alexander 2011; Davis and Richter 2014; Saxena and Hrubiak 2014; Han et al. 2015; Wood et al. 2019). The most primitive nebular phases survive in distinctive components of chondrite meteorites, including calcium-aluminum-rich inclusions (MacPherson 2014), amoeboid olivine aggregates (Grossman and Steele 1976; Krot et al. 2004), and ultra-refractory inclusions (El Goresy et al. 2002; Ma et al. 2014a). These ancient quasi-spheroidal to irregularly shaped objects, ranging in size from less than 1 mm to more than a centimeter in diameter, have received extensive scrutiny and have been the subject of several comprehensive reviews (Brearley and Jones 1998; Ebel 2006; MacPherson 2014; Scott and Krot 2014; Rubin and Ma 2017, 2020). What follows, therefore, summarizes and codifies information that has been collated and reviewed by previous researchers.

Mineral evolution in the early solar nebula was driven by a succession of heating events, initially associated with the premain-sequence life of the Sun (Desch et al. 2012; Connolly and Jones 2016). Processes within this dynamic, evolving system are not fully understood, but include radiative heating, FU Orionis-type flares (Bertout 1989), bipolar outflows (Sahai et al. 2003), shock waves induced by infalling of gas (Iida et al. 2001), bow shocks from planetary embryos (Desch and Connolly 2002; Boss and Durisen 2005) and associated magnetic effects (Mann et al. 2016; Mai et al. 2018), current sheets (Joung et al. 2004; Hubbard et al. 2012), and nebular lightning (Sorrell 1995; Desch and Cuzzi 2000), as well as cooling through thermal emission from the nebula. As larger objects grew through gravitational accretion, impact processes and magma formation increasingly played key roles. Therefore, primary mineralization in the early solar nebula occurred through condensation from a vapor enriched in O, Si, Mg, Al, Ca, and Fe (Fig. 1c), followed by melt crystallization, and solid-state reactions. The formation of these primary nebular minerals has been the subject of extensive theoretical modeling (Urey 1955; Yoneda and Grossman 1995; Ebel and Grossman 2000; Ebel 2006), as well as experimental research under high-temperature, low-pressure conditions (Hashimoto 1983; Nagahara et al. 1993; Davis and Richter 2014).

The following section reviews the three most primitive types of chondrite objects, all of which contain primary condensation minerals of the early solar nebula: calcium-aluminum-rich inclusions, amoeboid olivine aggregates, and ultra-refractory inclusions (Fig. 3).

In Part III of this series, we will consider primary minerals in chondrules, which are abundant in many kinds of chondrite meteorites. Chondrules are igneous droplets thought to have formed between 1.5 and 3 million years after CAIs (e.g., Connolly and Jones 2016). Note that additional chondritic components, including opaque assemblages (also known as fremdlinge), dark inclusions, and fine-grained matrices, often contain similar suites of primary phases, but their histories are complicated by a succession of secondary processes associated with thermal, aqueous, and impact alteration (Blum et al. 1988; Brearley and Jones 1998; MacPherson 2014; Rubin and Ma 2017). Thus, with the exception of primary metal alloys, the mineralogy of these additional chondritic components will be considered in Parts IV and V.

Calcium-aluminum-rich inclusions (CAIs): CAIs are the most ancient objects formed in the solar nebula, with radiometric ages 4567.3 ± 0.16 Ma (Amelin et al. 2002, 2010; Connelly et al. 2008, 2012; Krot 2019). These discrete components of primitive meteorites range in size from approximately 100 μm to more than a centimeter in diameter, and they possess distinctive suites of minerals reminiscent of ceramics—mineralogy that points to the earliest phase of solar nebular cooling and condensation (Brearley and Jones 1998; MacPherson 2014). Collectively, the refractory phases in CAIs represent the first ~5% of the solar nebula's condensable matter, as reflected in primitive CI chondrite meteorites (Grossman 1972; Davis and Richter 2014).

Detailed observations of CAIs from diverse types of chondrite meteorites reveal significant variations in bulk composition, mineralogy, and morphology—differences that reflect nebular heterogeneities in space and time (Liu et al. 2009; Kööp et al. 2018; MacPherson 2014 and references therein), as well as subsequent processing through re-melting, distillation, and a variety of secondary processes (the subject of Parts IV and V of this series). Owing to their diversity, CAIs have been divided into several groups according to size, shape, and mineralogy (Grossman 1975; Wark 1987; Beckett and Stolper 1994; MacPherson 2014):

- *Compact Type A CAIs* are spheroidal objects, evidently a consequence of partial melting. Melilite is often the dominant mineral with spinel, hibonite, perovskite, and other refractory phases (Fig. 3a).
- *Fluffy Type A CAIs* have similar mineralogy to compact type A CAIs, but their shapes are irregular, suggesting minimal melting (Fig. 3b).
- *Type B CAIs* are spheroidal objects characterized by their relatively large size (up to several centimeters) and mineralogy that commonly includes melilite, spinel, anorthite, forsterite, and the Al-Ti-rich calcic clinopyroxene called fassaite (Fig. 3c). Type B CAIs are further divided into subcategories based on mineralogical details.
- *Type C CAIs* consist primarily of spinel, fassaite, and anorthite with textures characteristic of igneous processes (Fig. 3d).
- In addition to A-, B-, and C-type CAIs, researchers recognize other fine-grained (i.e., <200 μm) objects with CAI affinities. *Spinel-hibonite-rich spherules*

(sometimes abbreviated SHIBs) are CAIs that contain a relatively unaltered assemblage of spinel, hibonite, and perovskite, with associated melilite, fassaite, and anorthite (Ireland 1988; Kööp et al. 2016a).

- *Platy hibonite crystals*, known as PLACs, are CAIs that consist of lath-like crystals of hibonite, sometimes surrounded by a silicate glass or fassaite, often with hibonite, grossite, and melilite, but typically lacking spinel (Ireland 1988; Kööp et al. 2016b).
- A mineralogically curious type of CAI, dubbed *"FUN" CAIs* by Wasserburg et al. (1977), displays "Fractionation and Unidentified Nuclear effects"—specifically, large mass-dependent fractionations of Mg, Si, and O isotopes, as well as other isotopic anomalies. In terms of primary mineralogy FUN CAIs are, for the most part, similar to type B CAIs. However, the discovery of dmisteinbergite ($CaAl_2Si_2O_8$), a rare hexagonal high-temperature polymorph of anorthite, points to an unusual formation environment close to the protosun with $T > 1500$ K and $P < 10^{-6}$ (i.e., significantly lower pressure than the ~10^{-4} atm modeled for most other CAIs; Ma et al. 2013a).

In our review, we focus on the primary mineralogy of CAIs and do not make distinctions among these varieties of calcium-aluminum-rich inclusions. Note, however, that we do distinguish CAIs from ultra-refractory inclusions, as the latter are chemically and mineralogically distinct from CAIs.

Isotopic evidence, including surprisingly uniform anomalous Mg and O isotopes across all types of CAIs (McKeegan et al. 1998; MacPherson 2014 and references therein) and age determinations by various methods (Connelly et al. 2012; see also Amelin et al. 2002, 2010; Connelly et al. 2008; Krot 2019), reveal that CAIs formed at ~4567.3 ± 0.16 Ga over a span of ~200 000 yr. However, detailed chemical and isotopic investigations point to at least two stages of CAI formation as a consequence of rapid protosun evolution during the earliest stages of the solar system.

The earliest nebular condensates are represented by a relatively small population of platy hibonite-bearing "PLAC" CAIs, which appear to have formed prior to an influx of ^{26}Al to the solar nebula, as measured by diagnostic ^{26}Mg (Liu et al. 2009). Hibonite in these CAIs contains helium and neon excesses that could only have formed under an intense flux of energetic particles, albeit at a heliocentric distance significantly beyond the inner disk edge, where temperatures were cooler (Kööp et al. 2018).

A second generation of CAIs of the spinel-hibonite-bearing "SHIB" type display at least three important differences from PLAC CAIs: (1) they contain excess ^{10}B formed by the decay of short-lived ^{10}Be, which points to condensation near the inner edge of the nebular disk in a single zone close to the Sun (McKeegan et al. 2000; MacPherson et al. 2003; Krot 2019); (2) they incorporated significant short-lived ^{26}Al (preserved as diagnostic ^{26}Mg), pointing to formation after PLAC CAIs (Kööp et al. 2016a, 2016b); and (3) they lack the anomalous helium and neon contents of PLAC hibonite (Kööp et al. 2018). According to current models, these CAIs were later dispersed beyond Jupiter's orbit by strong solar winds

(Shu et al. 1996). Further studies of CAI isotopic and mineralogical variations are likely to refine our understanding of the earliest stages of solar system evolution.

CAIs rarely represent unaltered primordial nebular condensates. They typically have been subjected to multiple stages of partial alteration from reheating, including annealing, melting, and distillation; impact melting, volatilization, and metamorphism; and secondary alteration, including oxidation, sulfidization, and hydration (MacPherson and Davis 1993; Beckett et al. 2000; Rubin and Ma 2017). Here we focus exclusively on the so-called "primary" mineralization in the sense of MacPherson (2014)—i.e., mineralization that results from "direct condensation, melt solidification, or solid-state recrystallization." Note that in this context solid-state recrystallization includes only the first phase of reaction and replacement of earlier high-temperature phases by exsolution, element ordering, or structural phase transition, during equilibrium cooling of CAIs below their initial condensation temperature and prior to their incorporation into larger bodies (e.g., Yoneda and Grossman 1995; Ebel 2006). Chondrite mineralization through subsequent secondary processes, including oxidation, sulfidation, aqueous and thermal alteration (metamorphism), shock processes, and planetesimal differentiation, will be considered in Parts IV and V of this series.

Only seven minerals, all of which occur in calculations of nebular condensation sequences between ~1800 and 1100 K are common primary minerals in CAIs (e.g., Grossman 1972; Brearley and Jones 1998; Lodders 2003; Davis and Richter 2014; MacPherson 2014, Table 1 therein; Wood et al. 2019). In order of appearance, they are hibonite, perovskite, gehlenite/åkermanite (both members of the melilite group), spinel, Al-Ti-rich calcic clinopyroxene ("fassaite"), forsterite, and anorthite. Note that corundum is calculated to be the highest-temperature oxide condensate (Lattimer et al. 1978; Anders and Grevesse 1989; Lodders 2003; Wood et al. 2019), yet it is usually absent owing to subsequent reactions with nebular vapor to hibonite, spinel, or melilite. Additional phases, though less common, include the oxides grossite, krotite, panguite, and tistarite; the calcium-titanium silicate rhönite; and alloys of Fe-Ni and platinum group elements (see Table 3).

An unresolved question related to CAIs is the paragenesis of ubiquitous thin outer layers, first described by Wark and Lovering (1977) and now known as "Wark-Lovering rims" (MacPherson et al. 1981; Ruzicka 1997; Wark and Boynton 2001). These layers are typically a few tens of micrometers thick and consist of both refractory condensates, often spinel, melilite, and fassaite, occasionally with hibonite, perovskite, anorthite, and forsterite, as well as such secondary minerals as nepheline, Fe-rich spinel, hedenbergite, and andradite (MacPherson 2014, and references therein). No new obviously primary minerals occur in these rims; therefore, for the purposes of this review, even though they may represent a distinct timing and mode of mineral formation, we do not consider Wark-Lovering rims as representing distinct natural kinds. Note, however, an important feature of this evolutionary system of mineralogy is that specialists have the option of splitting mineral natural kinds into finer and finer sub-categories, based on their distinctive modes of origin, as reflected in diagnostic suites of physical and chemical attributes.

Amoeboid olivine aggregates (AOAs): Amoeboid olivine aggregates (AOAs) represent a second common refractory constituent of chondrite meteorites. Originally described from the Allende CV chondrite by Grossman and Steele (1976) and subsequently identified from a wide variety of carbonaceous meteorites (Grossman et al. 1979; Kornacki and Wood 1984; MacPherson et al. 1988; Aléon et al. 2002; Chizmadia et al. 2002; Krot et al. 2004; Rubin 2013), AOAs are thought to have formed after CAIs, though before chondrules that were forming at ~4565 ± 0.5 Ma (Connolly and Jones 2016), and at generally lower condensation temperatures and at pressures consistent with 10^{-3} atm (Weisberg et al. 2004). They typically occur as irregularly shaped assemblages up to 0.5 mm in diameter, constituting a few percent of some carbonaceous chondrites (Scott and Krot 2014; Fig. 3e). AOAs consist of sintered accumulations of nebular condensates, primarily forsterite (typically fine-grained, <20 μm), with Fe-Ni metal alloys and a refractory assemblage, commonly including fassaite, spinel, and anorthite, and occasionally with perovskite and/or melilite. Models of AOA evolution suggest that other refractory phases, including corundum, grossite, and hibonite, may have initially formed but were transformed to melilite, clinopyroxene, spinel, and/or anorthite through continuous solid-state reactions of the fine-grained constituents on cooling (Weisberg et al. 2004).

Many AOAs also hold a rich variety of secondary minerals, including phyllosilicates, feldspathoids, sulfides, and other phases, which will be considered in Part V.

Ultra-Refractory Inclusions (URIs).—Ultra-refractory inclusions (URIs) are a scarce population of mineralogically important prechondrule objects, usually grouped with CAIs, that are extremely enriched in Sc, Zr, Y, and other refractory elements by factors of as much as 10^3 (El Goresy et al. 2002). A consequence of these enrichments is the appearance of more than a dozen rare oxide and silicate minerals (Rubin and Ma 2017), including allendeite ($Sc_4Zr_3O_{12}$), thortveitite ($Sc_2Si_2O_7$), and lakargite ($CaZrO_3$), as well as Sc- and Ti^{3+}-bearing clinopyroxenes and garnets (Table 3). The unusual chemistry of URIs points to an early stage of nebular evolution. URIs are often found as inclusions in later chondrite objects, including AOAs, chondrules, and fine-grained matrix (El Goresy et al. 2002; Ma et al. 2009a, 2014a).

A note regarding opaque assemblages

Some researchers have suggested that Fe-Ni-metal-rich opaque assemblages (also referred to as “fremdlinge”), which are found associated with some CAIs (e.g., Brearley and Jones 1998; MacPherson 2014), represent some of the earliest primary condensates of the solar nebula (El Goresy et al. 1978; Armstrong et al. 1985, 1987). Others posit a later origin of these objects with a complex history of alteration, for example by oxidation, sulfidation, and exsolution through exposure to heterogeneous nebular environments (Wark and Lovering 1982a; Blum et al. 1988, 1989; MacPherson 2014). We include the primary metals of opaque assemblages—Fe-Ni and platinum group element alloys—in the list of CAI minerals. However, the lower-temperature mineral suites of opaque assemblage minerals, including fayalite, wollastonite, feldspathoids, tungstate-molybdates, and varied sulfides and phosphates, will be considered in Parts IV and V.

Systematic evolutionary mineralogy: Part IIB—Primary nebular mineralogy

In the following section we outline the mineralogy of primary nebular phases, including minerals in CAIs, AOAs, and URIs formed by condensation, melt crystallization, and their initial solid-state reactions (see also Table 3). We tabulate 59 natural kinds of primary minerals, corresponding to more than 40 IMA-approved species plus nebular silicate glass. We also include one low-temperature solar nebular condensate, cubic H_2O ice, which has been observed through telescopic observations in the cool (~100 K) outer regions of other stellar environments. Each mineral natural kind is given a binomial designation: the first name indicates the paragenetic context (e.g., *CAI*, *AOA*, or *URI*), whereas the second name for the most part conforms to approved IMA mineral species' names. However, in several instances we deviate from IMA conventions:

- *Refractory metal alloys:* CAIs, URIs, and associated opaque assemblages often contain micrometer-scale "nuggets" in which refractory metals such as Mo, Ir, Os, Ru, Rh, Re, Pt, W, and Ru occur in hexagonal ($P6_3/mmc$) alloys with widely varied elemental proportions (e.g., Weber and Bischoff 1997; Berg et al. 2009; MacPherson 2014; Chi Ma, personal communication). For example, Berg et al. (2009) report the compositions of 88 refractory metal nuggets from the Murchison meteorite, most with significant concentrations of Mo, Os, and Ru, with each of those elements dominant in some grains. IMA protocols require naming each alloy based on the most abundant element; therefore, ruthenium, osmium, molybdenum, and other metals have all been officially recognized as separate native element mineral species. However, because these alloys form continuous solid solutions in chondrite nuggets and they are all formed by the same paragenetic process of condensation from a high-temperature nebular gas, we lump them together into platinum group element (PGE) alloys. Similarly, we lump the cubic ($Fm3m$) iron-molybdenum alloys hexaferrum (Fe,Os,Ir,Mo) and hexamolybdenum (Mo,Ru,Fe) into one natural kind: Fe-Mo alloys.
- *Anosovite:* The name "anosovite" for pseudobrookite-type Ti_3O_5 was discredited by Bowles (1988), as it was only known as an anthropogenic phase in Ti-rich slags. However, Zhang et al. (2015) have discovered this phase as a primary nebular condensate and we resurrect the name anosovite, pending IMA's decision on the naming of this mineral.
- *Melilite:* In the case of the melilite group, a complete solid solution exists between gehlenite ($Ca_2Al_2SiO_7$) and åkermanite ($Ca_2MgSi_2O_7$), with primary meteoritic compositions ranging from $Åk_{01}$ to $Åk_{100}$ (Brearley and Jones 1998). Individual grains, furthermore, may be zoned such that cores are technically gehlenite and rims technically åkermanite. These variations occur within a continuous solid solution and represent a single mode of formation. Therefore, we classify melilite samples as "*CAI melilite*," "*AOA melilite*," or *"URI melilite*."
- *Fassaite:* A fourth deviation from standard IMA nomenclature relates to primary CAI, AOA, and URI pyroxenes, typically a Ca-Mg-dominant, Fe-poor

clinopyroxene with significant Al and Ti (both Ti^{3+} and Ti^{4+}) in solid solution. The IMA-approved name for most of these occurrences is diopside, because the closest compositional end-member is $CaMgSi_2O_6$. However, the great majority of near-end-member diopside occurrences in CAIs are of secondary origin (Brearley and Jones 1998), and thus should be distinguished from the primary Al-Ti-bearing nebular calcic clinopyroxene phase, [$Ca(Mg,Al,Ti^{3+},Ti^{4+})(Al,Si)SiO_6$]. This complex solid solution has long been called “fassaite” in the meteoritics literature, based on its similarity to iron-poor calcic clinopyroxenes from the Fassa Valley, Trento Province, Italy (Thompson 1818; Deer et al. 1963; Sack and Ghiorso 2017). The name fassaite was discredited during a reclassification of pyroxene nomenclature (Morimoto et al. 1988; see also Hazen 1989), but it continues to be used by many meteorite experts to describe the distinctive primary calcic clinopyroxenes in chondrite meteorites (e.g., Brearley and Jones 1998; MacPherson 2014; Rubin and Ma 2017; Sack and Ghiorso 2017). Primary clinopyroxene from meteorites possesses several diagnostic attributes, including extensive Al, Ti^{3+}, Ti^{4+}, and (less commonly) Sc and/or V solid solution—compositional complexities that lead to a suite of distinctive optical properties, including refractive indices, birefringence, extinction angle, optic axial angle, and dispersion (e.g., Deer et al. 1963). Therefore, we retain the name fassaite for Al-Ti-bearing clinopyroxene.

- *Rhönite:* Finally, we lump two rare primary CAI minerals of the sapphirine group, rhönite [$Ca_2(Mg,Al,Ti)_6(Si,Al)_6O_{20}$] and addibischoffite [$Ca_2(Al,Mg,V,Ti)_6(Al,Si)_6O_{20}$]. These similar phases represent a continuous solid solution and occur via the same paragenetic mode.

Native elements

Iron-nickel alloys are common primary and secondary phases associated with CAIs, AOAs, URIs, and associated opaque aggregates (Brearley and Jones 1998; Rubin and Ma 2020). Chondrites also often incorporate micrometer-scale nuggets of highly refractory metal alloys, which contain Ir, Os, Ru, Mo, and other siderophile elements (Sylvester et al. 1993; Berg et al. 2009). In addition, refractory mineral assemblages occasionally incorporate metal grains with significant amounts of both Fe and Mo (Ma et al. 2014a; Zhang et al. 2015; Rubin and Ma 2017).

Platinum Group Element (PGE) alloys (Os,Ir,Ru,Rh,Pt,W,Mo,Re).

CAIs often incorporate micrometer-scale “refractory metal nuggets” (hexagonal, $P6_3/mmc$), containing elements of the platinum group (Os, Ir, Ru, Rh, and Pt), as well as Mo, W, and Re (Palme et al. 1994; Brearley and Jones 1998; MacPherson 2014), which condensed at temperatures between 1800 and 1300 K at 10^{-4} atm (Berg et al. 2009; Harries et al. 2012; Scott and Krot 2014). Some individual sub-micrometer-scale grains are close to pure Pt, Ru, or Re, whereas others are multielement alloys with Os, Ir, Ru, or Pt as the most abundant metal (e.g., El Goresy et al. 1978; Wark and Lovering 1978; Bischoff and Palme 1987; Brearley and Jones 1998; Berg et al. 2009). Because these elements form extensive solid

solutions by the same nebular condensation mechanism, we lump them together as "*PGE alloys*."

CAI PGE alloys.—Refractory metal nugget alloys of PGEs plus W, Mo, and Re are commonly found as micrometer-scale grains, often as inclusions in oxides or silicates, in CAIs (e.g., El Goresy et al. 1978, 1979, 1984; Wark and Lovering 1982b; Sylvester et al. 1993; Endress et al. 1994; Geiger and Bischoff 1995; Weber and Bischoff 1997; Berg et al. 2009; MacPherson 2014).

URI PGE alloys.—Micrometer-scale grains of Os-dominant PGE alloys are found in ultra-refractory inclusions in association with typical CAI phases, including fassaite (often Sc- and Ti-rich), perovskite, and spinel (Ma and Rossman 2008; Ma 2011; Ma et al. 2014a).

Iron-Nickel alloys.

Iron-nickel alloys condensed from the solar nebula at temperatures estimated between 1350 and 1450 K (Campbell et al. 2005). Consequently, metal alloys with iron dominant, typically incorporating significant Ni and at times with minor amounts of other siderophile elements, are common as a minor phase in CAIs, AOAs, and URIs from many types of chondrites. They occur as the minerals iron (also known as "kamacite"), taenite, and awaruite.

Here we accept iron and taenite as primary nebular condensates. Note that awaruite, an isometric (*Pm*3*m*) Ni-dominant alloy of iron and nickel, is also a common minor metallic phase in opaque aggregates associated with CAIs (Taylor et al. 1981; Rubin and Kallemeyn 1989; Ikeda 1992; Smith et al. 1993; Casanova and Simon 1994; Moggi-Cecchi et al. 2007). However, it appears that most occurrences of awaruite in CAIs are of secondary origin (Brearley and Jones 1998; Rubin and Ma 2020).

Iron (α-Fe).

Native iron, also known as kamacite (a discredited though often used mineral name in the context of meteorites), is the most stable low-Ni alloy of Fe and Ni. This cubic (*Im*3*m*) phase has nickel contents that are typically less than 10 wt% Ni, while Co is less than 1 wt% (Brearley and Jones 1998). Native iron is common as an opaque phase associated with CAIs, AOAs, and URIs (Bevan and Axon 1980; Zinner et al. 1991; Simon and Grossman 1992; Caillet et al. 1993; Zhang et al. 1995; Shibata 1996; Ma and Rossman 2008).

CAI iron.—Native iron has been reported as a primary phase (Campbell et al. 2005; Scott and Krot 2014; Rubin and Ma 2017) in type A (MacPherson and Grossman 1984; Ulyanov et al. 1982), type B (Blander and Fuchs 1975; Sylvester et al. 1992; Caillet et al. 1993), and rarely in type C CAIs (Blander et al. 1980).

AOA iron.—Iron-nickel alloys, typically with 5 to 7 wt% Ni, are ubiquitous components of amoeboid olivine aggregates (Weisberg et al. 1993, 2004; Chizmadia et al. 2002; Krot et al. 2004). They occur as blebs up to 10 μm in diameter, often as inclusions in refractory oxides and silicates.

URI iron.—Ma and Rossman (2008) recorded sub-micrometer grains of Fe-Ni alloy associated with zirconolite, tazheranite, and PGE alloys in an ultra-refractory inclusion from the Allende chondrite.

Taenite [γ-(Fe,Ni)].

Taenite is an isometric ($Pm\bar{3}m$) alloy of γ-iron, typically with 10 to more than 50 wt% Ni (Affiatalab and Wasson 1980; Nagahara 1982). Taenite often occurs in CAIs and opaque assemblages as a minor phase, typically in close association with kamacite (Zinner et al. 1991; Simon and Grossman 1992; Sylvester et al. 1992; Caillet et al. 1993; Brearley and Jones 1998), in some instances as exsolution lamellae in kamacite (Noguchi 1994; Ichikawa and Ikeda 1995). Taenite and kamacite are also associated in fine-grained mixtures known as “plessite” (Massalkski et al. 1966; Scott and Rajan 1979).

CAI taenite.—Taenite commonly occurs, both as isolated grains and as exsolution lamellae in kamacite, in types A and B CAIs (MacPherson and Davis 1993; Ichikawa and Ikeda 1995; Campbell et al. 2005; Rubin and Ma 2017).

Iron-Molybdenum alloys (Fe,Mo).

Iron and molybdenum, in combination with refractory metals, notably Ir, Os, and Ru, occasionally form micrometer-scale nuggets of hexagonal ($P6_3/mmc$) alloys, which must have condensed or solidified at temperatures intermediate between the ultra-refractory platinum group alloys and the lower-temperature Fe-Ni alloys described above. At least two IMA-approved species have been identified from CAIs in the Allende meteorite—hexaferrum [(Fe,Os,Ir,Mo); Ma 2012; Zhang et al. 2015] and hexamolybdenum [(Mo,Ru,Fe); Ma et al. 2011b, 2014a]. Ma et al. (2014a) provide a review of this “continuum of meteoritic refractory alloys with the $P6_3/mmc$ structure.”

CAI Fe-Mo alloys.—Ma et al. (2011a, 2012) described micrometer-scale nuggets of hexagonal alloys with varying proportions of Fe, Mo, Ru, and other metals from CAIs in the Allende and NWA 1934 meteorites.

URI Fe-Mo alloys.—Ma et al. (2014a) found hexamolybdenum in association with allendeite in an ultra-refractory inclusion, while Zhang et al. (2015) report hexaferrum.

Carbides

Khamrabaevite (TiC) is the only confirmed refractory carbide with characteristics of primary nebular phases (Ma and Rossman 2009a). Iron carbide minerals, including cohenite [$(Fe,Ni)_3C$], edscottite (Fe_5C_2), and haxonite [$(Fe,Ni)_{23}C_6$], are known from highly reduced chondrules in carbonaceous chondrites and enstatite chondrites (e.g., MacPherson 2014; Rubin and Ma 2017; Ma and Rubin 2019), but they have not been documented as primary phases in CAIs, AOAs, or URIs. Consequently, they are considered in Part III of this series.

URI khamrabaevite.—Titanium carbide (TiC) was identified by Ma and Rossman (2009c) as a 10 μm diameter grain associated with corundum and tistarite from the Allende carbonaceous chondrite.

Nitrides

Nitrides are rare in meteorites. Nierite (Si_3N_4) is known as a stellar mineral (Hazen and Morrison 2020), but has not to our knowledge been reported in CAIs, AOAs, or URIs. Sinoite (Si_2N_2O) is known as both a primary chondrule mineral and as an impact product in enstatite chondrites (Lin et al. 2011; El Goresy et al. 2011; see Parts III and IV).

The only known candidate for a primary nebular condensate mineral is osbornite (TiN), which is known from chondrules of enstatite chondrites (e.g., El Goresy et al. 2011), as well as from CAIs in several carbonaceous chondrites (Weisberg et al. 1988; Grokhovsky 2006; Krot et al. 2006; MacPherson 2014). Note that osbornite is also known as a secondary mineral in enstatite chondrite impact melts (Rubin and Ma 2020).

CAI osbornite.—Osbornite (TiN) was identified in CAIs from the Isheyevo (Grokhovsky 2006; Krot et al. 2006) and Allan Hills 85085 (Weisberg et al. 1988) carbonaceous chondrites. Osbornite was also found in Stardust samples that were presumed to be CAI fragments (Weisberg et al. 2006).

Silicides

The silicide perryite [$(Ni,Fe)_5(Si,P)_2$] is a refractory phase with characteristics of primary condensates (MacPherson 2014; Rubin and Ma 2017). However, perryite is found principally in the highly reduced mineral assemblages of enstatite chondrite chondrules and will be described in Part III of this series.

Phosphides

At least two phosphides, monipite (MoNiP) and schreibersite [$(Fe,Ni)_3P$], have been described as primary phases in chondrite meteorites. The exact mode of formation of these grains is uncertain; plausible hypotheses include reaction of a P-bearing nebular gas-phase with an Fe-Ni alloy (Schaefer and Fegley 2010), crystallization from a P-rich immiscible melt that exsolved from Fe-Ni melt, or exsolution from a solidified Fe-Ni alloy (Ma et al. 2014b). In this tabulation we list only monipite, which was discovered in a CAI. Schreibersite is known principally from highly reduced assemblages in enstatite chondrite chondrules and will be considered in Part III.

CAI monipite.—Monipite with composition [$(Mo_{0.84}Fe_{0.06}Co_{0.04}Rh_{0.03})$ $(Ni_{0.89}Ru_{0.09})P$] was described by Ma et al. (2014b) from a 1 × 2 μm crystal in a type B CAI from the Allende meteorite. It occurs in association with primary phases melilite, fassaite, and spinel, as well as probable alteration minerals, including awaruite, the rare oxides kamiokite ($Fe_2Mo_3O_8$), tugarinovite (MoO_2), and an unnamed Nb-rich oxide [$(Nb,V,Fe)O_2$].

Sulfides

Several sulfide minerals, including niningerite (MgS), oldhamite (CaS), pentlandite [$(Fe,Ni)_9S_8$], and troilite (FeS), probably formed early in the history of the solar nebula (Rubin and Ma 2017, 2020). However, all of these phases, as well as numerous subsequent sulfides, either formed by igneous processes in chondrules (e.g., Rubin et al. 1999; MacPherson 2014; see Part III), by sulfidation of earlier phases through reaction with an S-

rich vapor, or by solid-state reactions (Rubin and Ma 2017). Therefore, we do not list any sulfide minerals as primary nebular condensates in Part II.

Troilite represents a difficult case. In some instances, it appears to be a primary chondrule mineral (e.g., Rubin et al. 1999; El Goresy et al. 2011) and thus will be included in Part III of this series. However, many occurrences in meteorites, including in CAIs of enstatite chondrites, appear to represent secondary mineralization by sulfidation (Fagan et al. 2000; Guan et al. 2000; MacPherson 2014). Therefore, in spite of instances where troilite in CAIs is associated with primary oxide and silicate phases and a primary origin for the sulfide cannot be ruled out (Fagan et al. 2001), we do not list any sulfides as primary nebular condensates in CAIs, AOAs, or URIs.

Oxides

Oxygen is the most abundant element in the solar nebula after hydrogen and helium, and it played a dominant role in the condensation of primary refractory phases in CAIs, AOAs, and URIs. The most common primary nebular oxides in CAIs, AOAs, and URIs contain Mg, Ca, Al, and/or Ti, with rare minor oxides of Mo, Sc, V, and Zr. We also include ice (cubic H_2O) as the only molecular crystal likely to have condensed in the cool (~100 K) outer regions of the solar nebula.

Note that more than two dozen other refractory oxides are recorded as primary minerals from chondrules (MacPherson 2014; Rubin and Ma 2017). The distinction between primary condensates in CAIs, AOAs, and URIs (the subject of this contribution) vs. primary igneous phases in chondrules (which will be summarized in Part III) is important. The limited number of confirmed CAI, AOA, and URI oxide phases listed below are thought to have formed by condensation via cooling of high-temperature, low-pressure vapor or their subsequent solid-state reactions in the earliest solar nebula at ~4.567 Ga. Subsequent primary phases in chondrules were formed by partial melting of nebular materials at least 1.5 million years later—a time when planetesimal formation and nebular heterogeneities had become well established (e.g., Gilmour and Saxton 2001; Connolly and Jones 2016). Primary chondrule minerals thus crystallized at a later time by a different combination of processes; i.e., at generally lower temperatures, during relatively short heating events, and on nebular material that had already undergone a preliminary stage of chemical and isotopic fractionation.

Confusion can arise as to what constitutes a primary CAI, AOA, or URI phase. For example, the rare mineral tistarite (Ti_2O_3) was described from a single 1 × 2 μm grain in a chondrule from the Allende carbonaceous chondrite (Ma and Rossman 2009c). Because of its presumed primordial character, MacPherson (2014, Table 1 therein) listed tistarite as one of only 15 CAI primary minerals. However, coexisting rutile (TiO_2) is not included in this tabulation of the earliest primary nebular minerals, because it appears to represent a later stage of nebular mineralization (Ma 2019). Numerous other meteoritic oxide minerals will be considered in Parts III, IV, and V of this series.

Ice (H_2O).—Primary solar nebular mineralogy consists almost exclusively of high-temperature (T > 1100 K) refractory phases that form by condensation from a vapor phase or

melt crystallization in close proximity to the central star. However, infrared telescopic observations reveal the presence of crystalline H_2O, presumably condensed as thin mantles (<0.05 μm thick) on oxide and silicate dust grains in the cold circumstellar regions of some oxygen-rich stars (Omont et al. 1990). We therefore include ice as a primary nebular condensate.

The distinction between crystalline and amorphous condensed H_2O in the context of circumstellar environments is important. Crystalline water, which is revealed by sharp IR emission features at 44 and 60 μm, can only condense directly at temperatures >50 K under relatively low molecular fluxes (estimated at ~10^4 molecules per cm^2 per second in circumstellar environments; Kouchi and Yamamoto 1995). By contrast, at the significantly lower temperatures and greater molecular fluxes of interstellar clouds, amorphous H_2O with diagnostic broad emission peaks (notably at 3.1 μm) is more likely to form.

Water that initially condenses in the amorphous form will not crystallize to cubic ice unless T rises above 110 K and it has sufficient time to anneal. However, 110 K is close to the sublimation temperature, while the sublimation rate of amorphous H_2O may be an order of magnitude greater than that of crystalline H_2O (Léger et al. 1983). Therefore, condensed H_2O phases may disappear (Kouchi et al. 1994). Indeed, one line of evidence for amorphous H_2O (as opposed to a crystalline form) in comets is the anomalously high sublimation rate of some comets (Mukai 1986).

Laboratory experiments on ice formation under low-pressure, cryogenic conditions suggest that the stable crystalline form of H_2O under circumstellar conditions is “cubic ice” (Gaffney and Matson 1980; Bartels-Rausch et al. 2012; Fuentes-Landete et al. 2015; Salzmann 2018). Note that fewer than 100 H_2O molecules are required to form a localized phase with the structural properties of crystalline ice (Moberg et al. 2019; Jordan 2019). We recognize one likely circumstellar, low-temperature condensate, designated “*Circumstellar ice*.”

Circumstellar ice.: Occurring as <0.05 μm thick mantles on oxide and silicate dust grains, circumstellar cubic ice (H_2O) condenses in relatively cool ($50 < T < 150$ K) toroidal volumes surrounding some solar nebulas and O-rich stars (Omont et al. 1990).

Corundum (Al_2O_3).—Corundum is thought to be the highest temperature oxide condensate at $T \sim 1770$ K (Grossman 1972; Davis and Richter 2014; Wood et al. 2019). However, because corundum reacts with the cooling gas to form other oxides such as hibonite or melilite it is a relatively rare mineral in CAIs.

CAI corundum.: End-member Al_2O_3 with minor Mg and Fe is a rare mineral in CAIs. Sub-micrometer grains have been recorded in CAI cores, as inclusions in spinel or hibonite, or enclosing a central core of hibonite (Bar-Matthews et al. 1982; MacPherson et al. 1984; Wark 1986; Greshake et al. 1996).

URI corundum.: Ma and Rossman (2009c) reported corundum associated with khamrabaevite and tistarite in an ultra-refractory inclusion from the Allende meteorite.

Tistarite (Ti_2O_3).—The refractory mineral tistarite $\left(Ti_2^{3+}O_3\right)$, a member of the corundum group, is known from a single 5 × 7 μm subhedral grain form a chondrule in the Allende carbonaceous chondrite (Ma and Rossman 2009c; Ma et al. 2009a). It occurs in association with the primary phases corundum, khamrabaevite (TiC), and kaitianite $\left(Ti_2^{3+}Ti^{4+}O_5\right)$, as well as rutile ($TiO_2$).

URI tistartite.: Tistarite has been found as a single grain in an ultra-refractory inclusion contained within a chondrule from the Allende carbonaceous chondrite (Ma and Rossman 2009c).

Kaitianite $\left(\mathbf{Ti_2^{3+}Ti^{4+}O_5}\right)$.—Two crystals of the mixed-valence titanium oxide mineral, kaitianite, were discovered by Ma (2019) in association with the primary phases corundum, tistarite, and khamrabaevite (TiC), as well as rutile (TiO_2). Micrometer-scale kaitianite crystals have the monoclinic (*C*2/*c*) oxyvanite (V_3O_5) structure.

URI kaitianite.: Kaitianite has been found as two grains in an ultra-refractory inclusion; the observed composition is $\left(Ti_{1.75}^{3+}Al_{0.05}Ti_{0.10}^{+}Mg_{0.08}Fe_{0.02}\right)Ti^{4+}O_5$ (Ma 2019).

Rutile (TiO_2).—Rutile has been reported in association with tistarite and kaitianite by Ma and coworkers (Ma and Rossman 2009c; Ma et al. 2009a; Ma 2019), who suggest it is a primary phase in some URIs.

URI rutile.: Occurs as micrometer-scale grains in an ultra-refractory inclusion from the Allende meteorite (Ma 2019).

Baddeleyite (ZrO_2).—Presumably primary baddeleyite was described from meteorite MAC 88107, while grains of ZrO_2 (lacking structural details) have also been reported from Murchison and Allende chondrites (Krot et al. 2019). It occurs in association with allendeite and zirkelite.

URI baddeleyite.: Occurs as micrometer-scale grains in URIs (Krot et al. 2019).

Anosovite [$(Ti^{4+},Ti^{3+},Mg,Sc,Al)_3O_5$].—A second polymorph of Ti_3O_5 (in addition to kaitianite) was reported by Zhang et al. (2015) from an ultra-refractory inclusion in the Sayh al Uhaymir 290 (CH3) carbonaceous chondrite. This Sc-bearing phase has the orthorhombic (*Cmcm*) pseudobrookite structure and thus is equivalent to the discredited mineral “anosovite,” which was originally identified in Ti-rich slags (Bowles 1988). It occurs as micrometer-scale grains in association with fassaite, spinel, anorthite, perovskite, panguite, davisite, and Fe-Ir-Mo-Os alloy nuggets.

URI anosovite.: Two grains of ultra-refractory anosovite with the average composition of $\left(Ti_{1.36}^{4+}Ti_{0.59}^{3+}Mg_{0.34}Sc_{0.20}Al_{0.20}\ V_{0.05}Ca_{0.05}Si_{0.03}Fe_{0.03}Cr_{0.03}Zr_{0.03}\right)O_5$ were reported by Zhang et al. (2015).

Spinel ($MgAl_2O_4$).—Spinel is perhaps the most ubiquitous primary mineralogical component of CAIs in most chondrite types except CI (MacPherson 2014), as well as a common phase in Wark-Lovering rims. Fe-rich varieties of spinel group minerals, including chromite and hercynite, have also been described from CAIs (e.g., Brearley and Jones 1998), but they are always of secondary origins.

CAI spinel.: Most CAIs incorporate near end-member $MgAl_2O_4$ spinel, though with a wide range of observed trace and minor elements—notably Fe, Ti, V, Cr, and Zn (Brearley and Jones 1998). Spinel occurs in a variety of habits, including euhedral octahedral crystal inclusions in melilite, fassaite, or anorthite (Grossman 1980); as framboidal aggregates (El Goresy et al. 1979); surrounding a hibonite core (Steele 1995); as spinel-hibonite or spinel-perovskite spherules (Macdougall 1981); as spherical shells, or “palisades,” of spinel enclosing melilite, fassaite, and/or anorthite, within larger CAIs (Wark and Lovering 1982b; Simon and Grossman 1997); in association with grossite-bearing inclusions (Brearley and Jones 1998); and as a common layer in Wark-Lovering rims (Wark and Lovering 1977).

AOA spinel.: Spinel, typically in sub-micrometer grains, occurs as a primary phase associated with perovskite, fassaite, and anorthite in amoeboid olivine aggregates (Krot et al. 2004; Weisberg et al. 2004).

URI spinel.: Spinel occurs in ultra-refractory inclusions in association with Sc-rich fassaite, REE-enriched perovskite, and other distinctive Sc, Zr, Ti, and REE phases (e.g., Ma and Rossman 2009b; Ma et al. 2013b, 2014a).

Hibonite ($CaAl_{12}O_{19}$).—Hibonite, nominally $CaAl_{12}O_{19}$ but commonly incorporating significant $Mg+Ti^{4+} \leftrightarrow 2Al$ (up to ~4.5 and 9 wt% MgO and TiO_2, respectively) as well as minor V, Fe, Si, Cr, and Sc, is an important mineralogical component of CAIs in most types of chondrite meteorites (Keil and Fuchs 1971; Brearley and Jones 1998; MacPherson 2014). As much as a quarter of hibonite Ti may be present as Ti^{3+}—an indication of the highly reducing formation conditions of some CAIs (Ihinger and Stolper 1986; Beckett et al. 1988).

Hibonite is thought to form initially by reaction of the gas phase with corundum at $T > 1700$ K. Because of its high temperature of condensation (Davis and Richter 2014; Wood et al. 2019), hibonite is often the earliest preserved mineral in a CAI. As a consequence, hibonite petrology, major and trace element composition, and stable isotopes have been extensively studied to provide clues regarding primitive stellar environments (Hinton et al. 1988; Ireland 1988; Ireland et al. 1988; Brearley and Jones 1998; MacPherson 2014 and references therein; Kööp et al. 2016a, 2016b, 2018).

CAI hibonite.: CAI hibonite occurs in a variety of contexts and morphologies (Ireland 1988), including acicular crystals associated with spinel, melilite, and perovskite in compact type A inclusions (Grossman 1975; Sylvester et al. 1993); as a common constituent of fluffy type A CAIs (Grossman 1975; Kornacki and Wood 1984); as 1 to 25 μm laths near the exterior of type B CAIs in the Allende CV chondrite (Blander and Fuchs 1975); in fine-grained spinel-rich inclusions (Kornacki and Wood 1985); as up to 1 mm diameter grains in CAI cores (Allen et al. 1980; Armstrong et al. 1982; MacPherson et al. 1983); in clusters of

tabular crystals surrounded by spinel in a CAI core (Steele 1995); as inclusions in spinel, fassaite, melilite, and grossite CAI cores (Wark and Lovering 1977; Kornacki and Wood 1985; Mao et al. 1990; Weber and Bischoff 1994); in association with corundum (MacPherson et al. 1984; Hinton et al. 1988); as isolated crystal fragments (MacPherson et al. 1983; Ireland 1988); in spinel-hibonite spherules as 5 to 20 μm bladed crystals (Macdougall 1981) and rims (MacPherson et al. 1984); and as layers in Wark-Lovering rims.

Perovskite ($CaTiO_3$).—Near-stoichiometric calcium titanate perovskite, albeit with trace or minor Mg, Al, Si, Cr, Sc, V, Fe, Y, Zr, Nb, REE, Th, and U, is an important mineralogical component of CAIs in most chondrite types (Kornacki and Wood 1985; Weber and Bischoff 1994; Brearley and Jones 1998; MacPherson 2014). Twinning in perovskite crystallites suggest that they were heated above the cubic-orthorhombic transition at 1573 K.

CAI perovskite.: Near end-member perovskite is a common phase in CAIs (Brearley and Jones 1998). Perovskite generally occurs as very fine-grained (<15 μm) inclusions in melilite, spinel, and fassaite, and less commonly hibonite and grossite (Macdougall 1981; Fahey et al. 1994; Kojima et al. 1995; Steele 1995; Weber et al. 1995). It is also a common component in Wark-Lovering rims (Weisberg et al. 1993; Keller and Buseck 1994).

AOA perovskite.: Perovskite, often as sub-micrometer grains in association with spinel, is a common primary phase in amoeboid olivine aggregates (Weisberg et al. 2004).

URI perovskite.: Perovskite enriched in REE occurs in ultra-refractory inclusions, for example from the Allende carbonaceous chondrite in association with Sc-rich fassaite, spinel, and kangite (Ma and Rossman 2009b; Ma 2011; Ma et al. 2013b, 2014a, 2015).

Lakargiite ($CaZrO_3$).—Ma (2011) identified sub-micrometer grains of a Zr-dominant perovskite in an ultra-refractory inclusion from the Acfer 094 carbonaceous chondrite. Lakargiite [$Ca_{0.95}(Zr_{0.87}Ti_{0.16})O_3$] is found as inclusions in hibonite and in association with perovskite [$Ca_{0.94}(Ti_{0.98}Zr_{0.06})O_3$], tazheranite, an Os-dominant alloy, and other refractory phases (Krot et al. 2019).

URI lakargiite.: Ma (2011) identified Zr-rich perovskite from an ultra-refractory inclusion in Acfer 094.

Grossite ($CaAl_4O_7$).—Grossite is one of several high-temperature calcium aluminate minerals that forms in CAIs, presumably in environments with low Mg and Si shortly after the condensation of corundum and hibonite (Michel-Lévy et al. 1982; Weber and Bischoff 1994; Aléon et al. 2002). Samples are near stoichiometric, though they commonly incorporate minor Mg, Si, Ti, and Fe.

CAI grossite.: Grossite typically occurs as 5 to 10 μm diameter crystallites, often as inclusions in association with melilite, perovskite, spinel, hibonite, fassaite, and anorthite (Greenwood et al. 1992; Simon et al. 1994).

Krotite ($CaAl_2O_4$).—Krotite is one of several refractory calcium aluminates that occur as primary condensates in CAIs with low Mg and Si (Ivanova et al. 2002; Ma et al. 2011b). Mikouchi et al. (2009) identified a second polymorph of $CaAl_2O_4$, dmitryivanovite, which is thought to be a high-pressure form that results from impact transformation (see Part IV of this series).

CAI krotite.: The single known occurrence of krotite was found as aggregates of crystals from 10 to 350 μm diameter in the central and mantle portions of a CAI from the NWA 1934 CV3 carbonaceous chondrite (Ivanova et al. 2002; Ma et al. 2011b). It is found in association with perovskite, melilite, grossite, hibonite, and spinel.

Machiite ($Al_2Ti_3O_9$).—Krot et al. (2020) identified machiite, a new ultra-refractory oxide mineral from the Murchison carbonaceous chondrite that probably formed by direct condensation from a gas phase or by crystallization from a Ca-Al-rich melt in CAI-forming nebular regions. The ideal composition is $Al_2Ti_3O_9$ but, as is typical with ultra-refractory oxide phases, machiite incorporates significant Sc, Y, and Zr, as well. It was found as a single 4.4 μm diameter euhedral grain in association with euhedral corundum. Electron diffraction studies suggest a monoclinic (*C*2/*c*) schreyerite-type structure.

URI machiite.: Krot et al. (2020) describe a single 4.4 μm diameter crystallite with empirical composition $\left(Al_{1.17}Sc_{0.56}Y_{0.10}Ti^{4+}_{0.08}Fe_{0.06}Ca_{0.03}Mg_{0.01}\right)\left(Ti^{4+}_{2.71}Zr_{0.28}Si_{0.01}\right)O_9$.

Zirkelite [$(Ti,Ca,Zr)O_{2-x}$].—Krot et al. (2019) record a possible grain of zirkelite, a complex Ti-Ca-Zr oxide with a defect cubic fluorite structure, as a micrometer-scale phase in an ultra-refractory inclusion from meteorite MAC 88107.

URI zirkelite: Zirkelite was identified as a micrometer-scale grain from MAC 88107 (Krot et al. 2019).

Kangite [$(Sc,Ti,Al,Zr,Mg,Ca)_{1.8}O_3$] and Panguite [$(Ti^{4+},Sc,Al,Mg,Zr,Ca)_{1.8}O_3$]: Ma and coworkers described two closely related Ti-Sc oxides—Sc-dominant kangite (Ma et al. 2013b) and Ti-dominant panguite (Ma et al. 2012) from ultra-refractory inclusions in the Allende carbonaceous chondrite, as well as an occurrence of panguite from the Murchison chondrite (Ma et al. 2011a). Both minerals occur as micrometer-scale grains in association with Sc-rich davisite, perovskite, and spinel, and both have cation-deficient bixbyite structures. Thus, kangite and panguite might be lumped into a single natural kind; however, kangite is reported to be cubic $Ia\bar{3}$, whereas the panguite structure occurs in the orthorhombic subgroup *Pbca*. Therefore, we list two different natural kinds, subject to further structural and compositional details. Note that Ma et al. (2012) also report several Zr-rich grains of panguite.

URI kangite.: Sc-dominant kangite was described from an ultra-refractory inclusion in the Allende carbonaceous chondrite (Ma et al. 2013b).

URI panguite.: Micrometer-scale crystallites of Ti-dominant panguite are associated with fassaite in ultra-refractory inclusions (Ma et al. 2012; Krot et al. 2019). The most complete description is from a 20 × 30 μm amoeboid olivine aggregate in the Allende carbonaceous chondrite, while additional occurrences have been reported from the Allende, Murchison, and Sayh al Uhaymir 290 meteorites (Ma et al. 2012; Zhang et al. 2015).

Zirconolite ($CaZrTi_2O_7$).—Ma and Rossman (2008) reported zirconolite in an ultra-refractory inclusion in an amoeboid olivine aggregate from the Allende carbonaceous chondrite. It is associated with micrometer-scale inclusions of cubic zirconia (tazheranite) and Fe-Ni and PGE alloys.

URI zirconolite.: Zirconolite from the Allende meteorite was recorded by Ma and Rossman (2008).

Tazheranite [$(Zr,Sc,Ca,Y,Ti)O_{1.75}$].—Ma and Rossman (2008) described natural Sc-Ti-rich cubic zirconia as crystals up to 1.2 μm diameter from ultra-refractory inclusions within an AOA in the Allende meteorite. Tazheranite occurs as inclusions in zirconolite; associated minerals include fassaite and Fe-Ni and PGE alloys. A second occurrence from an Allende URI in fine-grained matrix (Ma et al. 2014a) is associated with allendeite, spinel, fassaite, and perovskite.

URI tazheranite.: Tazheranite is a rare mineral from ultra-refractory inclusions from the Allende meteorite (Ma and Rossman 2008; Ma et al. 2014a; Krot et al. 2019).

Allendeite ($Sc_4Zr_3O_{12}$).—Allendeite was described by Ma et al. (2014a), who examined grains up to 25 μm diameter in an ultra-refractory inclusion in the Allende carbonaceous carbonate. It contains inclusions of spinel and hexamolybdenum, and is closely associated with fassaite, perovskite, tazheranite, and Os-dominant PGE alloys.

URI allendeite.: Allendeite was discovered in an ultra-refractory inclusion from the Allende meteorite (Ma et al. 2014a; Krot et al. 2019).

Silicates

Refractory silicates are major components of CAIs, AOAs, and URIs. Several major rock-forming mineral groups, including olivine, garnet, pyroxene, and feldspar, are represented, as well as rare ultra-refractory Ti, Sc, and Zr silicates.

Quartz (SiO_2).—Komatsu et al. (2018) reported an unusual occurrence of silica condensation within the solar nebula in a region with low Mg/Si—an example of nebular element fractionation in the period following CAI formation. Quartz occurs as grains up to 20 μm diameter in association with fassaite, anorthite, and spinel in an amoeboid olivine aggregate from the Yamato-793261 carbonaceous chondrite.

AOA quartz.: Quartz occurs as primary grains associated with fassaite, forsterite, anorthite, and spinel in an AOA (Komatsu et al. 2018).

Olivine group [$(Mg,Fe,Ca,Mn)_2SiO_4$].—Nebular olivine represents a solid solution among four principal end-members, forsterite (Mg), fayalite (Fe), monticellite (Ca), and tephroite (Mn). Primary olivine that formed by direct condensation or melt solidification in CAIs and AOAs is typically close to end-member forsterite (Brearley and Jones 1998). Davis et al. (1991) describe rare instances where CAI forsterite (replaced by akermanite) and fassaite (replaced by gehlenite and perovskite) have been partially evaporated, resulting in a different mode of mineral formation due to a reheating event (and loss of Si and Mg) to at least 1700 K, possibly by remixing close to the Sun (Davis and Richter 2014).

CAI forsterite.: Forsteritic olivine is a minor primary phase in CAIs. It occurs, for example, as <5 μm diameter grains associated with spinel and fassaite, as well as in Wark-Lovering rims, in a variety of carbonaceous chondrites (Greenwood et al. 1994; MacPherson and Davis 1994), and as an interstitial phase with anorthite and melilite in a CAI from PCA91082 (Birjukov and Ulyanov 1996).

AOA forsterite.: Mg-rich olivine (Fo > 98), in some cases with rims enriched in Mn (Mn > Fe), is the principal constituent of AOA's (Krot et al. 2004; Weisberg et al. 2004). Micrometer-scale crystals (<10 μm) occur in irregular-shaped aggregates up to 1 mm in diameter. Klöck et al. (1989) suggest that the Mn enrichment arose from condensation of a tephroite component directly from the solar nebular at temperatures close to 1100 K, compared to the ~1440 K condensation of pure forsterite, and far above the ~500 K reaction of Fe metal with forsterite to form fayalite.

Garnet group [$Ca_3(Al,Ti^{3+},V,Sc)_2Si_3O_{12}$].—Ca-Al garnet with significant Ti^{3+} and/or Sc is a scarce primary phase in the earliest nebular condensates. Garnet with composition close to the grossular end-member (ideally $Ca_3Al_2Si_3O_{12}$) is known almost exclusively as a secondary phase in chondrites (Fuchs 1974; Wark et al. 1987; Brearley and Jones 1998; Rubin and Ma 2017). In addition, Simon and Grossman (1992) reported goldmanite [$Ca_3(V,Al,Fe,Ti)_2Si_3O_{12}$] in a Fremdlinge from the Leoville chondrite (see Part III). However, Ma and coworkers have discovered two rare primary garnets with the general formula $Ca_3(Ti^{3+},Sc,Mg,Y)Si_3O_{12}$ in chondrite meteorites (Ma 2012; Ma et al. 2017a), including the end-members eringaite ($Ca_3Sc_2Si_3O_{12}$) and rubinite $\left(Ca_3Ti_2^{3+}Si_3O_{12}\right)$. These compositional extremes reveal fascinating heterogeneities in the early solar nebula.

Eringaite (Ma 2012), the Sc-dominant, Al-poor garnet $Ca_3(Sc,Y,Ti)_2Si_3O_{12}$, was discovered with rubinite in an ultra-refractory inclusion within an AOA from the Vigarano carbonaceous chondrite. It occurs as micrometer-scale crystals within davisite and in association with spinel, tazheranite, and hexaferrum.

The Ti^{3+} end-member, dubbed rubinite by Ma et al. (2017a), was discovered as crystals up to 20 μm diameter in type A CAIs from both the Allende and Efremovka carbonaceous chondrites, where it occurs with the major primary CAI minerals, as well as eringaite and Ti^{3+}-dominant fassaite (grossmanite). Rubinite significantly enriched in Y, Sc, and Zr was found in an ultra-refractory inclusion in the Vigarano meteorite with spinel, panguite, fassaite, and davisite, which is enclosed in an AOA.

CAI rubinite.: Rubinite occurs in type A CAIs from the Allende and Efremovka carbonaceous chondrites (Ma 2012).

URI rubinite.: Rubinite significantly enriched in Y, Sc, and Zr occurs with eringaite in an ultra-refractory inclusion in the Vigarano chondrite (Ma et al. 2017a).

URI eringaite.: Eringaite occurs with rubinite in an ultra-refractory inclusion in the Vigarano chondrite (Ma et al. 2017a).

Melilite group [gehlenite ($Ca_2Al_2SiO_7$) to åkermanite ($Ca_2MgSi_2O_7$)].—The calcium silicates of the melilite group, which feature complete solid solution between Al_2 (gehlenite) and MgSi (åkermanite) end-members, are major mineralogical constituents of CAIs. Unlike many igneous examples, CAI melilite contains minimal Fe and Na. Wood et al. (2019), in revised calculations of condensation temperatures that take trace elements into account, suggest that gehlenite-dominant melilite condenses first, between 1550 and 1600 K, following the appearance of corundum and hibonite. As condensation temperatures fall, melilite crystals typically develop zoning from gehlenite-rich cores to åkermanite-dominant rims. Because melilite in CAIs spans the complete compositional range from Al_2 to MgSi end-members, we lump CAI gehlenite and åkermanite into a single natural kind. Melilite is common in most types of CAIs, as well as in AOAs.

CAI melilite.: Melilite is among the commonest primary condensed phases in CAIs, ranging in composition from $Åk_{01}$ to $Åk_{100}$ (Grossman 1975, 1980; Wark et al. 1987; Davis et al. 1991; Podosek et al. 1991), often with zoning from more gehlenite-rich cores to more åkermanite-rich rims. It occurs as coarse-grained (2 to 3 mm) crystals in the cores of many CAIs (e.g., MacPherson 2014); as rims on spinel (Holmberg and Hashimoto 1992); in nodular aggregates with spinel and fassaite (Weisberg et al. 1993); as a component of hibonite-, spinel-, and grossite-bearing inclusions (J.N. Grossman et al. 1988; Weber et al. 1995); and as layers in Wark-Lovering rims (Wark and Lovering 1977).

AOA melilite.: Gehlenite-rich melilite ($Ge_{80–85}$) is an occasional primary phase in AOAs, typically associated with anorthite and spinel (Krot et al. 2004). Weisberg et al. (2004) suggest that some AOA melilite underwent solid-state reactions on cooling to form anorthite.

URI melilite.: Ma et al. (2015) reported gehlenitic melilite in a Sc-rich ultra-refractory inclusion in the Vigarano carbonaceous chondrite, associated with warkite, davisite, perovskite, and spinel.

Clinopyroxene group [$Ca(Mg,Al,Ti^{3+},Ti^{4+},Sc,V)(Al,Si)SiO_6$].—Fassaite and related calcic clinopyroxenes are abundant primary phases in CAIs, AOAs, and URIs (Brearley and Jones 1998; Davis and Richter 2014; MacPherson 2014; Sack and Ghiorso 2017). Ca-Mg-dominant, Fe-poor clinopyroxene with significant Al and Ti (both Ti^{3+} and Ti^{4+}), and occasionally Sc or V, is closest compositionally to the IMA-approved species diopside ($CaMgSi_2O_6$), though end-member diopside has not been confirmed as a primary nebular

condensate (Brearley and Jones 1998). The discredited name “fassaite” (Morimoto et al. 1988) is still widely used by the meteoritics community and the name is retained here.

The crystal chemistry of fassaite can be modeled with four dominant ideal end-members (Sack and Ghiorso 1994a, 1994b, 1994c, 2017). In addition to diopside, rare Al-rich grains are closer to ($CaAl_2SiO_6$), the IMA-approved end-member kushiroite (Kimura et al. 2009), though long called the “calcium Tschermak’s pyroxene” (e.g., Ma et al. 2009b). Other examples are closer in composition to grossmanite ($CaTi^{3+}AlSiO_6$; Ma and Rossman 2009a), while Sack and Ghiorso (1994a, 1994c, 2017) also recognize “alumino-buffonite” $\left(CaMg_{0.5}\ Ti^{4+}_{0.5}\ AlSiO_6\right)$ as an important additional end-member with the maximum possible octahedral Ti^{4+} content. Phase equilibria in this four-component fassaite system are complex; Sack and Ghiorso (2017) suggest as many as four miscibility gaps, based on both thermodynamic modeling and observed coexistence of fassaite rims and cores of different compositions that appear to be in equilibrium (Wark and Lovering 1982). Additional complexity arises from the occurrence of rare micrometer-scale grains of burnettite ($CaV^{3+}AlSiO_6$; Ma and Beckett 2016) and davisite ($CaSc^{3+}AlSiO_6$; Simon et al. 1996; Ma and Rossman 2009b).

How many natural kinds of primary nebular clinopyroxene should be recognized remains an open question. Evidence for fassaite miscibility gaps points to the need for multiple natural kinds; however, until more analyses and other diagnostic attributes are available for cluster analysis, we lump primary nebular clinopyroxenes from the quadrilateral defined by diopside, kushiroite, grossmanite, and “alumino-buffonite” into one natural kind, “fassaite” [$Ca(Mg,Al,Ti^{3+},Ti^{4+})(Al,Si)SiO_6$].

The fassaite phase region may extend to Sc- and/or V-rich compositions; however, only two examples of these extremes have been reported and both appear idiosyncratic. Burnettite is an oddity, with octahedral M2 site composition $\left[\left(V^{3+}_{0.29}Sc_{0.24}Ti^{3+}_{0.13}Al_{0.09}\right)Ti^{4+}_{0.12}Mg_{0.08}\right]$ (Ma and Beckett 2016); thus, V, Sc, and Ti are present in roughly equal amounts and no cation is present at greater than 29 mol% M2 occupancy. Burnettite is therefore far from any ideal end-member composition. We designate the only known occurrence, from an unusual V-rich fluffy type A CAI, as “*CAI burnettite*.”

Davisite [$Ca(Sc,Ti^{3+},Ti^{4+},Mg,Zr)AlSiO_6$], is a minor phase that occurs occasionally in ultra-refractory inclusions (Ma and Rossman 2009b). Common associations include fassaite (with significantly less Sc than in coexisting davisite), as well as perovskite, spinel, and a host of rare Sc-bearing minerals, including eringaite, kangite, panguite, rubinite, thortveitite, and warkite (Ma et al. 2011a, 2012, 2013b, 2015, 2017a; Ma 2012; Krot et al. 2019).

CAI fassaite.: Ca-rich, Fe-poor pyroxenes are, in combination with spinel, the most common CAI phases, occurring in types A, B, and C CAIs and URIs (Grossman 1980; Wark 1987; Wark et al. 1987; Podosek et al. 1991; Brearley and Jones 1998), as well as layers in Wark-Lovering rings (Wark and Lovering 1977). Primary fassaite commonly occurs with anorthite, melilite, forsterite, and spinel as CAI cores, mantles, and rims (Macdougall 1979, 1981; Doukhan et al. 1991; Kimura et al. 1993; Kojima et al. 1995; Simon et al. 1996). Of

special note regarding CAI fassaite is the occurrence of both trivalent and tetravalent Ti—a consequence of the extremely reducing conditions of its formation (Beckett 1986), perhaps dominated by hot H_2 gas, as well as conditions in which C/O > 0.5.

AOA fassaite.: Al-Ti-rich calcic clinopyroxene with Al and Ti as high as 20 and 13 wt%, respectively, is a common primary phase in AOAs, especially in Al-rich refractory inclusions where it occurs in close association with forsterite and anorthite, as well as melilite, spinel, and perovskite (Hashimoto and Grossman 1987; Krot et al. 2004; Weisberg et al. 2004; Ma et al. 2012).

URI fassaite.: Fassaite enriched in Sc, Ti^{3+}, and/or V^{3+} occurs as sub-millimeter grains in ultra-refractory inclusions in association with davisite, spinel, perovskite, melilite, and a variety of rare oxides and silicates (Ma and Rossman 2009a, 2009b; Ma et al. 2013b, 2014a, 2015).

CAI burnettite.: V-dominant, Sc- and Ti-rich calcic clinopyroxene was identified by Ma and Beckett (2016) from one fluffy type A CAI in the Allende meteorite.

URI davisite.: Davisite is a Sc-dominant calcic clinopyroxene that occurs in association with fassaite, perovskite, spinel, and rare Sc-bearing phases in ultra-refractory inclusions (Ma and Rossman 2009b).

FELDSPAR GROUP [$(NA,CA)(AL,SI)_4O_8$]

Anorthite ($Ca_2Al_2SiO_8$).

End-member (i.e., Na-free) anorthite is common as both a primary and secondary mineral, notably in type B and type C CAIs (Podosek et al. 1991; Caillet et al. 1993; Brearley and Jones 1998). Condensing initially at ~1410 K (Davis and Richter 2014), anorthite is the last of the common CAI primary phases to appear; it crystallizes from a melt and is often found in close association with melilite or spinel (MacPherson and Davis 1993; Kojima et al. 1995). Note that plagioclase feldspar, typically with a significant albitic component ($NaAlSi_3O_8$), is a common secondary phase in chondrite meteorites, including as a fine-grained alteration phase in CAIs and their Wark-Lovering rims, as a common minor phase in AOAs, and in chondrules (see Part III).

CAI anorthite.—The last major primary phase to condense from the solar nebula, anorthite is commonly found as coarse-grained laths in CAIs (Brearley and Jones 1998).

AOA anorthite.—Near end-member Ca plagioclase is a common, if volumetrically minor, constituent of AOAs (Weisberg et al. 2004).

Dmisteinbergite ($CaAl_2Si_2O_8$).

Rare individual crystals of dmisteinbergite, a hexagonal high-temperature polymorph of anorthite, have been documented from a type B FUN CAI in the Allende carbonaceous chondrite (Ma et al. 2013a). This phase points to an origin environment with $T > 1500$ K and $P < 10^{-6}$ atm (Abe et al. 1991; Mendybaev et al. 2009), likely close to the protosun, where it

crystallized directly from a silicate vapor or melt phase. Ma et al. (2013a) also note a Ba-rich grain of dmisteinbergite with up to 27 atom % Ba substituting for Ca.

CAI dmisteinbergite.—Dmisteinbergite occurs as 100 to 600 μm diameter crystals in association with melilite, fassaite, and spinel (Ma et al. 2013a).

Baghdadite [$Ca_3(Zr,Ti)Si_2O_9$].

Ma (2018) reported the first extraterrestrial occurrence of baghdadite, a CAI silicate mineral from the Allende carbonaceous chondrite that may be one of the earliest primary silicate condensates. A single 0.8 μm diameter euhedral grain is associated with primary spinel, perovskite, hibonite, fassaite, refractory metal nuggets, and the rare phases burnettite and paqueite as inclusions in melilite. The baghdadite structure is monoclinic ($P2_1/a$).

CAI baghdadite.—Ma (2018) reported a single baghdadite grain with composition $(Ca_{2.77}Mg_{0.08})(Zr_{0.55}Ti_{0.35}Nb_{0.02})(Si_{1.89}Al_{0.35})O_9$.

Rhönite [$Ca_2(Mg,Al,Ti)_6(Si,Al)_6O_{20}$], addibischoffite [$Ca_2(Al,Mg,V,Ti)_6(Al,Si)_6O_{20}$), and warkite [$Ca_2(Sc,Ti,Al,Mg,Zr)_6Al_6O_{20}$].

Rhönite, a rare refractory member of the sapphirine group (triclinic, $P\bar{1}$), was first reported by Fuchs (1971), and was subsequently identified in both type A and type B CAIs in association with melilite, spinel, fassaite, and perovskite (Fuchs 1978; Grossman 1980; Podosek et al. 1991; Jambon and Boudouma 2011). Ma and colleagues subsequently identified two closely related Ca-Al oxides/silicates, also with the $P\bar{1}$ sapphirine structure. Addibischoffite, with the general formula $[Ca_2(Al,Mg,V,Ti)_6(Al,Si)_6O_{20}]$, was discovered as a 9 μm diameter crystal in a CAI from the Acfer 214 carbonaceous chondrite. Like rhönite, it occurs in association with typical CAI phases—Al-dominant fassaite (kushiroite), hibonite, spinel, melilite, perovskite, anorthite, and Fe-Ni alloy (Ma et al. 2017b). We conclude that rhönite and addibischoffite are part of a continuous solid solution and form in similar environments. Therefore, we combine these minerals into one natural kind: "*CAI rhönite*."

Warkite was identified by Ma et al. (2015) from ultra-refractory inclusions in the Murchison and Vigarano carbonaceous chondrites. Warkite, general formula $[Ca_2(Sc,Ti,Al,Mg,Zr)_6Al_6O_{20}]$, occurs as aggregates of crystals up to 4 μm diameter in association with perovskite, davisite, spinel (in Murchison), and melilite (in Vigarano). Warkite may well form a continuous solid-solution with rhönite and addibischoffite; however, because it forms in a different mineralogical environment and appears to be Si-poor, we recognize "URI warkite" as a distinct natural kind.

CAI rhönite.—Rhönite has been identified in both A and B type CAIs from several carbonaceous chondrites (Fuchs 1971; Ma et al. 2017b).

URI warkite.—Warkite was described by Ma et al. (2015) from ultra-refractory inclusions in the Murchison and Vigarano meteorites (see also, Krot et al. 2019).

Paqueite [$Ca_3TiSi_2(Al,Ti,Si)_3O_{14}$].

Ma and Beckett (2016) identified a new Ca-Ti silicate from a fluffy type A CAI in the Allende carbonaceous chondrite. It occurs as micrometer-scale euhedral crystals in association with melilite, spinel, V-rich perovskite, fassaite, hibonite, and refractory metal grains.

CAI paqueite.—Paqueite was discovered by Ma and Beckett (2016) in a V-rich fluffy type A CAI.

Thortveitite ($Sc_2Si_2O_7$).—Ma et al. (2011a) and Ma (2012) report the occurrence of thortveitite in an ultra-refractory inclusion from the Murchison meteorite. It occurs with fassaite, davisite, panguite, and spinel as subhedral crystals up to 9 μm maximum dimension.

URI thortveitite.—Thortveitite occurs in an ultra-refractory inclusion in the Murchison chondrite (Ma et al. 2011a; Krot et al. 2019).

Silicate glass (Ca,Mg,Al,Si,O).

A glass of aluminous pyroxene composition is a significant component of hibonite-silicate spherules, a type of CAI less than 200 μm in diameter (Kimura et al. 1993; Beckett and Stolper 1994; Russell et al. 1998; MacPherson 2014). Silicate glass occurs with fassaite and hibonite, often in association with perovskite, melilite, and grossite. These spherules contain primary phases that crystallized from a melt or, in the case of hibonite, may represent unmelted relict crystals. Note that we distinguish nebular silicate glass, which formed from a melt, from stellar amorphous silicate, which condenses from the gas phase (Hazen and Morrison 2020).

CAI silicate glass.—Silicate glass is a significant component of hibonite-silicate spherules (MacPherson 2014).

Network graph of stellar and primary nebular minerals

The evolutionary system of mineralogy is illustrated using bipartite mineral network graphs (Fruchterman and Reingold 1991; Asratian et al. 1998; Morrison et al. 2017), which display relationships among mineral phases and their attributes, in this instance their paragenetic modes (Hazen et al. 2019; Hazen and Morrison 2020; Morrison et al. 2020). Figure 4 displays a bipartite force-directed network graph of primary stellar, interstellar, and nebular minerals formed prior to ~4565 Ma, in which 69 different phases, including 10 amorphous condensed phases, are represented by diamond-shaped nodes. Each of these mineral nodes is linked to one or more node representing a paragenetic mode of formation. Three different star-shaped nodes (AGB, SN-II, and CNova) represent stellar environments that impart distinctive isotopic signatures to minerals. A cloud-shaped node indicates interstellar dense molecular clouds (DMC), whereas four flattened disk icons represent different primary mineral-forming nebular environments (Circumstellar, CAI, AOA, and URI).

Node size, shape, and color convey information. Mineral compositions are indicated by the color of diamond-shaped mineral nodes: black (C-bearing), green (lacking C or O), blue

(contains O, but not C or Si), and red (contains Si+O). The sizes of mineral nodes correspond to the numbers of paragenetic modes to which they are linked. Similarly, the sizes of the star-, cloud-, and disk-shaped symbols indicate the numbers of different minerals to which they are associated.

Network graphs often display structures that reveal genetic relationships. For example, note that the three stellar nodes are tightly grouped on the right side of the graph, whereas nodes for CAIs, AOAs, and URIs are grouped to the left. In future contributions, this pattern will expand outward, creating an embedded timeline of mineral evolution. At this early stage of mineral evolution, 8 different low-temperature interstellar and nebular condensed molecular phases ($T < 100$ K) form a separate network from 56 high-temperature stellar and nebular condensates ($T > 1100$ K). In future parts of this series, phases formed at intermediate temperatures in planetary surface environments will provide links between these two mineral-forming environments.

This bipartite network of mineral evolution is a visual representation of all confirmed stellar, interstellar, and primary nebular minerals described in Parts I and II of the evolutionary system of mineralogy. As new parts are introduced, and new nodes for minerals and paragenetic processes are added, this information-rich graphical approach will provide a dynamic, expanding, interactive view of the entire sweep of mineral evolution.

Implications

Stage II of mineral evolution introduces for the first time several mineral groups that played important roles in planetary evolution, including garnet, melilite, clinopyroxene, and quartz. Like several of the phases described among the stellar condensation minerals of Stage I, many of which occur in two or three different natural kinds based on very different isotopic signatures associated with different kinds of stars (Hazen and Morrison 2020), several primary nebular minerals occur as condensates in CAIs, AOAs, and URIs—different mineral-forming environments that impart distinctive combinations of compositional, morphological, and petrologic attributes.

As with Part I of this series, we emphasize that this contribution is a preliminary foray into a rich and rapidly evolving topic of mineralogical investigation. New nebular minerals, notably micrometer-scale refractory phases, are being discovered every year; unusual varieties of chondrite meteorites continue to be discovered; and new and more precise analytical measurements of mineral ages, isotopic idiosyncrasies, and nanoscale chemical and textural features refine our understanding of this earliest stage of solar system evolution. We also note that condensed non-crystalline phases play an important role in interstellar and nebular mineralogy, as they do in other episodes of Earth's mineral evolution. Further efforts to characterize glasses and amorphous condensates will undoubtedly reveal new natural kinds, as they clarify our understanding of heating and cooling events in the dynamic, heterogeneous nebular environment.

This contribution, the second in a series that considers chronologically the evolutionary sequence of mineral formation, will be followed by an examination of the primary igneous

minerals of chondrules, which are the most abundant constituents of chondrite meteorites (Part III). The primary minerals of differentiated asteroidal bodies, as well as numerous secondary minerals that arise through thermal, aqueous, and impact alteration of chondrite minerals in planetesimal environments—minerals as preserved in altered chondrite and achondrite meteorites—will provide the focus of Parts IV and V.

Acknowledgments

We thank Anirudh Prabhu, who developed the bipartite network representation of stellar, interstellar, and nebular mineralogy. We are grateful to Denton Ebel, Alexander Krot, and Chi Ma for providing images of refractory inclusions. Denton Ebel, Chi Ma, Alan Rubin, and B.J. Tkalcec contributed invaluable detailed reviews of the manuscript. The sections on nebular condensate mineralogy, in particular, benefitted from the advice of Rubin and Ma, who provided access to highly relevant work in press, including a draft of their forthcoming book, *Meteorite Mineralogy*. We are grateful to Conel M.O'D. Alexander, Asmaa Boujibar, Carol Cleland, Robert T. Downs, Olivier Gagné, Sergey Krivovichev, Glenn MacPherson, Michael Walter, and Shuang Zhang for thoughtful discussions and comments.

Funding

This publication is a contribution to the Deep Carbon Observatory. Studies of mineral evolution and mineral ecology have been supported by the Deep Carbon Observatory, the Alfred P. Sloan Foundation, the W.M. Keck Foundation, the John Templeton Foundation, the NASA Astrobiology Institute ENIGMA team, a private foundation, and the Carnegie Institution for Science. Any opinions, findings, or recommendations expressed herein are those of the authors and do not necessarily reflect the views of the National Aeronautics and Space Administration.

References cited

Abe T, Tsukamoto K, and Sunagawa I (1991) Nucleation, growth and stability of $CaAl_2Si_2O_8$ polymorphs. Physics and Chemistry of Minerals, 17, 257–281.

Affiatalab F, and Wasson JT (1980) Composition of the metal phases in ordinary chondrites: Implications regarding classification and metamorphism. Geochimica et Cosmochimica Acta, 44, 431–446.

Aléon J, Krot AN, and McKeegan KD (2002) Calcium–aluminum-rich inclusions and amoeboid olivine aggregates from the CR carbonaceous chondrites. Meteoritics & Planetary Science, 37, 1729–1755.

Alexander CMO'D, Fogel M, Yabuta H, and Cody GD (2007) The origin and evolution of chondrites recorded in the elemental and isotopic compositions of their macromolecular organic matter. Geochimica et Cosmochimica Acta, 71, 4380–4403.

Alexander CMO'D, McKeegan KD, and Altwegg K (2018) Water reservoirs in small planetary bodies: meteorites, asteroids, and comets. Space Science Reviews, 214, 36–83. Doi: 10.1007/s11214-018-0474-9. [PubMed: 30842688]

Allamandola LJ, Bernstein MP, Sandford SA, and Walker RL (1999) Evolution of interstellar ices. Space Science Reviews, 90, 219–232. [PubMed: 11543288]

Allen JM, Grossman L, Lee T, and Wasserburg GJ (1980) Mineralogy and petrography of HAL, an isotopically unusual Allende inclusion. Geochimica et Cosmochimica Acta, 44, 685–699.

Amelin Y, Krot AN, Hutcheon ID, and Ulyanov AA (2002) Lead isotopic ages of chondrules and calcium–aluminum-rich inclusions. Science, 297, 1678–1683. [PubMed: 12215641]

Amelin Y, Kaltenbach A, Iizuka T, Stirling CH, Ireland TR, Petaev M, and Jacobsen SB (2010) U–Pb chronology of the solar system's oldest solids with variable $^{238}U/^{235}U$. Earth and Planetary Science Letters, 300, 343–350.

Anders E, and Grevesse N (1989) Abundances of the elements: Meteoritic and solar. Geochimica et Cosmochimica Acta, 53, 197–214.

Armstrong JT, Meeker GP, Huneke JC, and Wasserburg GJ (1982) The Blue Angel: I. mineralogy and petrogenesis of a hibonite inclusion from the Murchison meteorite. Geochimica et Cosmochimica Acta, 46, 575–595.

Armstrong JT, El Goresy A, and Wasserburg GJ (1985) Willy: A prize noble Ur-Fremdling—its history and implications for the formation of Fremdlinge and CAI. Geochimica et Cosmochimica Acta, 49, 1001–1022.

Armstrong JT, Hutcheon ID, and Wasserburg GJ (1987) Zelda and company: Petrogenesis of sulfide-rich fremdlinge and constraints on solar nebula processes. Geochimica et Cosmochimica Acta, 51, 3155–3173.

Asratian AS, Denley TMJ, and Häggkvist R (1998) Bipartite Graphs and their Applications. Cambridge University Press.

Bar-Matthews M, Hutcheon ID, MacPherson GJ, and Grossman L (1982) A corundum-rich inclusion in the Murchison carbonaceous chondrite. Geochimica et Cosmochimica Acta, 46, 31–41.

Bartels-Rausch T, Bergeron V, Cartwright JHE, Escribano R, Finney JL, Grothe H, Gutirrez PJ, Haapala J, Kuhs WF, Pettersson JBC, and others. (2012) Ice structures, patterns, and processes: A view across the icefields. Reviews of Modern Physics, 84, 885–944.

Beckett JR (1986) The origin of calcium-, aluminum-rich inclusions from carbonaceous chondrites: An experimental study. Ph.D.dissertation, University of Chicago, Illinois.

Beckett JR, and Stolper E (1994) The stability of hibonite, melilite and other aluminous phases in silicate melts: Implications for the origin of hibonite-bearing inclusions from carbonaceous chondrites. Meteoritics, 29, 41–65.

Beckett JR, Live D, Tsay F-D, Grossman L, and Stolper E (1988) Ti^{3+} in meteoritic and synthetic hibonite. Geochimica et Cosmochimica Acta, 52, 1479–1495.

Beckett JR, Simon SB, and Stolper E (2000) The partitioning of Na between melilite and liquid: Part II. Applications to Type B inclusions from carbonaceous chondrites. Geochimica et Cosmochimica Acta, 64, 2519–2534.

Berg T, Maul J, Schönhense G, Marosits E, Hoppe P, Ott U, and Palme H (2009) Direct evidence for condensation in the early solar system and implications for nebular cooling rates. The Astrophysical Journal, 702, L172–L176.

Bertout C (1989) T Tauri stars—wild as dust. Annual Reviews of Astronomy and Astrophysics, 27, 351–395.

Bevan AWR, and Axon HJ (1980) Metallography and thermal history of the Tieschitz unequilibrated meteorite—metallic chondrules and the origin of polycrystalline taenite. Earth and Planetary Science Letters, 47, 353–360.

Birjukov V, and Ulyanov V (1996) Petrology and classification of new Antarctic carbonaceous chondrites PCA91082, TIL91722, and WIS91600. Proceedings of the NIPR Symposium on Antarctic Meteorites, 9, 8–19.

Bischoff A, and Palme H (1987) Composition and mineralogy of refractory-metal-rich assemblages from a Ca,Al-rich inclusion in the Allende meteorite. Geochimica et Cosmochimica Acta, 51, 2733–2748.

Bisschop SE, Fuchs GW, Boogert ACA, van Dishoeck EF, and Linnartz H (2007) Infrared spectroscopy of HCOOH in interstellar ice analogues. Astronomy & Astrophysics, 470, 749–759.

Blander L, and Fuchs LH (1975) Calcium-aluminum-rich inclusions in the Allende meteorite: Evidence for a liquid origin. Geochimica et Cosmochimica Acta, 39, 1605–1619.

Blander L, Fuchs LH, Horowitz C, and Land R (1980) Primordial refractory metal particles in the Allende meteorite. Geochimica et Cosmochimica Acta, 44, 217–223.

Blum JD, Wasserburg GJ, Hutcheon ID, Beckett JR, and Stopler EM (1988) “Domestic” origin of opaque assemblages in refractory inclusions in meteorites. Nature, 331, 405–409.

——— (1989) Origin of opaque assemblages in CV3 meteorites: Implications for nebular and planetary processes. Geochimica et Cosmochimica Acta, 53, 543–556.

Boogert ACA, and Ehfrenfreund P (2004) Interstellar ices. In Witt AN, Clayton GC, and Draine BT, Eds., Astrophysics of Dust. ASP Conference Series, 309, 547–573.

Boogert ACC, Schutte WA, Tielens AGGM, Whittet DCB, Helmich FP, Ehrenfreund P, Wesselius PR, de Graauw T, and Prusti T (1996) Solid methane toward deeply embedded protostars. Astronomy & Astrophysics, 315, L377–L380.

Boogert ACC, Schutte WA, Helmich FP, Tielens AGGM, and Wooden DH (1997) Infrared observations and laboratory simulations of interstellar CH_4 and SO_2. Astronomy & Astrophysics, 317, 929–941.

Boogert ACC, Helmich FP, van Dishoeck EF, Schutte WA, Tielens AGGM, and Whittet DCB (1998) The gas/solid methane abundance ratio toward deeply embedded protostars. Astronomy & Astrophysics, 336, 352–358.

Boss AJ, and Durisen RH (2005) Sources of shock waves in the protoplanetary disk. ASP Conference Series, 341, 821–838.

Bowles JFW (1988) Definition and range of composition of naturally occurring minerals with the pseudobrookite structure. American Mineralogist, 73, 1377–1383.

Brearley AJ, and Jones RH (1998) Chondritic meteorites. Reviews in Mineralogy, 36, 3.01–3.398.

Burke EAJ (2006) The end of CNMMN and CCM—Long live the CNMNC! Elements, 2, 388.

Caillet C, Zinner EK, and MacPherson GJ (1993) Petrologic and Al–Mg isotopic clues to the accretion of two refractory inclusions onto the Leoville parent body: One was hot, the other wasn't. Geochimica et Cosmochimica Acta, 57, 4725–4743.

Campbell AJ, Zanda B, Perron C, Meiborn A, and Petaev MI (2005) Origin and thermal history of Fe-Ni metal in primitive chondrites. In Krot AN, Scott ERD, and Reipurth B, Eds., Chondrites and the Protoplanetary Disk. Astronomical Society of the Pacific Conference Series, 341, 407–431.

Casanova I, and Simon SB (1994) Opaque minerals in CAIs, and classification of the Axtell (CV3) chondrite. Meteoritics, 29, 454–455.

Chiar JE, Adamson AJ, Kerr TH, and Whittet DCB (1995) High-resolution studies of solid CO in the Taurus Dark Cloud: Characterizing the ices in quiescent clouds. The Astrophysical Journal, 455, 234–243.

Chiar JE, Adamson AJ, and Whittet DCB (1996) Three micrometer hydrocarbon and methanol absorption in taurus. The Astrophysical Journal, 472, 665.

——— (1998) Detection of abundant CO_2 ice in the quiescent dark cloud medium toward Elias 16. The Astrophysical Journal, 498, L159–L163.

Chiar JE, Tielens AGGM, Whittet DCB, Schutte WA, Boogert ACA, Lutz D, van Dishoeck EF, and Bernstein MP (2000) The composition and distribution of dust along the line of sight toward the galactic center. The Astrophysical Journal, 537, 749–762.

Chizmadia LJ, Rubin AE, and Wasson JT (2002) Mineralogy and petrology of amoeboid olivine inclusions in CO3 chondrites: relationship to parent-body aqueous alteration. Meteoritics & Planetary Sciences, 37, 1781–1796.

Clark FO, Buhl D, and Snyder LE (1974) Observational evidence for the excitation of HCN and H_2O in protostellar molecular clouds. The Astrophysical Journal, 190, 545–556.

Cleland CE (2011) Prediction and explanation in historical natural science. British Journal of the Philosophy of Science, 62, 551–582.

——— (2013) Common cause explanation and the search for the smoking gun. The Geological Society of America Special Paper, 502, 1–9. doi: 10.1130/2013.2502(01)

Collings MP, Dever JW, Fraser HJ, McCoustra MRS, and Williams DA (2003) Carbon monoxide entrapment in interstellar ice analogs. The Astrophysical Journal, 583, 1058–1062.

Connolly HC Jr., and Jones RH (2016) Chondrules: The canonical and noncanonical views. Journal of Geophysical Research: Planets, 121, 1885–1899.

Connelly JN, Amelin Y, Krot AN, and Bizzarro M (2008) Chronology of the solar system's oldest solids. The Astrophysical Journal, 67, L121–L124.

Connelly JN, Bizzarro M, Krot AN, Nordlund Å, Wielandt D, and Ivanova MA (2012) The absolute chronology and thermal processing of solids in the solar protoplanetary disk. Science, 338, 651–655. [PubMed: 23118187]

Cronin JR, and Pizzarello S (1990) Aliphatic hydrocarbons of the Murchison meteorite. Geochimica et Cosmochimica Acta, 54, 2859–2868. [PubMed: 11537195]

Dana JD (1850) A System of Mineralogy, Comprising the Most Recent Discoveries, Including Full Descriptions of Species and their Localities, Chemical Analyses and Formulas, Tables for the

Determination of Minerals, and a Treatise on Mathematical Crystallography and the Drafting of Figures of Crystals. Third ed., Rewritten, Rearranged, and Enlarged. Putnam George P..

Daranlot J, Hincelin U, Bergeat A, Costes M, Loison J-C, Wakelam V, and Hickson KM (2012) Elemental nitrogen partitioning in dense interstellar clouds. Proceedings of the National Academy of Sciences, 109, 10,233–10,238. doi: 10.1073/pnas.1200017109.

Dartois E, d'Hendecourt L, Thi W, Pontoppidan KM, and van Dishoeck EF (2002) Combined VLT ISAAC/ISO SWS spectroscopy of two protostellar sources. Astronomy & Astrophysics, 394, 1057–1068.

Davis AM, and Richter FM (2014) Condensation and evaporation of solar system materials. In Davis AM, Holland HD, and Turekian KK, Eds., Treatise on Geochemistry, Vol. 1: Meteorites, Comets, and Planets, Second ed. pp.335–360. Elsevier-Pergamon.

Davis AM, Hashimoto A, Clayton RN, and Mayeda TK (1990) Isotope mass fractionation during evaporation of forsterite (Mg_2SiO_4). Nature, 347, 655–658.

Davis AM, MacPherson GJ, Clayton RN, Mayeda TK, Sylvester PJ, Grossman L, Hinton RW, and Laughlin JR (1991) Melt solidification and late-stage evaporation in the evolution of a FUN inclusion from the Vigarano C3V condrite. Geochimica et Cosmochimica Acta, 55, 621–637.

Deer WA, Howie RA, and Zussman J (1963) Rock-Forming Minerals, vol. 2, Chain Silicates, p. 161–166. Wiley.

Desch SJ, and Connolly HC Jr. (2002) A model for the thermal processing of particles in solar nebula shocks: Application to the cooling rates of chondrules. Meteoritics & Planetary Science, 37, 183–207.

Desch SJ, and Cuzzi JN (2000) The generation of lightning in the solar nebula. Icarus, 143, 87–105.

Desch SJ, Morris MA, Connolly HC Jr., and Boss AP (2012) The importance of experiments: Constraints on chondrule formation models. Meteoritics & Planetary Science, 47, 1139–1156.

d'Hendecourt LB, and de Muizon MJ (1989) The discovery of interstellar carbon dioxide. Astronomy & Astrophysics, 223, L5–L8.

d'Hendecourt L, Jourdain de Muizon M, Dartois E, Breitfellner M, Ehrenfreund P, Benit J, Boulanger F, Puget JL, and Habing HJ (1996) ISO-SWS observations of solid state features towards RAFGL 7009S. Astronomy & Astrophysics, 315, L365–L368.

Di Francesco J, Evans NJ II, Caselli P, Myers PC, Shirley Y, Aikawa Y, and Tafalla M (2006) An observational perspective of low-mass dense cores I: Internal physics and chemical properties. Protostars and Planets V, pp. 18–32. University of Arizona Press.

Doukhan N, Doukhan JC, and Poirier JP (1991) Transmission electron microscopy of a refractory inclusion from the Allende meteorite: Anatomy of a pyroxene. Meteoritics, 26, 105–109.

Ebel DS (2006) Condensation of rocky materials in astrophysical environments. In Lauretta DS and McSween HY Jr., Eds., Meteorites and the Early solar system II, pp. 253–277. University of Arizona Press, Tucson.

Ebel DS, and Alexander CMO'D (2011) Equilibrium condensation from chondritic porous IDP enriched vapor: Implications for Mercury and enstatite chondrite origins. Planetary and Space Science, 59, 1888–1894.

Ebel DS, and Grossman L (2000) Condensation in dust-rich systems. Geochimica et Cosmochimica Acta, 65, 469–477.

Ehrenfreund P, and Cami J (2010) Cosmic carbon chemistry: From the interstellar medium to early Earth. In Deamer D and Szostak JW, Eds., Perspectives on the Origins of Life, pp. 1–14. Cold Spring Harbor Press.

Ehrenfreund P, and Charnley SB (2000) Organic molecules in the interstellar medium, comets, and meteorites: A voyage from dark clouds to the early Earth. Annual Reviews in Astronomy and Astrophysics, 38, 427–483.

Ehrenfreund P, and Fraser H (2003) Ice chemistry in space. In Pirronello V, Krelowski K, and Manico G, Eds., Solid State Astrochemistry, pp. 317–356. Kluwer Academic Publishers.

Ehrenfreund P, Robert F, d'Hendecourt L, and Behar F (1991) Comparison of interstellar and meteoritic organic matter at 3.4 microns. Astronomy & Astrophysics, 252, 712–717.

Ehrenfreund P, Boogert ACA, Gerakines PA, Tielens AGGM, and van Dishoek EF (1997) Infrared spectroscopy of interstellar apolar ice analogs. Astronomy & Astrophysics, 328, 649–669.

El Goresy A, Nagel K, and Ramdohr P (1978) Fremdlinges and their noble relatives. Proceedings of the Lunar and Planetary Science Conference, 9, 1279–1303.

——— (1979) Spinel framboids and Fremdlinge in Allende inclusions: Possible sequential markers in the early history of the solar system. Proceedings of the Lunar and Planetary Science Conference, 10, 833–850.

El Goresy A, Palme H, Yabuki H, Nagel K, Herrwerth I, and Ramdohr P (1984) A calcium-aluminum inclusion from Essebi (CM2) chondrite: Evidence for captured spinel-hibonite spherules and for an ultra-refractory rimming sequence. Geochimica et Cosmochimica Acta, 48, 2283–2298.

El Goresy A, Zinner E, Matsunami S, Palme H, Spettel B, Lin Y, and Nazarov M (2002) Efremovka 101.1: A CAI with ultra-refractory REE patterns and enormous enrichments of Sc, Zr, and Y in fassaite and perovskite. Geochimica et Cosmochimica Acta, 66, 1459–1491.

El Goresy A, Boyer M, and Miyahara M (2011) Almahata Sita MS-17 EL-3 chondrite fragment: contrasting oldhamite assemblages in chondrules and matrix and significant oldhamite REE-patterns. Meteoritics & Planetary Sciences, 46, Abstract 5079.

Elsila J, Allamandola LJ, and Sandford SA (1997) The 2140 cm^{-1} (4.673 microns) solid CO band: The case for interstellar O2 and N2 and the photochemistry of nonpolar interstellar ice analogs. The Astrophysical Journal, 479, 818–838. [PubMed: 11540158]

Endress M, Keil K, Bischoff A, Spettel B, Clayton RN, and Mayeda TK (1994) On the origin of dark clasts in Acfer 059/El Djouf 001 CR2 chondrite. Meteoritics, 29, 26–40.

Fagan TJ, Krot AN, and Keil K (2000) Calcium–aluminum-rich inclusions in enstatite chondrites: I. Mineralogy and textures. Meteoritics & Planetary Science, 35, 771–781.

Fagan TJ, McKeegan KD, Krot AN, and Keil K (2001) Calcium–aluminium-rich inclusions in enstatite chondrites: II. Oxygen isotopes. Meteoritics & Planetary Science, 36, 223–230.

Fahey AJ, Zinner E, Kurat K, and Kracher A (1994) Hibonite-hercynite inclusions HH-1 from the Lance (CO_3) meteorite: The history of an ultra-refractory inclusion CAI. Geochimica et Cosmochimica Acta, 58, 4779–4793.

Ferriere D (2001) The interstellar environment of our galaxy. Reviews of Modern Physics, 73, 1031–1066.

Freeman A, and Millar TJ (1983) Formation of complex molecules in TMC-1. Nature, 301, 402–404.

Fruchterman TMJ, and Reingold EM (1991) Graph drawing by force-directed placement. Software: Practice and Experience, 21, 1129–1164.

Fuchs LH (1971) Occurrence of wollastonite, rhönite and andradite in the Allende meteorite. American Mineralogist, 56, 2053–2068.

——— (1974) Grossular in the Allende (Type III carbonaceous) meteorite. Meteoritics, 9, 11–18.

——— (1978) The mineralogy of a rhönite-bearing calcium aluminum rich in the Allende meteorite. Meteoritics, 13, 73–88.

Fuentes-Landete V, Mitterdorfer C, Handle PH, Ruiz GN, Bernard J, Bogdan A, Seidl M, Amann-Winkel K, Stern J, Fuhrmann S, and Loerting T (2015) Crystalline and amorphous ices. Proceedings of the International School of Physics, 187. doi: 10.3254/978-1-61499-507-4-173.

Gaffney ES, and Matson DL (1980) Water ice polymorphs and their significance on planetary surfaces. Icarus, 44, 511–519.

Geiger T, and Bischoff A (1995) Formation of opaque minerals in CK chondrites. Planetary & Space Science, 43, 485–498.

Gerakines PA, Whittet DCB, Ehrenfreund P, Boogert ACA, Tielens AGGM, Schutte WA, Chiar JE, van Dishoeck EF, Prusti T, Helmich FP, and de Graauw T (1999) ISO-SWS observations of solid carbon dioxide in molecular clouds. The Astrophysical Journal, 522, 357–377.

Ghose J, Methikkalam RRJ, Bhuin RG, Ragupathy G, Choudhary N, Kumar R, and Pradeep T (2019) Clathrate hydrates in interstellar environment. Proceedings of the National Academy of Sciences, 116, 1526–1531.

Gibb EL, Whittet DCB, Boogert ACA, and Tielens AGGM (2004) Interstellar ice: The Infrared Space Observatory legacy. The Astrophysical Journal Supplement Series, 151, 35–73.

Gillet FC, and Forrest WJ (1973) Spectra of the Becklin-Neugebauer point source and the Kleinmann-Low nebula from 2.8 to 13.5 microns. The Astrophysical Journal, 179, 483–491.

Gilmour JD, and Saxton JM (2001) A time-scale of formation of the first solids. Philosophical Transactions of the Royal Society London, A, 359, 2037–2048.

Greenberg JM (1991) Interstellar dust-gas relationships. In Shapiro MM, Silberberg R, and Wefel JP, Eds., Cosmic Rays, Supernovae, and the Interstellar Medium. NATO ASI Series: Mathematical and Physical Sciences, 120, 57–68.

Greenberg JM, Li A, Mendoza-Gomez CX, Schutte WA, Gerakines PA, and de Groot M (1995) Approaching the interstellar grain organic refractory component. The Astrophysical Journal Letters, 455, L177–L180.

Greenwood RC, Hutchison R, Huss GR, and Hutcheon ID (1992) CAIs in CO3 meteorites: Parent body or nebular alteration? Meteoritics, 27, 229.

Greenwood RC, Lee MR, Hutchison R, and Barber DJ (1994) Formation and alteration of CAIs in Cold Bokkeveld (CM2). Geochimica et Cosmochimica Acta, 58, 1913–1935.

Greshake A, Bischoff A, Putnis A, and Palme H (1996) Corundum, rutile, periclase, and CaO in Ca,Al-rich inclusions from carbonaceous chondrites. Science, 272, 1316–1318. [PubMed: 8662462]

Grim RJA, Bass F, Geballe TR, Greenberg JM, and Schutte WA (1991) Detection of solid methanol toward W33A. Astronomy & Astrophysics, 243, 473–477.

Grishko VI, and Duley WW (2000) Detection of new infrared spectral features in hydrogenated amorphous carbon. The Astrophysical Journal, 543, L85–L88.

Grokhovsky VI (2006) Osbornite in CB/CH-like carbonaceous chondrite Isheyevo. Meteoritics & Planetary Science, 41, A68.

Grossman L (1972) Condensation in the primitive solar nebula. Geochimica et Cosmochimica Acta, 36, 597–619.

——— (1975) Petrography and mineral chemistry of Ca-rich inclusions in the Allende meteorite. Geochimica et Cosmochimica Acta, 39, 433–453.

——— (1980) Refractory inclusions in the Allende meteorite. Annual Reviews of Earth and Planetary Sciences, 8, 559–608.

Grossman L, and Steele IM (1976) Amoeboid olivine aggregates in the Allende meteorite. Geochimica et Cosmochimica Acta, 40, 149–155.

Grossman L, Ganapathy R, Methot RL, and Davis AM (1979) Trace elements in the Allende meteorite amoeboid olivine aggregates. Geochimica et Cosmochimica Acta, 43, 817–829.

Grossman JN, Rubin AE, and MacPherson GJ (1988) ALH 85085: A unique volatile-poor carbonaceous chondrite with implications for nebular fractionation practices. Earth and Planetary Science Letters, 91, 33–54.

Grundy WM, and Schmitt B (1998) The temperature-dependent near-infrared absorption spectrum of hexagonal H_2O ice. Journal of Geophysical Research, 103, 25809.

Guan Y, Huss GR, MacPherson GJ, and Wasserburg GJ (2000) Calcium–aluminum-rich inclusions from enstatite chondrites: Indigenous or foreign? Science, 289, 1330–1333. [PubMed: 10958775]

Güsten R, Wiesemeyer H, Neufeld D, Menten KM, Graf UU, Jacobs K, Klein B, Ricken O, Risacher C, and Stutzki J (2019) Astrophysical detection of the helium hydride ion HeH^+. Nature, 568, 357–360. [PubMed: 30996316]

Hagen W, Tielens AGGM, and Greenberg JM (1981) The infrared spectra of amorphous solid water and ice between 10 and 140 K. Chemical Physics, 56, 367–379.

Han J, Brearley AJ, and Keller LP (2015) Microstructural evidence for a disequilibrium condensation origin for hibonite-spinel inclusions in the ALHA77307 CO3.0 chondrite. Meteoritics & Planetary Science, 50, 2121–2136.

Harries D, Berg T, Langenhorst F, and Palme H (2012) Structural clues to the origin of refractory metal alloys as condensates of the solar nebula. Meteoritics & Planetary Sciences, 47, 2148–2159.

Hashimoto A (1983) Evaporation metamorphism in the early solar nebula—evaporation experiments on the melt FeO-MgO-SiO_2-CaO-Al_2O_3 and chemical fractionations of primitive materials. Geochemical Journal, 17, 111–145.

——— (1992) The effect of H_2O gas on volatilities of planet-forming major elements: I. Experimental determination of thermodynamic properties of C-, Al-, and Si-hydroxide gas molecules, and its application to the solar nebula. Geochimica et Cosmochimica Acta, 56, 511–532.

Hashimoto A, and Grossman L (1987) Alteration of Al-rich inclusions inside amoeboid olivine aggregates in the Allende meteorite. Geochimica et Cosmochimica Acta, 51, 1685–1704.

Hazen RM (1989) A farewell to obsolete pyroxenes. The Lattice, 2, 1989, 6–7.

——— (2018) Titan mineralogy: A window on organic mineral evolution. American Mineralogist, 103, 341–342.

——— (2019) An evolutionary system of mineralogy: Proposal for a classification based on natural kind clustering. American Mineralogist, 104, 810–816.

Hazen RM, and Ferry JM (2010) Mineral evolution: Mineralogy in the fourth dimension. Elements, 6, 1, 9–12.

Hazen RM, and Morrison SM (2020) An evolutionary system of mineralogy. Part I: Stellar mineralogy (>13 to 4.6 Ga). American Mineralogist, 105, 627–651.

Hazen RM, Papineau D, Bleeker W, Downs RT, Ferry JM, McCoy TL, Sverjensky DA, and Yang H (2008) Mineral evolution. American Mineralogist, 93, 1693–1720.

Hazen RM, Sverjensky DA, Azzolini D, Bish DL, Elmore SC, Hinnov L, and Milliken RE (2013) Clay mineral evolution. American Mineralogist, 98, 2007–2029.

Hazen RM, Downs RT, Elesish A, Fox P, Gagné O, Golden JJ, Grew ES, Hummer DR, Hystad G, Krivovichev SV, and others. (2019) Data-driven discovery in mineralogy: Recent advances in data resources, analysis, and visualization. China Engineering, 5, 397–405.

Henning T, and Salama E (1998) Carbon in the universe. Science, 282, 2204–2210. [PubMed: 9856936]

Henning T, Jager C, and Mutschke H (2004) Laboratory studies on carbonaceous dust. In Witt AN, Clayton GC, and Draine BT, Eds., Astrophysics of Dust. ASP Conference Series, 309, 603–628.

Herbst E (1995) Chemistry in the interstellar medium. Annual Review of Physical Chemistry, 46, 27–54.

Herbst E, and Klemperer W (1973) The formation and depletion of molecules in dense interstellar clouds. The Astrophysical Journal, 185, 505–533.

Hinton RW, Davis AM, Scalena-Wachel DE, Grossman L, and Draus RJ (1988) A chemical and isotopic study of hibonite-rich refractory inclusions in primitive meteorites. Geochimica et Comsochimica Acta, 52, 2573–2598.

Hobbs PV (1974) Ice Physics. Oxford University Press.

Hollenbach D, Kaufman MJ, Bergin EA, and Melnick GJ (2009) Water, O_2, and ice in molecular clouds. The Astrophysical Journal, 690, 1497–1521.

Holmberg AA, and Hashimoto H (1992) A unique (almost) unaltered spinel-rich fine-grained inclusion in Kainsaz. Meteoritics, 27, 149–153.

Hubbard A, McNally CP, and MacLow M-M (2012) Short circuits in thermally ionized plasmas: A mechanism for intermittent heating of protoplanetary disks. The Astrophysical Journal, 761, 58–67.

Ichikawa O, and Ikeda Y (1995) Petrology of the Yamato-8559 CR chondrite. Proceedings of the NIPR Symposium on Antarctic Meteorites, 8, 63–78.

Ihinger PD, and Stolper E (1986) The color of meteoritic hibonite: An indicator of oxygen fugacity. Earth and Planetary Science Letters, 78, 67–79.

Iida A, Nakamoto T, Susa H, and Nakagawa Y (2001) A shock model for chondrule formation in a protoplanetary disk. Icarus, 153, 430–450.

Ikeda Y (1992) An overview of the research consortium, “Antarctic carbonaceous chondrites with CI affinities,” Yamato-86720, Yamato-82162, and Belgica-7904. Proceedings of the NIPR Symposium on Antarctic Meteorites, 5, 49–73.

Ireland TR (1988) Correlated morphological, chemical, and isotopic characteristics of hibonites from the Murchison carbonaceous chondrite. Geochimica et Cosmochimica Acta, 52, 2827–2839.

Ireland TR, Fahey AJ, and Zinner EK (1988) Trace element abundances in hibonites from the Murchison carbonaceous chondrite: Constraints on high-temperature processes in the solar nebula. Geochimica et Cosmochimica Acta, 52, 2841–2854.

Ivanova MA, Petaev MI, MacPherson GJ, Nazarov MA, Taylor LA, and Wood JA (2002) The first known natural occurrence of $CaAl_2O_4$, in a Ca–Al-rich inclusion from the CH chondrite NWA470. Meteoritics & Planetary Science, 37, 1337–1344.

Jambon A, and Boudouma O (2011) Evidence for rhönite in angrites D'Orbigny and Sahara 99555. 74th Annual Meeting of the Meteoritical Society, Meteoritics & Planetary Science Supplement, id.5167 (Sept 2011).

Jeans JH (1902) The stability of a spherical nebula. Philosophical Transactions of the Royal Society A, 199, 1–53.

Jenniskens P, and Blake DF (1994) Structural transitions in amorphous water ice and astrophysical implications. Science, 265, 753–756. [PubMed: 11539186]

——— (1996) Crystallization of amorphous water ice in the solar system. The Astrophysical Journal, 473, 1104–1113. [PubMed: 11539415]

Jordan KD (2019) Smallest water clusters supporting the ice I structure. Proceedings of the National Academy of Sciences, 116, 24383–24385.

Joung RMK, MacLow MM, and Ebel DS (2004) Chondrule formation and protoplanetary disk heating by current sheets in nonideal magnetohydrodynamic turbulence. The Astrophysical Journal, 606, 532–541.

Keil K, and Fuchs LH (1971) Hibonite from the Leoville and Allende chondritic meteorites. Earth and Planetary Science Letters, 12, 184–190.

Keller LP, and Buseck PR (1994) Twinning in meteoritic and synthetic perovskite. American Mineralogist, 79, 73–79.

Kerridge JF (1983) Isotopic composition of carbonaceous-chondrite kerogen: Evidence for an interstellar origin of organic matter in meteorites. Earth and Planetary Science Letters, 64, 186–200.

Kimura M, El Goresy A, Palme H, and Zinner E (1993) Ca-Al-rich inclusions in the unique chondrite ALH85085: Petrology, chemistry, and isotopic compositions. Geochimica et Cosmochimica Acta, 57, 2329–2359.

Kimura M, Mikouchi T, Suzuki A, Miyahara M, Ohtani E, and El Goresy A (2006) Kushiroite, $CaAlAlSiO_6$: A new mineral of the pyroxene group from the ALH 85085 CH chondrite, and its genetic significance in refractory inclusions. American Mineralogist, 94, 1479–1482.

Klöck W, Thomas KL, McKay DS, and Palme H (1989) Unusual olivine and pyroxene compositions in interplanetary dust and unequilibrated ordinary chondrites. Nature, 339, 126–128.

Knauth DC, Andersson B-G, McCandliss SR, and Moos HW (2004) The interstellar N_2 abundance towards HD 124314 from far-ultraviolet observations. Nature, 429, 636–638. [PubMed: 15190346]

Kojima T, Yada S, and Tomeoka K (1995) Ca-Al-rich inclusion in three Antarctic CO3 chondrites, Y-81020, Yamato-82050 and Yamato-790992: Record of low temperature alteration processes. Proceedings of the NIPR Symposium on Antarctic Meteorites, 8, 79–86.

Komatsu M, Fagan TJ, Krot AN, Nagashima K, Petaev MI, Kimura M, and Yamaguchi A (2018) First evidence for silica condensation within the solar protoplanetary disk. Proceedings of the National Academy of Sciences, 115, 7497–7502.

Kööp L, Nakashima D, Heck PR, Kita NT, Tenner TJ, Krot AN, Nagashima K, Park C, and Davis AM (2016a) New constraints on the relationship between ^{26}Al and oxygen, calcium, and titanium isotopic variation in the early solar system from a multielement isotopic study of spinel-hibonite inclusions. Geochimica et Cosmochimica Acta, 184, 151–172.

Kööp L, Davis AM, Nakashima D, Park C, Krot AN, Nagashima K, Temmer TJ, Heck PR, and Kita NT (2016b) A link between oxygen, calcium and titanium isotopes in ^{26}Al-poor hibonite-rich CAIs from Murchison and implications for the heterogeneity of dust reservoirs in the solar nebula. Geochimica et Cosmochimica Acta, 189, 70–95.

Kööp L, Heck PR, Busemann H, Davis AM, Greer J, Maden C, Meier MMM, and Wieler R (2018) High early solar activity inferred from helium and neon excess in the oldest meteorite inclusions. Nature Astronomy, 2, 709–713.

Kornacki AS, and Wood JA (1984) Petrography and classification of Ca,Al-rich and olivine-rich inclusions in the Allende CV3 chondrite. Proceedings of the Lunar and Planetary Science Conference, 14, B573–B587.

——— (1985) The identification of Group II inclusions in carbonaceous chondrites by electron microprobe analysis of perovskite. Earth and Planetary Science Letters, 72, 74–86.

Kouchi A (1987) Vapour pressure of amorphous H_2O ice and its astrophysical implications. Nature, 330, 550–552.

——— (1990) Evaporation of H_2O-CO ice and its astrophysical implications. Journal of Crystal Growth, 99, 1220–1226.

Kouchi A, and Kuroda T (1990) Amorphization of cubic ice by ultraviolet irradiation. Nature, 344, 134–135.

Kouchi A, and Yamamoto T (1995) Cosmoglaciology: Evolution of ice in interstellar space and the early solar system. Progress in Crystal Growth and Characterization of Materials, 30, 83–107.

Kouchi A, Yamamoto T, Kozasa T, Kuroda T, and Greenberg JM (1994) Conditions for condensation and preservation of amorphous water ice and crystallinity of astrophysical ices. Astronomy & Astrophysics, 290, 1009–1018.

Krivovichev SV (2012) Topological complexity of crystal structures: quantitative approach. Acta Crystallographica, A68, 393–398.

——— (2013) Structural complexity of minerals: information storage and processing in the mineral world. Mineralogical Magazine, 77, 275–326.

Krot AN (2019) Refractory inclusions in carbonaceous chondrites: Records of early solar systems processes. Meteoritics & Planetary Science, 54, 1647–1691. [PubMed: 31379423]

Krot AN, Petaev MI, Russell SS, Itoh S, Fagan TJ, Yurimoto H, Chizmadia L, Weisberg MK, Komatsu M, Ulyanov AA, and Keil K (2004) Amoeboid olivine aggregates and related objects in carbonaceous chondrites: records of nebular and asteroid processes. Chemie der Erde Geochemistry, 64, 185–239.

Krot AN, Ulyanov AA, and Ivanova MA (2006) Refractory inclusions and aluminum-rich chondrules in the CB/CH-like carbonaceous chondrite Isheyevo. Proceedings of the Lunar and Planetary Science Conference, 37, 1226.

Krot AN, Keil K, Scott ERD, Goodrich CA, and Weisberg MK (2014) Classification of meteorites and their genetic relationships. In Davis AM, Ed., Treatise on Geochemistry (2nd ed.), vol. 1, pp. 1–63. Elsevier.

Krot AN, Ma C, Nagashima K, Davis AM, Beckett JR, Simon SB, Komatsu M, Fagan TJ, Brenker F, Ivanova MA, and Bischoff A (2019) Mineralogy, petrology, and oxygen isotopic compositions of ultra-refractory inclusions from carbonaceous chondrites. Geochemistry, 79, 125519 (29 pp.).

Krot AN, Nagashima K, and Rossman GR (2020) Machiite, $Al_2Ti_3O_9$, a new oxide mineral from the Murchison carbonaceous chondrite: A new ultra-refractory phase from the solar nebula. American Mineralogist, 105, 239–243.

Lacy JH, Carr JS, Evans NJ II, Baas F, Achtermann JM, and Arens JF (1991) Discovery of interstellar methane: Observations of gaseous and solid CH_4 absorption toward young stars in molecular clouds. The Astrophysical Journal, 376, 556–560.

Lattimer JM, Schramm DN, and Grossman L (1978) Condensation in supernova ejecta and isotopic anomalies in meteorites. The Astrophysical Journal, 219, 230–249.

Léger A, Gauthier S Defourneau D, and Rouan D (1983) Properties of amorphous H_2O ice and origin of the 3.1 micron absorption. Astronomy & Astrophysics, 117, 164–169.

Lin Y, El Goresy A, Boyer M, Feng L, Zhang J, and Hao J (2011) Earliest solid condensates consisting of the assemblage oldhamite, sinoite, graphite and excess ^{36}S in lawrencite from Almahata Sitta MS-17 EL3 chondrite. Workshop on Formation of the First Solids in the solar system, Abstract 9040.

Liu M-C, McKeegan KD, Goswami JN, Marhas KK, Sahijpal S, Ireland TR, and Davis AM (2009) Isotopic records in CM hibonites: Implications for timescales of mixing of isotope reservoirs in the solar nebula. Geochimica et Cosmochimica Acta, 73, 5051–5079.

Lodders K (2003) Solar system abundances and condensation temperatures of the elements. The Astrophysical Journal, 591, 1220–1247.

Longair MS (2008) Galaxy Formation, Second edition. Springer.

Luhman KL, Allen PR, Espaillat C, Hartmann L, and Calvet N (2010) The disk population of the Taurus star-forming region. The Astrophysical Journal Supplement Series, 186, 111–174.

Ma C (2011) Discovery of meteoritic lakargiite ($CaZrO_3$), a new ultra-refractory mineral from the Acfer 094 carbonaceous chondrite. Proceedings of the Annual Meeting of the Meteoritical Society, 74, 5169.

——— (2012) Discovery of meteoritic eringaite, $Ca_3(Sc,Y,Ti)_2Si_3O_{12}$, the first solar garnet? Meteoritics & Planetary Science, 47, A256.

——— (2018) Discovery of meteoritic baghdadite, $Ca_3(Zr,Ti)Si_2O_9$, in Allende: The first solar silicate with structurally essential zirconium? Meteoritics & Planetary Science, 53 (S1), Abstract No. 6358.

——— (2019) Discovery of kaitianite, $Ti_1^{+}Ti^{4+}O_5$, in Allende: A new refractory mineral from the solar nebula. Proceedings of the Annual Meeting of the Meteoritical Society, 82, 6098.

Ma C, and Beckett JR (2016) Burnettite, $CaVAlSiO_6$, and paqueite, $Ca_3TiSi_2(Al_2Ti)O_{14}$, two new minerals from Allende: Clues to the evolution of a V-rich Ca-Al-inclusion. Proceedings of the Lunar and Planetary Science Conference, 47, 1595.

Ma C, and Rossman GR (2008) Discovery of tazheranite (cubic zirconia) in the Allende meteorite. Geochimica et Cosmochimica Acta, 72, A577.

——— (2009a) Grossmanite, $CaTi^{3+}AlSiO_6$, a new pyroxene from the Allende meteorite. American Mineralogist, 94, 1491–1494.

——— (2009b) Davisite, $CaScAlSiO_6$, a new pyroxene from the Allende meteorite. American Mineralogist, 94, 845–848.

——— (2009c) Tistarite, Ti_2O_3, a new refractory mineral from the Allende meteorite. American Mineralogist, 94, 841–844.

Ma C, and Rubin AE (2019) Edscottite, Fe_5C_2, a new iron carbide mineral from the Ni-rich Wedderburn IAB iron meteorite. American Mineralogist, 104, 1351–1355.

Ma C, Beckett JR, Rossman GR, Connolly HC Jr., Guan Y, Eiler JM, and Hofmann AE (2009a) In-situ discovery of a cluster of refractory grains in an Allende ferromagnesiam chondrule. Proceedings of the Lunar and Planetary Science Conference, 40, 2138.

Ma C, Simon SB, Rossman GR, and Grossman L (2009b) Calcium Tschermak's pyroxene, $CaAlAlSiO_6$, from the Allende and Murray meteorites: EBSD and micro-Raman characterizations. American Mineralogist, 94, 1483–1486.

Ma C, Beckett JR, Tschauner O, and Rossman GR (2011a) Thortveitite ($Sc_2Si_2O_7$), the first solar silicate? Proceedings of the Annual Meeting of the Meteoritical Society, 74, 5171.

Ma C, Kampf AR, Connolly HC Jr., Beckett JR, Rossman GR, Sweeney Smith SA, and Schrader DL (2011b) Krotite, $CaAl_2O_4$, a new refractory mineral from the NWA 1934 meteorite. American Mineralogist, 96, 709–715.

Ma C, Tschauner O, Beckett JR, Rossman GR, and Liu W (2012) Panguite, $(Ti^{4+},Sc,Al,Mg,Zr,Ca)_{1.8}O_3$, a new ultra-refractory titania mineral from the Allende meteorite: synchrotron micro-diffraction and EBSD. American Mineralogist, 97, 1219–1225.

Ma C, Krot AN, and Bizzarro M (2013a) Discovery of dmisteinbergite (hexagonal $CaAl_2Si_2O_8$) in the Allende meteorite: A new member of refractory silicates formed in the solar nebula. American Mineralogist, 98, 1368–1371.

Ma C, Tschauner O, Beckett JR, Rossmann GR, and Liu W (2013b) Kangite, $(Sc,Ti,Al,Zr,Mg,Ca,\square)_2O_3$, a new ultra-refractory scandia mineral from the Allende meteorite: Synchrotron micro-Laue diffraction and electron backscatter diffraction. American Mineralogist, 98, 870–878.

Ma C, Beckett JR, and Rossman GR (2014a) Allendeite ($Sc_4Zr_3O_{12}$) and hexamolybdenum (Mo,Ru,Fe), two new minerals from an ultra-refractory inclusion from the Allende meteorite. American Mineralogist, 99, 654–666.

——— (2014b) Monipite, MoNiP, a new phosphide mineral in a Ca-Al-rich inclusion from the Allende meteorite. American Mineralogist, 99, 198–205.

Ma C, Krot AN, Beckett JR, Nagashima K, and Tschauner O (2015) Discovery of warkite, $Ca_2Sc_6Al_6O_{20}$, a new Sc-rich ultra-refractory mineral in Murchison and Vigarano. Proceedings of the Annual Meeting of the Meteoritical Society, 78, 5025.

Ma C, Yoshizaki T, Krot AN, Beckett JR, Nakamura T, Nagashima K, Muto J, and Ivanova MA (2017a) Discovery of rubinite, $Ca_3Ti_2^{3+}Si_3O_{12}$, a new garnet mineral in refractory inclusions from carbonaceous chondrites. Proceedings of the Annual Meeting of the Meteoritical Society, 80, 6023.

Ma C, Krot AN, and Nagashima K (2017b) Addibischoffite, $Ca_2Al_6Al_6O_{20}$, a new calcium aluminate mineral from the Acfer 214 CH carbonaceous chondrite: A new refractory phase from the solar nebula. American Mineralogist, 102, 1556–1560.

Macdougall JD (1979) Refractory-element-rich inclusions in C2 meteorites. Earth and Planetary Science Letters, 42, 1–6.

——— (1981) Refractory spherules in the Murchison meteorite: Are they chondrules? Geophysical Research Letters, 8, 966–969.

MacPherson GJ (2014) Calcium-aluminum-rich inclusions in chondritic meteorites. In Davis AM, Holland HD, and Turekian KK, Eds., Treatise on Geochemistry, Vol. 1: Meteorites, Comets, and Planets, Second edition. pp.139–179. Elsevier-Pergamon.

MacPherson GJ, and Davis AM (1993) A petrologic and ion microprobe study of a Vigarano Type B2 refractory inclusion: Evolution by multiple stages of melting and alteration. Geochimica et Cosmochimica Acta, 57, 231–243.

——— (1994) Refractory inclusions in the prototypical CM chondrite, Mighei. Geochimica et Cosmochimica Acta, 58, 5599–5625.

MacPherson GJ, and Grossman L (1984) Fluffy Type-A inclusions in the Allende meteorite. Geochimica et Cosmochimica Acta, 48, 29–46.

MacPherson GJ, Grossman L, Allen JM, and Beckett JR (1981) Origin of rims on coarse-grained inclusions in the Allende meteorite. Proceedings of the Lunar and Planetary Science Conference, 12, 1079–1091.

MacPherson GJ, Bar-Matthews M, Tanaka T, Olsen E, and Grossman L (1983) Refractory inclusions in the Murchison meteorite. Geochimica et Cosmochimica Acta, 47, 823–839.

MacPherson GJ, Paque JM, Stolper E, and Grossman L (1984) The origin and significance of reverse zoning in melilite from Allende Type B inclusions. Journal of Geology, 92, 289–305.

MacPherson GJ, Wark DA, and Armstrong JT (1988) Primitive material surviving in chondrites: refractory inclusions. In Kerridge JF and Matthews MS, M.S., Eds., Meteorites and the Early solar system, p. 746–807. University of Arizona Press.

MacPherson GJ, Huss GR, and Davis AM (2003) Extinct ^{10}Be in Type A CAIs from CV chondrites. Geochimica et Cosmochimica Acta, 67, 3165–3179.

Mai C, Desch SJ, Boley AC, and Weiss BP (2018) Magnetic fields recorded by chondrules formed in nebular shocks. The Astrophysical Journal, 857, 96 (13 pp.).

Mann CR, Boley AC, and Morris MA (2016) Planetary embryo bow shocks as a mechanism for chondrule formation. The Astrophysical Journal, 818, 103–123.

Mao XY, Ward BJ, Grossman L, and MacPherson GJ (1990) Chemical compositions of refractory inclusions from the Vigarano and Leoville carbonaceous chondrites. Geochimica et Cosmochimica Acta, 54, 2121–2132.

Maret S, Bergin EA, and Lada CJ (2006) A low fraction of nitrogen in molecular form in a dark cloud. Nature, 442, 425–427. [PubMed: 16871211]

Massalkski TB, Park FR, and Vassalmillet LF (1966) Speculations about plessite. Geochimica et Cosmochimica Acta, 30, 649–662.

Maynard-Casely HE, Cable ML, Malaska MJ, Vu TH, Choukroun M, and Hodyss R (2018) Prospects for mineralogy on Titan. American Mineralogist, 103, 343–349.

McKeegan KD, Leshin LA, Russell SS, and MacPherson GJ (1998) Oxygen isotope abundances in calcium-aluminum-rich inclusions from ordinary chondrites: implications for nebular heterogeneity. Science, 280, 414–418. [PubMed: 9545215]

McKeegan KD, Chaussidon M, and Robert F (2000) Incorporation of short-lived ^{10}Be in a calcium-aluminum-rich inclusion from the Allende meteorite. Science, 289, 1334–1337. [PubMed: 10958776]

Mendybaev RA, Richter FM, Georg RB, and Davis AM (2009) Evaporation kinetics of forsterite-rich melts and thermal histories of FUN CAIs. Proceedings of the Lunar and Planetary Science Conference, 40, 2461.

Michel-Lévy MC, Kurat G, and Brandstätter F (1982) A new calcium aluminate from a refractory inclusion in the Leoville carbonaceous chondrite. Earth and Planetary Science Letters, 61, 13–22.

Mikouchi T, Zolensky M, Ivanova M, Tachikawa O, Komatsu M, Le L, and Gounelle M (2009) Dmitryivanovite: A new high-pressure calcium aluminate from the Northwest Africa 470 CH3 chondrite characterized using electron backscatter diffraction analysis. American Mineralogist, 94, 746–750.

Mills SJ, Hatert F, Nickel EH, and Ferrais G (2009) The standardization of mineral group hierarchies: Application to recent nomenclature proposals. European Journal of Mineralogy, 21, 1073–1080.

Mizuno A, Onishi T, Hayashi M, Ohashi N, Sunada K, Hasegawa T, and Fukul Y (1994) Molecular cloud condensation as a tracer of low-mass star formation. Nature, 368, 719–721.

Moberg DR, Becker D, Dierking CW, Zurheide F, Bandow B, Buck U, Hudait A, Molinero V, Paesani F, and Zeuch T (2019) The end of ice I. Proceedings of the National Academy of Sciences, 116, 24,413–24,419.

Moggi-Cecchi V, Pratesi G, Salvadori A, Franchi IA, and Greenwood RC (2007) Textural and minerochemical features of NWA 1807 and 2180, two new CV3 chondrites from Northwest Africa. Lunar and Planetary Science Conference, 38, 2338.

Moore MH, and Hudson RL (1992) Far-infrared spectral studies of phase changes in water ice induced by proton radiation. The Astrophysical Journal, 401, 353.

Morimoto N, Fabries J, Ferguson AK, Ginzburg IV, Ross M, Seifert FA, Zussman J, Aoki K, and Gottardi G (1988) Nomenclature of pyroxenes. American Mineralogist, 73, 1123–1133.

Morrison SM, Liu C, Eleish A, Prabhu A, Liu C, Ralph J, Downs RT, Golden JJ, Fox P, Hummer DR, Meyer MB, and Hazen RM (2017) Network analysis of mineralogical systems. American Mineralogist, 102, 1588–1596.

Morrison SM, Downs RT, Eleish A, Fox P, Hummer DR, Hystad G, Golden JJ, Liu C, Prabhu A, Zahirovic S, and Hazen RM (2020) Visualizing carbon minerals: Recent advances in C mineral evolution, mineral ecology, and network analysis. Frontiers in Earth Sciences, in press, DOI: 10.3389/feart.2020.00208.

Mukai T (1986) Analysis of a dirty water-ice model for cometary dust. Astronomy & Astrophysics, 164, 397–407.

Mysen BO, and Kushiro I (1988) Composition, evaporation, melting and crystallization in the primitive solar nebula: Experimental data in the system MgO-SiO_2-H_2 to 1.0×10^{-9} bar and 1870 °C with variable oxygen fugacity. American Mineralogist, 73, 1–19.

Mysen BO, Virgo D, and Kushiro I (1985) Experimental studies at low pressures and high temperatures: Phase equilibra in the system $CaMgSi_2O_6$—H_2 in the temperature range 1200° −1500°C and the pressure range (PH2) 10^{-6} to 10^{-9} bar. Earth and Planetary Science Letters, 75, 139–147.

Nagahara H (1982) Fe-Ni metals in the type 3 ordinary chondrites. Symposium on Antarctic Meteorites, NIPR special Issue, 20, 86–96.

Nagahara H, Kushiro I, and Mysen BO (1993) Vaporization and condensation of chondritic materials —experimental studies. In Ohya H, Ed., Primitive Solar Nebula and Origin of Planets, pp. 427–446, Terra Scientific Publishing Company (TERRAPUB) Tokyo.

Newman SF, Buratti BJ, Brown RH, Jaumann R, Bauer J, and Momary T (2008) Photometric and spectral analysis of the distribution of crystalline and amorphous ices on Enceladus as seen by Cassini. Icarus, 193, 397–406.

Noguchi T (1994) Petrology and mineralogy of the Coolidge meteorite (CV4). Proceedings of the NIPR Symposium of Antarctic Meteorites, 7, 42–72.

Nummelin A, Whittet DCB, Gibb EL, Gerakines PA, and Chiar JE (2001) Solid carbon dioxide in regions of low-mass star formation. The Astrophysical Journal, 558, 185–193.

Öberg KI, Boogert ACA, Pontoppidian KM, Blake GA, Evans NJ, van Lahuis F, and Dishoeck EF (2008) The c2d Spitzer spectroscopic survey of ices around low-mass young stellar objects. III. CH_4. The Astrophysical Journal, 678, 1032–1041.

Omont A, Moseley SH, Forveille T, Glaccum WJ, Harvey PM, Likkel L, Lowenstein RF, and Lisse CM (1990) Observation of 40–70 micron bands of ice in IRAS 09371–1212 and other stars. The Astrophysical Journal, 355, L27–L30.

Palme H, Hutcheon ID, and Spettel B (1994) Composition and origin of refractory-metal-rich assemblages in a Ca,Al-rich Allende inclusion. Geochimica et Cosmochimica Acta, 58, 495–513.

Palumbo ME (2005) The morphology of interstellar water ice. Journal of Physics Conference Series, 6, 211–216.

Palumbo ME, Tielens AGGM, and Tokunaga AT (1995) Solid carbonyl sulphide (OCS) in W33A. The Astrophysical Journal, 449, 674–680.

Palumbo ME, Geballe TR, and Tielens AGGM (1997) Solid carbonyl sulfide (OCS) in dense molecular clouds. The Astrophysical Journal, 479, 839–844.

Pendleton YJ, and Allamandola LJ (2002) The organic refractory material in the diffuse interstellar medium: Mid-infrared spectroscopic constraints. The Astrophysical Journal Supplement, 138, 75–98.

Podosek FA, Zinner EK, MacPherson GJ, Lundberg LL, Brannon JC, and Fahey AJ (1991) Correlated study of initial $^{87}Sr/^{86}Sr$ and Al-Mg isotope systematics and petrologic properties in a suite of refractory inclusions from the Allende meteorite. Geochimica et Cosmochinica Acta, 55, 1083–1110.

Pontoppidan KM, Dartois E, van Dishoeck EF, Thi W-F, and d'Hendecourt L (2003) Detection of abundant solid methanol toward young low mass stars. Astronomy & Astrophysics, 404, L17–L20.

Pontoppidan KM, Boogert ACA, Fraser HJ, van Dishoeck EF, Blake GA, Lahuis F, Öberg KI, Evans J, and Salyk C (2008) The c2d spitzer spectroscopic survey of ices around low-mass young stellar objects. II. CO_2. The Astrophysical Journal, 678, 1005–1031.

Qasim D, Chuang K-J, Fedoseev G, Ioppolo S, Boogert ACA, and Linnartz H (2018) Formation of interstellar methanol ice prior to the heavy CO freeze-out stage. Astronomy & Astrophysics, 612, A83, 9 pp.

Richter FM, Davis AM, Ebel DS, and Hashimoto A (2002) Elemental and isotopic fractionation of Type B calcium-, aluminum-rich inclusions: Experiments, theoretical considerations, and constraints on their thermal evolution. Geochimica et Cosmochimica Acta, 66, 521–540.

Richter FM, Janney PE, Mendybaev RA, Davis AM, and Wadhwa M (2007) Elemental and isotopic fractionation of Type B CAI-like liquids by evaporation. Geochimica et Cosmochimica Acta, 71, 5544–5564.

Roser JE, Vidali G, Manicò G, and Pirronello V (2001) Formation of carbon dioxide by surface reactions on ices in the interstellar medium. The Astrophysical Journal, 555, L61–L64.

Rubin AE (2013) An amoeboid olivine inclusion (AOI) in CK3 NWA 1559, comparison to AOIs in CV3 Allende, and the origin of AOIs in CK and CV chondrites. Meteoritics & Planetary Science, 48, 432–441.

Rubin AE, and Kallemeyn GW (1989) Carlisle Lakes and Allan Hills 85151: members of a new chondrite grouplet. Geochimica et Cosmochimica Acta, 53, 3035–3044.

Rubin AE, and Ma C (2017) Meteoritic minerals and their origins. Chemie der Erde, 77, 325–385.

——— (2020) Meteorite Mineralogy. Cambridge University Press, in press.

Rubin AE, Sailer AL, and Wasson JT (1999) Troilite in the chondrules of type-3 ordinary chondrites. Geochimica et Cosmochimica Acta, 63, 2281–2298.

Russell SS, Huss GR, Fahey AJ, Greenwood RC, Hutchison R, and Wasserburg GJ (1998) An isotopic and petrologic study of calcium–aluminium-rich inclusions from CO3 meteorites. Geochimica et Cosmochimica Acta, 62, 689–714.

Ruzicka A (1997) Mineral layers around coarse-grained, Ca–Al-rich inclusions in CV3 carbonaceous chondrites: Formation by high-temperature metasomatism. Journal of Geophysical Research, 102, 13387–13402.

Sack NJ, and Baragiola RA (1993) Sublimation of vapor-deposited water ice below 170 K, and its dependence on growth conditions. Physical Review B, 48, 9973–9978.

Sack RO, and Ghiorso MS (1994a) Thermodynamic properties of multicomponent pyroxenes: I. Formulation of a general model. Contributions to Mineralogy and Petrology, 116, 277–286.

——— (1994b) Thermodynamic properties of multicomponent pyroxenes: II. Phase relations in the quadrilateral. Contributions to Mineralogy and Petrology, 116, 287–300.

——— (1994c) Thermodynamics of multicomponent pyroxenes III: Calibration of $Fe^{2+}(Mg)_{-1}$, $TiAl(MgSi)_{-1}$, $TiFe^{3+}(MgSi)_{-1}$, $AlFe^{3+}(MgSi)_{-1}$, $NaAl(CaMg)_{-1}$, $Al^{2}(MgSi)_{-1}$ and $Ca(Mg)_{-1}$ exchange reactions between pyroxenes and silicate melts. Contributions to Mineralogy and Petrology, 118, 271–296.

——— (2017) Ti^{3+}- and Ti^{4+}-rich fassaites at the birth of the solar system: Thermodynamics and applications. American Journal of Science, 317, 807–845.

Sahai R, Zijlstra A, Sánchez Contreras C, and Morris M (2003) An icy, bipolar proto-planetary nebula with knotty jets: IRAS 22036+5306. The Astrophysical Journal Letters, 586, L81–L85.

Salama F, Galazutdinov GA, Krelowski J, Biennier L, Beletsky Y, and Song I-O (2011) Polycyclic aromatic hydrocarbons and the diffuse interstellar bands: A survey. The Astrophysical Journal 728, 154–161.

Salzmann CG (2018) Advances in the experimental exploration of water's phase diagram. arXiv:1812.04333. doi: 1063/1.5085163.

Sandford SA, Allamandola LJ, Tielens AGGM, and Valero GJ (1988) Laboratory studies of the infrared spectral properties of CO in astrophysical ices. The Astrophysical Journal, 329, 498–510. [PubMed: 11538228]

Saxena SK, and Hrubiak R (2014) Mapping the nebular condensates and the chemical composition of the terrestrial planets. Earth and Planetary Science Letters, 393, 113–119.

Schaefer L, and Fegley B (2010) Volatile element chemistry during metamorphism of ordinary chondritic material and some of its implications for the composition of asteroids. Icarus, 205, 483–496.

Schertl H-P, Mills SJ, and Maresch WV (2018) A Compendium of IMA-Approved Mineral Nomenclature. International Mineralogical Association, Melbourne, Australia.

Schutte WA, Boogert ACA, Tielens AGGM, Whittet DCB, Gerakines PA, Chiar JE, Ehrenfreund P, Greenberg JM, van Dishoeck EF, and de Graauw T (1999) Weak ice absorption features at 7.24 and 7.41 microns in the spectrum of the obscured young stellar object W33A. Astronomy & Astrophysics, 343, 966–976.

Scott ERD, and Krot AN (2014) Chondrites and their components. In Davis AM, Holland HD, and Turekian KK, Eds., Treatise on Geochemistry, Vol. 1: Meteorites, Comets, and Planets, Second edition. pp. 65–137. Elsevier-Pergamon.

Scott ERD, and Rajan S (1979) Thermal history of the Shaw chondrite. Proceedings of the Lunar and Planetary Science Conference, 10, 1031–1043.

Seki J, and Hasegawa H (1983) The heterogeneous condensation of interstellar ice grains. Astrophysics and Space Science, 94, 177–189.

Shibata Y (1996) Opaque minerals in Antarctic CO3 carbonaceous chondrites: Yamato-74135, −790992, −791717, −81020, −81025, −82050, and Allan Hills 77307. Proceedings of the NIPR Symposium on Antarctic Meteorites, 9, 79–96.

Shu FH, Shang H, and Lee T (1996) Toward an astrophysical theory of chondrites. Science, 271, 1545–1552.

Simon SB, and Grossman L (1992) Low temperature exsolution in refractory siderophile element-rich opaque assemblages from the Leoville carbonaceous chondrite. Earth and Planetary Science Letters, 110, 67–75.

——— (1997) In situ formation of palisade bodies in calcium, aluminum-rich refractory bodies. Meteoritics & Planetary Science, 32, 61–70.

Smith RG, Sellgren K, and Tokunaga AT (1989) Absorption features in the 3-micron spectra of protostars. The Astrophysical Journal, 344, 413–426.

Simon SB, Yoneda S, Grossman L, and Davis AM (1994) A $CaAl_4O_7$-bearing refractory spherule from Murchison: Evidence for very high-temperature melting in the solar nebula. Geochimica et Cosmochimica Acta, 58, 1937–1949.

Simon SB, Davis AM, and Grossman L (1996) A unique ultra-refractory inclusion from the Murchison meteorite. Meteoritics, 31, 106–115.

Smith DGW, Miúra Y, and Launspach S (1993) Fe, Ni, and Co variations in the metals from some Antarctic chondrites. Earth and Planetary Science Letters, 120, 487–498.

Snow TP, and McCall BJ (2006) Diffuse atomic and molecular clouds. Annual Review of Astronomy and Astrophysics, 44, 367–414.

Snow T, and Witt A (1995) The interstellar carbon budget and the role of carbon in dust and large molecules. Science, 270, 1455–1460. [PubMed: 7491489]

Snyder LE, and Buhl D (1971) Observations of radio emission from interstellar hydrogen cyanide. The Astrophysical Journal, 163, L47–L52.

Snyder LE, Buhl D, Zuckerman B, and Palmer P (1969) Microwave detection of interstellar formaldehyde. Physical Review Letters, 22, 679–681.

Sorrell W (1995) Nebular lightning and the chondrule factory. Comments of Astrophysics, 18, 151–159.

Steele IM (1995) Mineralogy of a refractory inclusion in the Allende (C3V) meteorite. Meteoritics, 30, 9–14.

Sylvester PJ, Grossman L, and MacPherson GJ (1992) Refractory inclusions with unusual chemical compositions from the Vigarano carbonaceous chondrite. Geochimica et Cosmochimica Acta, 56, 1343–1363.

Sylvester PJ, Simon SB, and Grossman L (1993) Refractory inclusions from the Leoville, Efremovka, and Vigarano C3V chondrites: Major element differences between Types A and B, and extraordinary refractory siderophile element compositions. Geochimica et Cosmochimica Acta, 57, 3763–3784.

Taylor GJ, Okada A, Scott ERD, Rubin AE, Huss GR, and Keil K (1981) The occurrence and implications of carbide-magnetite assemblages in unequilibrated ordinary chondrites. Proceedings of the Lunar and Planetary Science Conference, 12, 1076–1078.

Thompson T (1818) Scientific intelligence, and notices of subjects connected with science. III. Notice concerning certain minerals lately discovered. Annals of Philosophy, or Magazine of Chemistry, Mineralogy, Mechanics, Natural History, Agriculture, and the Arts, 12, 310–312.

Tielens AGGM (2008) Interstellar polycyclic aromatic hydrocarbon molecules. Annual Review of Astronomy and Astrophysics, 46, 289–337.

Ulyanov AA, Korina MI, Nazarov MA, and Sherbovsky EY (1982) Efremovka CAIs: Mineralogical and petrological data. Proceedings of the Lunar and Planetary Science Conference, 13, 813–814.

Urey HC (1955) The cosmic abundances of potassium, uranium, and thorium and the heat balances of the Earth, the Moon, and Mars. Proceedings of the National Academy of Sciences, 15, 127–144.

Wakelam V, Bron E, Cazaux S, Dulieu F, Gry C, Guillard P, Habart E, Hornekaer L, Morisset S, Nyman G, and others. (2017) H_2 formation on interstellar dust grains: The viewpoints of theory, experiments, models, and observations. Molecular Astrophysics, 9, 1–36.

Wang S, Li A, and Jiang BW (2015) The interstellar oxygen crisis, or where have all the oxygen atoms gone? Monthly Notices of the Royal Astronomical Society, 454, 569–575.

Wark DA (1986) Evidence for successive episodes of condensation at high temperatures in a part of the solar nebula. Earth and Planetary Science Letters, 77, 129–148.

——— (1987) Plagioclase-rich inclusions in carbonaceous chondrite meteorites: Liquid condensates? Geochimica et Cosmochimica Acta, 51, 221–242.

Wark DA, and Boynton WV (2001) The formation of rims on calcium–aluminum-rich inclusions: Step I. Flash heating. Meteoritics & Planetary Science, 36, 1135–1166.

Wark DA, and Lovering JF (1977) Marker events in the early solar system: Evidence from rims on Ca–Al-rich inclusions in carbonaceous chondrites. Proceedings of the Lunar Science Conference, 8, 95–112.

Wark DA, and Lovering JF (1978) Refractory/platinum metals and other opaque phases in Allende Ca-Al-rich inclusions (CAI's). Proceedings of the Lunar Science Conference, 9, 1214–1216.

——— (1982a) Evolution of Ca-Al-rich bodies in the earliest solar system: growth by incorporation. Geochimica et Cosmochimica Acta, 46, 2595–2607.

——— (1982b) The nature and origin of type B1 and B2 inclusions in the Allende meteorite. Geochimica et Cosmochimica Acta, 46, 2581–2594.

Wark DA, Boynton WV, Keays RR, and Palme H (1987) Trace element and petrologic clues to the formation of forsterite-bearing Ca-Al-rich inclusions in the Allende meteorite. Geochimica et Cosmochimica Acta, 51, 607–622.

Wasserburg GJ, Lee T, and Papanastassiou DA (1977) Correlated O and Mg isotopic anomalies in Allende inclusions: II. Magnesium. Geophysical Research Letters, 4, 299–302.

Weber D, and Bischoff A (1994) The occurrence of grossite ($CaAl_4O_7$) in chondrites. Geochimica et Cosmochimica Acta, 58, 3855–3877.

——— (1997) Refractory inclusions in the CR chondrite Acler 059-El Djouf 001: Petrology, chemical composition, and relationship to inclusion populations in other types of carbonaceous chondrites. Chemie der Erde, 57, 1–24.

Weber D, Zinner E, and Bischoff A (1995) Trace element abundances and magnesium, calcium and titanium isotopic compositions of grossite containing inclusions from the carbonaceous chondrite, Acfer 182. Geochimica et Cosmochimioca Acta, 59, 803–823.

Weisberg MK, Prinz M, and Nehru CE (1988) Petrology of ALH85085: A chondrite with unique characteristics. Earth and Planetary Science Letters, 91, 19–32.

Weisberg MK, Prinz M, Clayton RN, and Mayeda TK (1993) The CR (Renazzo-tyoe) carbonaceous chondrite group. Geochimica et Cosmochimica Acta, 57, 1567–1586.

Weisberg MK, Connolly HC Jr., and Ebel DS (2004) Petrology and origin of amoeboid olivine aggregates in CR chondrites. Meteoritics & Planetary Science, 39, 1741–1753.

Weisberg MK, Connolly H, Zolensky M, Bland P, Brearley A, Bridges J, Brownlee D, Butterworth A, and 33 others. (2006) Stardust (comet) samples and the meteorite record. American Geophysical Union, Abstract P51E-1243.

Whittet DCB (2003) Dust in the Galactic Environment. Institute of Physics Publishing, Bristol.

Whittet DCB, Pendleton YJ, Gibb EL, Boogert ACA, Chiar JE, and Nummelin A (2001) Observational constraints on the abundance and evolution of "XCN" in interstellar grain mantles. The Astrophysical Journal, 550, 793–798.

Widowiak TJ, Cronin LW, Beegle LW, and Robinson MS (1995) Plasma processing of interstellar PAHs into solar system kerogen. Planetary and Space Sciences, 43, 1175–1182.

Williams DA (2005) Gas and dust in the interstellar medium. Journal of Physics Conference Series, 6, 1–17.

Wilson RW, Jeeferts KB, and Penzias AA (1971) Carbon monoxide in the Orion nebula. Astrophysical Journal Letters, 161, 43–44.

Winnewisser G, and Churchwell E (1975) Interstellar formic acid. Sterne und Weltraum, 14, 288–289 (in German).

Womack M, Ziurys LM, and Wyckoff S (1992) Estimates of N_2 abundances in dense molecular clouds. The Astrophysical Journal, 393, 188–192.

Wood JA, and Hashimoto A (1993) Mineral equilibrium in fractionated nebular systems. Geochimica et Cosmochimica Acta, 57, 2377–2388.

Wood BJ, Smythe DJ, and Harrison T (2019) The condensation temperatures of the elements. American Mineralogist, 104, 844–856.

Yan L, Chary R, Armus L, Teplitz H, Helou G, Frayer D, Fadda D, Surace J, and Choi P (2005) Spitzer detection of polycyclic aromatic hydrocarbon and silicate dust features in the mid-infrared spectra of z ~2 ultraluminous infrared galaxies. The Astrophysical Journal, 628, 604–610.

Yoneda S, and Grossman L (1995) Condensation of CaO-MgO-Al_2O_3-SiO_2 liquids from cosmic gases. Geochimica et Cosmochimica Acta, 59, 3413–3444.

Zasowski G, Kemper F, Watson DM, Furlan E, Bohac CJ, Hull C, and Green JD (2009) Spitzer infrared spectrograph observations of Class I/II objects in Taurus: Composition and thermal history of the circumstellar ices. The Astrophysical Journal, 694, 459–478.

Zhang A, Benoit PH, and Sears DWG (1995) The classification and complex thermal history of the enstatite chondrites. Journal of Geophysical Research, 100, 9417–9438.

Zhang A-C, Ma C, Sakamoto N, Wang R-C, Hsu W-B, and Yurimoto H (2015) Mineralogical anatomy and implications of a Ti-Sc-rich ultra-refractory inclusion from Sayh al Uhaymir 290 CH3 chondrite. Geochimica et Cosmochimica Acta, 163, 27–39.

Zinner EK, Caillet C, and El Goresy A (1991) Evidence for extraneous origin of magnesiowüstite–metal Fremdlinge from the Vigarano CV3 chondrite. Earth and Planetary Science Letters, 102, 252–264.

Zuckerman B, Ball JA, and Gottlieb CA (1971) Microwave detection of interstellar formic acid. The Astrophysical Journal, 163, L41–L45.

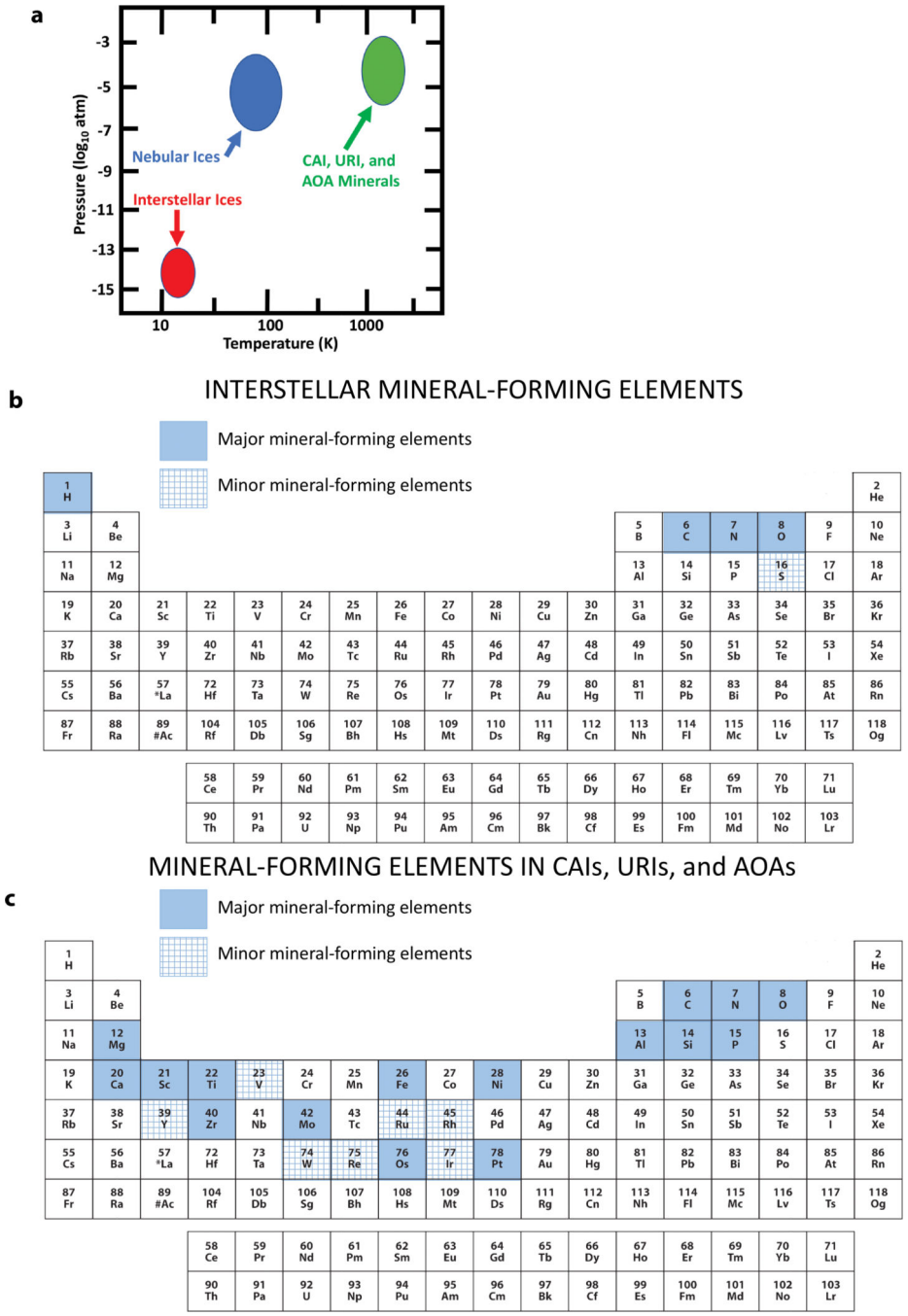

FIGURE 1.

The temperature, pressure, and compositional characteristics of primary interstellar and solar nebular condensates result in a distinctive second phase of the evolutionary system of mineralogy. (**a**) These minerals formed at a wide range of temperatures via low-pressure (P < 0.01 atm) condensation in interstellar and nebular environments. (**b**) Interstellar minerals formed primarily from C, H, N, O, and probably S—five of the most abundant elements in the cosmos. (**c**) Primary minerals in CAIs, URIs, and AOAs formed principally from 16

essential major elements, with important additional contributions from 7 minor elements. (Color online.)

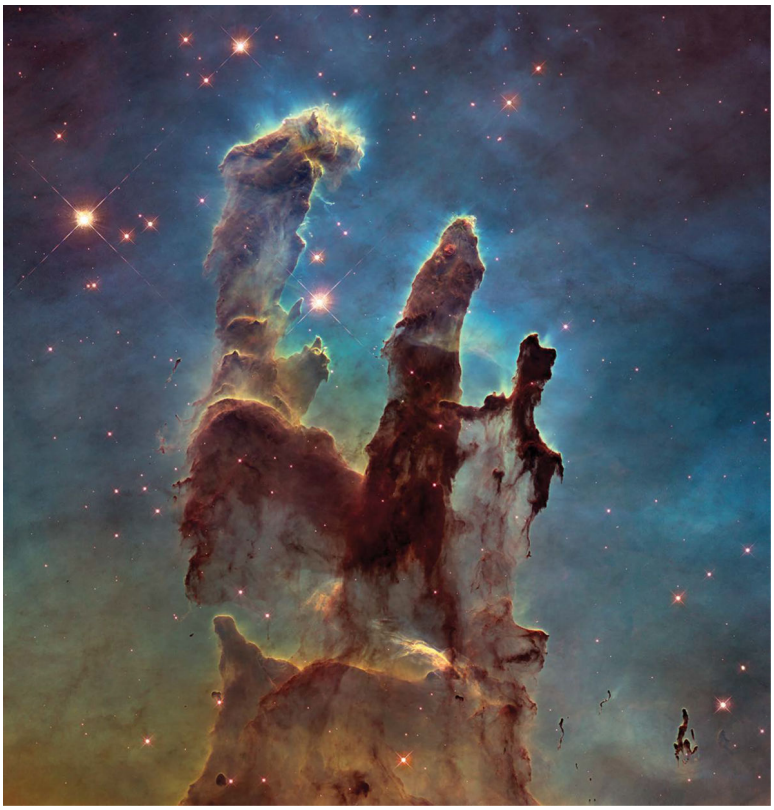

FIGURE 2.

A 2015 Hubble Space Telescope image of a portion of the Eagle Nebula (NGC 6611 and IC 4703), dubbed “The Pillars of Creation,” displays a star-forming region of a dense molecular cloud. The core regions of this structure are cooler areas, dense molecular clouds where molecular solids condense. [Image credit: NASA, ESA and the Hubble Heritage Team (STScI/AURA).] (Color online.)

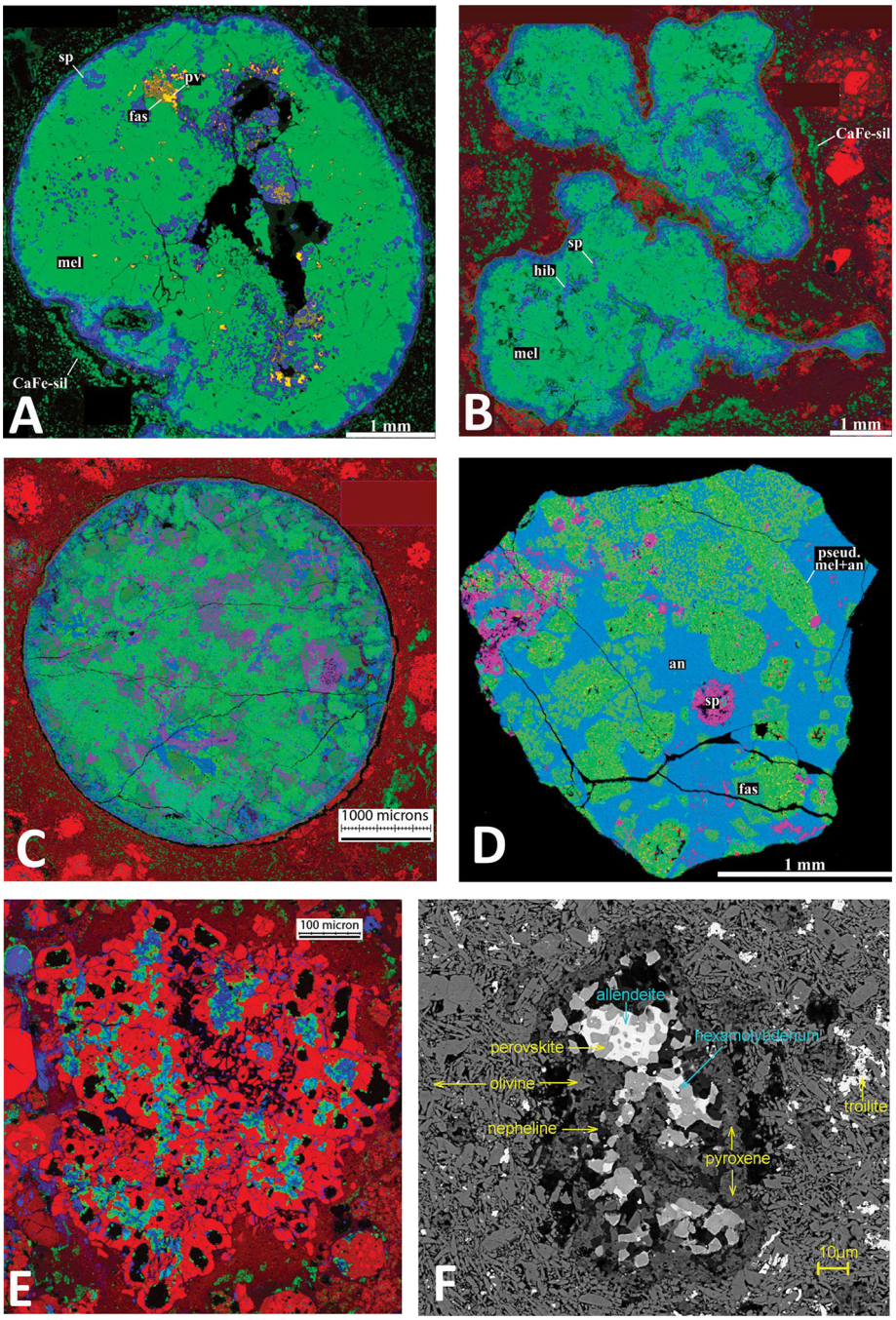

FIGURE 3.

Components of primitive chondrite meteorites with primary mineral phases include: calcium-aluminum-rich inclusions (CAIs), amoeboid olivine aggregates (AOAs), and ultra-refractory inclusions (URIs). (**a**) Compact type A CAI from the Adelaide meteorite with primarily melilite and spinel and minor perovskite and fassaite (Ti = red; Ca = green; Al = blue); (**b**) fluffy type A CAI from the Allende meteorite with melilite, spinel, fassaite, and anorthite (Mg = red; Ca = green; Al = blue); (**c**) type B CAI from the Allende meteorite with melilite, fassaite, spinel, and anorthite (Mg = red; Ca = green; Al = blue); (**d**) type C CAI

with anorthite, melilite, spinel, and fassaite (Mg = red; Ca = green; Al = blue); (**e**) forsterite-rich AOA from the Kainsaz meteorite with dominant forsterite plus Fe-Ni metal alloys, fassaite, spinel, and anorthite (Mg = red; Ca = green; Al = blue); (**f**) URI in matrix from the Allende carbonaceous chondrite. (Image credits: **a**, **b**, **d**, **e**, courtesy of Alexander Krot, University of Hawaii; **c**, courtesy of Denton Ebel, American Museum of Natural History; **f**, courtesy of Chi Ma, Caltech.) (Color online.)

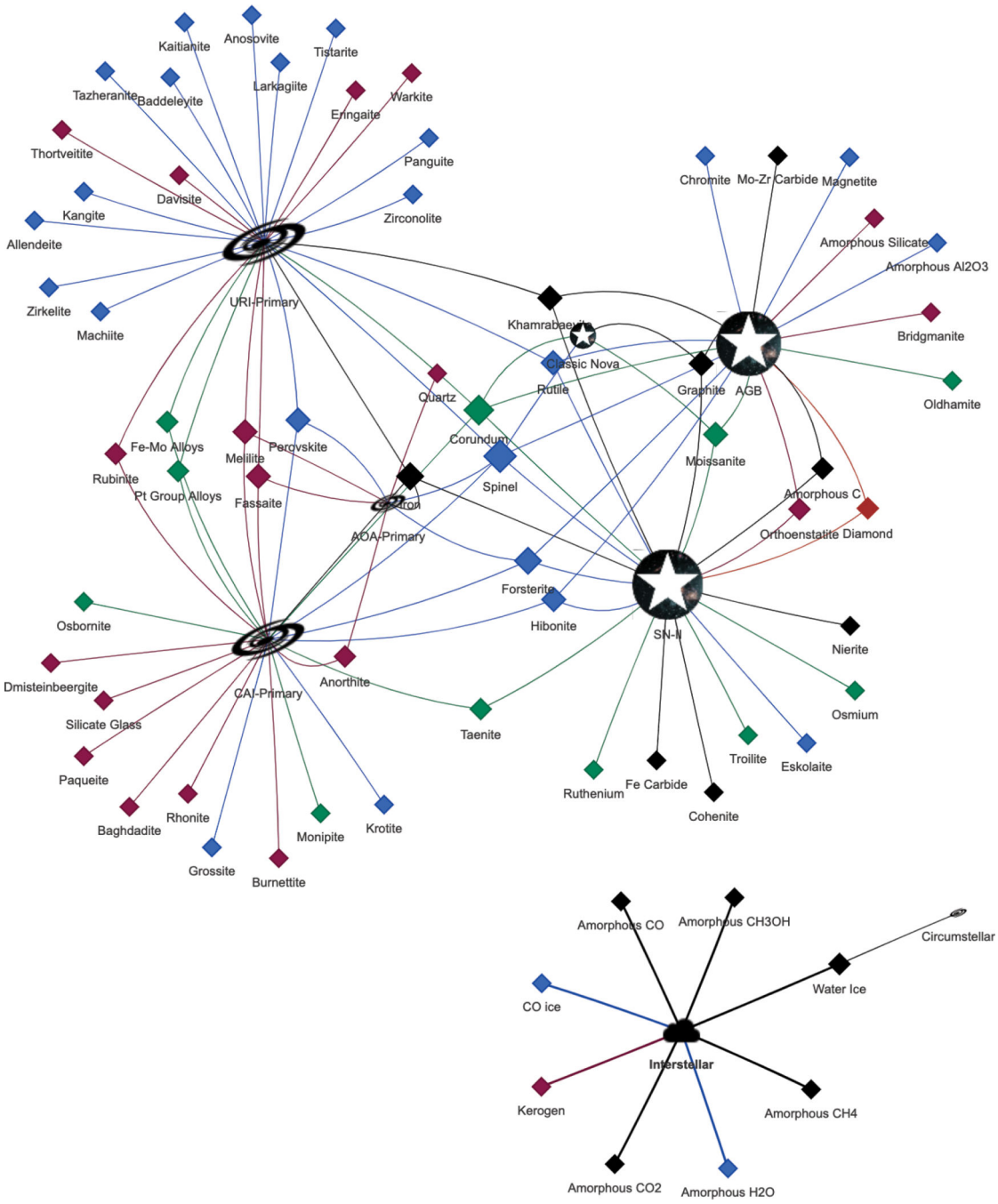

FIGURE 4.

Bipartite force-directed network graph (Morrison et al. 2017) of primary stellar, interstellar, and nebular minerals linked to their modes of paragenesis. Diamond-shaped nodes represent condensed crystalline and amorphous phases [black (C-bearing), green (not C or O), blue (contains O, but not C or Si), and red (contains Si+O)]. Star-shaped nodes represent three types of host stars—asymptotic giant branch stars (AGB), Type II supernovae (SN-II), and classical novae (CNova); the cloud-shaped node represents dense molecular clouds (DMC); and four disk-shaped nodes indicate circumstellar environments, CAIs, AOAs, and URIs.

The sizes of nodes correspond to the numbers of links to other nodes. Note that 8 low-temperature phases of the interstellar medium are not linked to 61 high-temperature primary phases of stellar and nebular environments. Network graph developed in collaboration with Anirudh Prabhu. (Color online.)

TABLE 1.

Seventeen paragenetic modes of meteorite minerals, after Rubin and Ma (2017)

Mode #	Description	Part
1	Condensation in the gaseous envelopes of stars (stellar mineralogy)	I
2	Condensation in the solar nebula	II
3	Crystallization in CAI and AOA melts	II
4	Crystallization in chondrule melts	III
5	Exsolution during cooling of CAIs	II
6	Exsolution during cooling of chondrules	III
7	Annealing of amorphous material	I, II, & III
8	Thermal metamorphism and exsolution	V
9	Aqueous alteration, hydrothermal alteration, and metasomatism	V
10	Shock metamorphism	IV
11	Condensation within impact plumes	IV
12	Crystallization from melts in differentiated bodies	IV
13	Condensation from late-stage vapors in differentiated bodies	IV
14	Exsolution, inversion, and subsolidus redox effects in cooling igneous rocks	IV
15	Solar heating near perihelion	III,V
16	Atmospheric passage	VI+
17	Terrestrial weathering[a]	VI+

Note: These modes of formation are not mutually exclusive. “Part” refers to proposed divisions of the evolutionary system of mineralogy, which will appear in multiple, ongoing contributions.

[a]Includes biological alteration, to be discussed in later contributions.

TABLE 2.

Diagnostic properties of circumstellar and interstellar condensed phases, with unconfirmed phases appearing in brackets

Species (formula)	Natural kind	Characteristics	References
		Native Elements	
Hydrogen (H_2)	[Interstellar hydrogen]	A fraction of H_2 may condense at $T \sim 10$ K	1
Nitrogen (N_2)	[Interstellar nitrogen]	Molecular nitrogen should condense heterogeneously at $T < 20$ K	2,3
Oxygen (O_2)	[Interstellar oxygen]	Most molecular oxygen reacts with H_2 to form H_2O	4,5
		Oxides	
Water (H_2O)	Interstellar cubic ice	Diagnostic sharp IR emission features at 44 and 60 μm	6–8
	Interstellar amorphous H_2O	Diagnostic O-H stretch at 3.05 μm	7–10
Carbon monoxide (CO)	Interstellar amorphous CO	Diagnostic absorption at 4.67 μm	11,12
	Interstellar CO	Forms when amorphous CO anneals at $T > 23$ K	13
Carbon dioxide (CO_2)	Interstellar amorphous CO_2	IR absorption features at 4.27 and 15.2 μm	14
Sulfur dioxide (SO_2)	[Interstellar SO_2]	Diagnostic absorption at ~7.6 μm	15,16
		Organic Molecular Solids	
Methanol (CH_3OH)	Interstellar amorphous CH_3OH	Diagnostic absorption at 3.54, 3.95, 8.9, and 9.75 μm	8,17
Methane (CH_4)	Interstellar amorphous CH_4	Diagnostic 7.676 μm absorption	8,18
Cyanide (XCN; X = H,O)	[Interstellar *X*CN]	Diagnostic absorption at 4.62 μm	8,19,20
Formaldehyde (H_2CO)	[Interstellar H_2CO]	5.81 and 5.83 μm absorption; 4830 MHz emission	8,21
Formic acid (HCOOH)	[Interstellar HCOOH]	Diagnostic absorption at 5.85 and 7.243 μm	8,22,23
Acetaldehyde (CH_3HCO)	[Interstellar CH_3HCO]	Diagnostic 7.414 μm absorption	8,23
Carbonyl sulfide (OCS)	[Interstellar OCS]	Diagnostic 4.91 μm absorption	8,24,25
Ammonia (NH_3)	[Interstellar NH_3]	Suggested by bands at 3.5 and ~9 μm	8,26
Kerogen (C,H,N,O)	Interstellar kerogen	Preserved in relatively unaltered carbonaceous chondrites; Diagnostic absorption at 3.3, 3.47, 6.2, 8.6, and 11.3 μm	8,27–31

References: 1 = Allamandola et al. (1999); 2 = Maret et al. (2006); 3 = Daranlot et al. (2012); 4 = Hollenbach et al. (2009); 5 = Wang et al. (2015); 6 = Omont et al. (1990); 7 = Whittet (2003); 8 = Gibb et al. (2004); 9 = Hagen et al. (1981); 10 = Newman et al. (2008); 11 = Chiar et al. (1996); 12 = Elsila et al. (1997); 13 = Kouchi (1990); 14 = Pontoppidian et al. (2008);15 = Boogert et al. (1997); 16 = Zasowski et al. (2009); 17 = Pontoppidian et al. (2003); 18 = Boogert et al. (1996); 19 = Clark et al. (1974); 20 = Whittet et al. (2001); 21 = Grim et al. (1991); 22 = Bisschop et al. (2007); 23 = Schutte et al. (1999); 24 = Palumbo et al. (1995); 25 = Palumbo et al. (1997); 26 = Smith et al. (1989); 27 = Cronin & Pizzarello (1990); 28 = Greenberg et al. (1995); 29 = Widowiak et al. (1995); 30 = Ehrenfreund- & Cami (2010); 31 = Ehrenfreund et al. (1991).

TABLE 3.

Properties of primary phases in the solar nebula formed by condensation, melt crystallization, and solid-state reactions

Group	Species (formula)	Natural kind	Characteristics	References
		Native elements		
	Pt group alloys (Pt,Ru,Os, etc.)	CAI PGE alloy	Nano- to micro-scale alloys, space group $P6_3/mmc$	1,2
		URI PGE alloys	Often Os-dominant	3–5
	Iron (Fe,Ni) [also called “kamacite”]	CAI iron	Occurs as a primary phase in type A, B, and C CAIs	1,6–8
		AOA iron	Ubiquitous in AOAs, typically with 5 to 7 wt% Ni	9–11
		URI iron	Sub-micrometer grains associated with ultra-refractory minerals	
	Taenite (Fe,Ni)	CAI taenite	Occurs in type A and B CAIs; typically 10 to 50 wt% Ni	1,6,8
	Fe-Mo alloys (Fe,Mo,Ru,Os,etc.)	CAI Fe-Mo alloys	Includes IMA-approved hexaferrum and hexamolybdenum	12–14
		URI Fe-Mo alloys	Includes IMA-approved hexaferrum and hexamolybdenum	4,5,14
		Carbides		
	Khamrabaevite (TiC)	URI khamrabaevite	Associated with corundum and tistarite	15
		Nitrides		
	Osbornite (TiN)	CAI osbornite	As a rare phase in CAIs	16,17
		Phosphides		
	Monipite (MoNiP)	CAI monipite	Known from micrometer-scale grains in the Allende meteorite	18
		Oxides		
	Ice (H_2O)	Nebular cubic ice	Condenses at $50 < T < 150$ K in the outer nebula	19
	Corundum (Al_2O_3)	CAI corundum	Near end-member; in CAI cores, inclusions in hibonite or spinel	1,20,21
		URI corundum	Associated with khrambaevite and tistarite	15
	Tistarite (Ti_2O_3)	URI tistarite	Associated with khrambaevite and corundum	15,22
	Kaitianite ($Ti_2^{3+}Ti^{4+}O_3$)	URI kaitianite	Known from two grains, both micrometer-scale	15,22
	Rutile (TiO_2)	URI rutile	Associated with tistarite and kaitianite	15,22
	Baddeleyite (ZrO_2)	URI baddeleyite	Associated with zirkelite	23
	Anosovite [$(Ti^4,Ti^{3+},Mg,Sc,Al)_3O_5$]	URI anosovite	Known from two grains, both micrometer-scale	14
	Spinel ($MgAl_2O_4$)	CAI spinel	Ubiquitous in CAIs; a component of Wark-Lovering rims	1,2
		AOA spinel	Associated with perovskite, fassaite, and anorthite	10,11
		URI spinel	Associated with Sc-rich fassaite, REE-enriched perovskite	5,24,25
	Hibonite ($CaAl_{12}O_{19}$)	CAI hibonite	Common in CAIs and Wark-Lovering rims	1,2

Group	Species (formula)	Natural kind	Characteristics	References
	Perovskite ($CaTiO_3$)	CAI perovskite	Common in CAIs and Wark-Lovering rims	1,2
		AOA perovskite	Common as sub-micrometer grains associated with spinel	1,11
		URI perovskite	Typically enriched in REE; associated with Sc minerals	4,5,24–26
	Lakargiite ($CaZrO_3$)	URI lakargiite	Sub-micrometer grains as inclusions in hibonite	4
	Grossite ($Ca_2Al_4O_7$)	CAI grossite	5- to 10-micrometer grains as inclusions in major CAI phases	27,28
	Krotite ($CaAl_2O_4$)	CAI krotite	One occurrence; in association with major CAI phases	29,30
	Machiite ($Al_2Ti_3O_9$)	URI machiite	Known from a single 4.4-micrometer diameter crystallite	31
	Zirkelite [$(Ti,Ca,Zr)O_{2-x}$]	URI zirkelite	Found in association with baddeleyite	23
	Kangite [$(Sc,Ti,Al,Zr,Mg,Ca)_{1.8}O_3$]	URI kangite	Cation-deficient, cubic bixbyite structure	25
	Panguite [$(Ti,Sc,Al,Mg,Zr,Ca)_{1.8}O_3$]	URI panguite	Cation-deficient, orthorhombic bixbyite structure	12,14,32,33
	Zirconolite ($CaZrTi_2O_7$)	URI zirconolite	Associated with tazheranite and metal alloys	3
	Tazheranite [$(Zr,Sc,Ca,Y,Ti)O_{1.75}$]	URI tazheranite	Associated with zirconolite and metal alloys	3,13
	Allendeite ($Sc_4Zr_3O_{12}$)	URI allendeite	Contains spinel and refractory metal inclusions	5
		Silicates		
	Quartz (SiO_2)	AOA quartz	Associated with fassaite, forsterite, anorthite, and spinel	
Olivine group [$(Mg,Fe,Ca,Mn)_2SiO_4$]				
	Forsterite Mg_2SiO_4	CAI forsterite	A minor primary CAI phase; with spinel and fassaite	1,2
		AOA forsterite	Defining major phase of AOAs	1,2
Garnet group [$Ca_3(Al, Ti^{3+},V,Sc)_2Si_3O_{12}$]				
	Rubinite ($Ca_3Ti_2^{3+}Si_3O_{12}$)	CAI rubinite	From type A CAIs	35
		URI rubinite	Significantly enriched in Y, Sc, and Zr; with eringaite	35
	Eringaite ($Ca_3Sc_2Si_3O_{12}$)	URI eringaite	Occurs with rubinite	13,35
Melilite group [gehlenite ($Ca_2Al_2SiO_7$) to åkermanite ($Ca_2MgSi_2O_7$)]				
		CAI melilite	Common in CAIs and Wark-Lovering rims	1,2
		AOA melilite	Gehlenite-rich, associated with anorthite and spinel	1,10
		URI melilite	Gehlenite-rich, associated with davisite, perovskite, spinel	26
Clinopyroxene group [$Ca(Mg,Al,Ti^{3+},Sc,V)(Al,Ti^{4+},Si)SiO_6$				
	Fassaite [$Ca(Mg,Al,Ti^{3+})(Si,Al,Ti^{4+})SiO_6$]	CAI fassaite	Common in CAIs and Wark-Lovering rims	1,2

Group	Species (formula)	Natural kind	Characteristics	References
		AOA fassaite	Common in association with forsterite and anorthite	10,11
		URI fassaite	Sub-millimeter grains with davisite, spinel, etc.	5,24,36
	Burnettite ($CaV^{3+}AlSiO_6$)	CAI burnettite	Identified by from one fluffy type A CAI	37
	Davisite ($CaSc^{3+}AlSiO_6$)	URI davisite	Associated with fassaite, perovskite, and spinel	12,15,24
Feldspar group [$(Na,Ca)(Al,Si)_4O_8$]				
	Anorthite ($CaAl_2Si_2O_8$)	CAI anorthite	Commonly as laths in CAIs; Primary anorthite is Na-free	1,2
		AOA anorthite	Common minor phase in AOAs	11
		CAI dmisteinbergite	A rare high-*T*, low-*P* polymorph of anorthite	38
		CAI baghdadite	Known from a single 0.8 μm euhedral grain	39
	Rhönite [$Ca_2(Mg,Al,Ti)_6(Si,Al)_6O_{20}$], Addibischoffite [$Ca_2(Al,Mg,V,Ti)_6(Al,Si)_6O_{20}$)], and Warkite [$Ca_2(Sc,Ti,Al,Mg,Zr)_6Al_6O_{20}$]			
		CAI rhönite	A rare constituent of A and B CAIs	40,41
		URI warkite	Micrometer-scale crystals with perovskite and davisite	26
	Paqueite [$Ca_3TiSi_2(Al,Ti,Si)_3O_{14}$]	CAI paqueite	From a fluffy type A CAI	37
	Thortveitite ($Sc_2Si_2O_7$)	URI thortveitite	Micrometer-scale crystals with fassaite and davisite	12
	Silicate glass (Ca,Mg,Al,Si,O)	CAI silicate glass	A component of hibonite-silicate spherules	2,42,43

Note: CAI = calcium-aluminum-rich inclusion; AOA = amoeboid olivine aggregate; URI = ultra-refractory inclusion.

References: 1 = Brearley & Jones (1998); 2 = MacPherson (2014); 3 = Ma & Rossman (2008); 4 = Ma (2011); 5 = Ma et al. (2014a); 6 = Campbell et al. (2005); 7 = Scott & Krot (2014); 8 = Rubin & Ma (2017); 9 = Chizmadia et al. (2002); 10 = Krot et al. (2004); 11 = Weisberg et al. (2004); 12 = Ma et al. (2011a); 13 = Ma (2012); 14 = Zhang et al. (2015); 15 = Ma & Rossman (2009c); 16 = Grokhovsky (2006); 17 = Weisberg et al. 1988; 18 = Ma et al. (2014b); 19 = Omont et al. (1990); 20 = Bar-Matthews et al. (1982); 21 = Greshake et al. (1996); 22 = Ma (2019); 23 = Krot et al. (2019); 24 = Ma and Rossman 2009b); 25 = Ma et al. (2013b); 26 = Ma et al. (2015); 27 = Greenwood et al. (1992); 28 = Simon et al. (1994); 29 = Ivanova et al. (2002); 30 = Ma et al. (2011b); 31 = Krot et al. (2020); 32 = El Goresy et al. (2002); 33 = Ma et al. (2012); 34 = Komatsu et al. (2018); 35 = Ma et al. (2017a); 36 = Ma and Rossman (2009a); 37 = Ma and Beckett (2016); 38 = Ma et al. (2013a); 39 = Ma (2018); 40 = Fuchs (1971); 41 = Ma et al. (2017b); 42 = Kimura et al. (1993); 43 = Beckett and Stolper (1994).